NASA Technical Paper 1844

Evaluation of Microwave Landing System (MLS) Effect on the Delivery Performance of a Fixed-Path Metering and Spacing System

Leonard Credeur, Christina M. Davis,
and William R. Capron

AUGUST 1981

NASA

NASA Technical Paper 1844

Evaluation of Microwave Landing System (MLS) Effect on the Delivery Performance of a Fixed-Path Metering and Spacing System

Leonard Credeur
Langley Research Center
Hampton, Virginia

Christina M. Davis
Research Triangle Institute
Research Triangle Park, North Carolina

William R. Capron
Kentron International, Inc.
Hampton, Virginia

National Aeronautics
and Space Administration

**Scientific and Technical
Information Branch**

1981

CONTENTS

GLOSSARY

ADC	analog-to-digital converter
ATC	air traffic control
ARTS	automated radar terminal system
DAC	digital-to-analog converter
DICE	direct-course-error
DME	distance measuring equipment
DSMT	desired scheduled marker time
EADI	electronic attitude director indicator
EHSI	electronic horizontal situation indicator
ETA	estimated time of arrival
FAA	Federal Aviation Administration
FCFS	first-come-first-serve
G	approach gate
H	heavy aircraft
IAF	initial arrival fix
IAS	indicated airspeed
IFR	instrument flight rules
ILS	instrument landing system
M & S	metering and spacing
MLS	microwave landing system
MSL	mean sea level
MSMT	metering scheduled marker time
OM	outer marker
RNAV	area navigation
SMT	scheduled outer-marker arrival time

SRT	synchronized real time
STAR	standard terminal arrival route
TAATM	Terminal Area Air Traffic Model
TCV	Terminal Configured Vehicle
TDZ	runway touchdown zone
VCWS	velocity control-wheel steering
VFR	visual flight rules
VOR	very high frequency omnidirectional range

SUMMARY

A simulation study was conducted to evaluate the delivery performance of an earlier proposed fixed-path metering and spacing (M & S) system and to determine if use of the microwave landing system (MLS) improved the system's delivery performance over that achieved with the current instrument landing system (ILS). The M & S algorithms used in the study are described with additional detail and flow charts included in the appendixes. The M & S system assumes an aircraft two-dimensional area navigation (RNAV) capability, and the three navigation systems compared were as follows: (1) Very high frequency omnidirectional range/distance measuring equipment (VOR/DME) and ILS; (2) VOR/DME and ±40° MLS; and (3) VOR/DME and ±60° MLS. The study was made with a computerized Terminal Area Air Traffic Model (TAATM), which contains pertinent en route effects, and the results of the study were compared to a full-crew, pilot-in-the-loop cockpit simulation.

The batch (fast-time) simulation results show that the aircraft interarrival-error standard deviation at the outer marker is only reduced from 9.2 to 7.9 sec when the ±60° MLS replaces the VOR/DME for navigation during final-spacing path-adjustment maneuvers. Though true for the particular geometry studied, further investigation showed this result reflects the interaction of two types of approach route. For only straight-in routes there was no verified difference between the interarrival-error standard deviation of the MLS and ILS systems; however, there was a 2.6-sec advantage for the MLS system with a geometry containing only direct-course-error (DICE) turn final-approach routes. For the system studied the wider coverage ±60° MLS offers no advantage over the basic ±40° MLS system.

Real-time cockpit data indicate that moving the gate closer to the runway threshold, although theoretically possible because of MLS precision, may affect the interarrival delivery precision of the M & S system. Interarrival delivery-error deviations achieved during the study were substantially less than those usually quoted for current manual vectoring procedures. The study also demonstrated that most of the terminal area holding is transferred to more fuel-efficient, higher altitude en route delay when the en route time-base metering is coupled to the terminal scheduling and spacing process in the M & S system. A reduction in terminal delay not only saves fuel but increases safety by reducing congestion and lowering the work load of both pilots and controllers.

1.0 INTRODUCTION

A study was undertaken in response to a Federal Aviation Administration (FAA) need to more completely evaluate a particular early-design fixed-path metering and spacing (M & S) system (refs. 1 to 4) and to determine if use of the microwave landing system (MLS) for approach guidance improved the system's delivery performance. The proposed fixed-path M & S system emphasizes the use of RNAV paths together with computer-derived indicated-airspeed commands to the

pilot in order to minimize route variations normally used in achieving a precise scheduled landing time. The regulation of the flow rate (metering) into the terminal is accomplished via a time-based process.

Limited simulation evaluations (refs. 1 to 4) of a metering and spacing system using speed control, transition vectoring, and two-dimensional RNAV with direct engage capability were encouraging. These studies demonstrated the workability of this type of system and yielded results comparable to M & S systems using only vectoring. Another evaluation, which used a single-aircraft root-sum-square error analysis (ref. 5), calculated the delivery performance of a strictly speed-control (fixed-path only) system and also that of a speed-control system with fine tuning through RNAV direct-engage time-to-turn maneuvers in the base-leg region. This analysis indicated that a wide-coverage MLS would have significant superiority over other navaids in its ability to support a fixed-path speed-control system.

A more rigorous investigation through simulation was deemed necessary to consider the system performance of the MLS fixed-path system. A more realistic and detailed simulation would evaluate the multiple aircraft interactions of the system subjected to various traffic demands. Also needed was verification of theoretical results on such man-machine issues as communication delays and pilot reaction under realistic work-load conditions.

Facilities used in the investigation are the Terminal Area Air Traffic Model (TAATM) and the Terminal Configured Vehicle (TCV) Aft Flight Deck Simulator at the Langley Research Center (ref. 6). The fixed-path M & S control logic was incorporated into TAATM and its geometry configured to the Denver Terminal Area used in references 1 to 5. Current operational geometry in Denver is different, but in order to make comparisons with previous results, the original configuration was used in this investigation. The TAATM is a flexible dynamic model of the airborne, navaid, ground control, and communications aspects of the terminal area environment which can run in either fast time (batch mode) or in real time. The TAATM also models pertinent en route effects. Pilot-in-the-loop experiments were conducted with the TAATM and the TCV simulator integrated together. The TAATM in conjunction with a simulation operator provided an operational environment and voice commands to the TCV simulator. The TCV simulator then became one of the aircraft to be controlled in the TAATM airspace.

The report is organized so that the system studied is first described and then the investigation results and conclusions follow. Sections 2.0 and 3.0 explain the terminal geometry and the fixed-path, speed-control M & S system evaluated. Section 4.0 describes the models used to represent navigation and system errors. Limitations in the M & S system were observed during the investigation and presented in section 5.0. Section 6.0 presents the fast-time (batch) study results whereas section 7.0 presents the real-time pilot-in-the-loop findings. The entire investigation results are summarized in section 8.0. Appendix A gives the derivation of a procedure for determining system interarrival time-error performance from single-aircraft, route-dependent arrival errors. This allows a direct comparison of real-time results with those obtained from system interarrival-error performance measured in fast-time runs.

Appendixes B and C give more details of the M & S system and aircraft navigation modes and appendix D contains M & S control-logic flow diagrams.

Several of the figures are exact duplicates of the displays used, and as such they contain measurements in feet. To convert these values to meters, use the following conversion: 1 ft = 0.3048 m. Also, knots are indicated in some figures as K.

Use of trade names or names of manufacturers in this report does not constitute an official endorsement of such products or manufacturers, either expressed or implied, by the National Aeronautics and Space Administration.

2.0 AIR TRAFFIC CONTROL (ATC) TERMINAL AREA METERING AND SPACING ENVIRONMENT FOR DENVER

The terminal area environment for the metering and spacing studies was designed based on the proposed specifications in reference 4. The overall configuration assuming MLS capability is depicted in figure 1, which shows the merger of two of the seven arrival routes into a single straight-in approach from the east (BYERS), merger of two routes into a north corner-post approach (LONGMONT), one southwest corner-post approach (SHAWNEE), and merger of the last two routes into a south corner-post approach path (ELIZABETH). The four ATC intersections (VOR/DME defined) for which the standard terminal arrival routes (STAR's) are named are the so-called metering or initial arrival fixes (IAF's) at which holding stacks are deployed when necessary. Each path from the terminal area perimeter to the final-approach gate is a two-dimensional area navigation (RNAV) path defined by navigation waypoints. Exceptions to this are the racetrack-shaped holding patterns and the delay vector areas. The waypoint names and locations do not necessarily represent reality in the Denver area but were chosen to satisfy the experimental requirements for the TAATM M & S simulation.

The differences in geometry between the MLS and conventional ILS configurations are associated with the location of the outer marker with respect to the runway touchdown zone (TDZ). In theory, the final-approach common path can be shortened if RNAV-equipped aircraft utilize the wider, high-precision coverage afforded by the MLS system to intercept the extended-runway centerline closer to the threshold. Thus, for the TAATM M & S, the outer marker locations are 3.5 and 5.5 n.mi. from the TDZ for MLS and ILS, respectively, with corresponding differences in the locations of the approach GATE, ALTURA, NORTH2, and SOUTH2 waypoints. The altitude objectives at the gate (glide-slope intercept altitudes at the outer marker) are 1981 and 2134 m (6500 and 7000 ft) for glide slopes of 3.00° and 2.75° for MLS and ILS approaches, respectively.

In general, the initial arrival clearance for the route segments from the perimeter to the IAF calls for a descent to the IAF altitude followed by a 250-knot speed command. The delivery time for the speed command is computed to provide earliest time of arrival at the IAF based on perimeter penetration

speed and nominal deceleration rate for the particular class of aircraft. In other words, the speed objective should be met just as the aircraft reaches the fix.

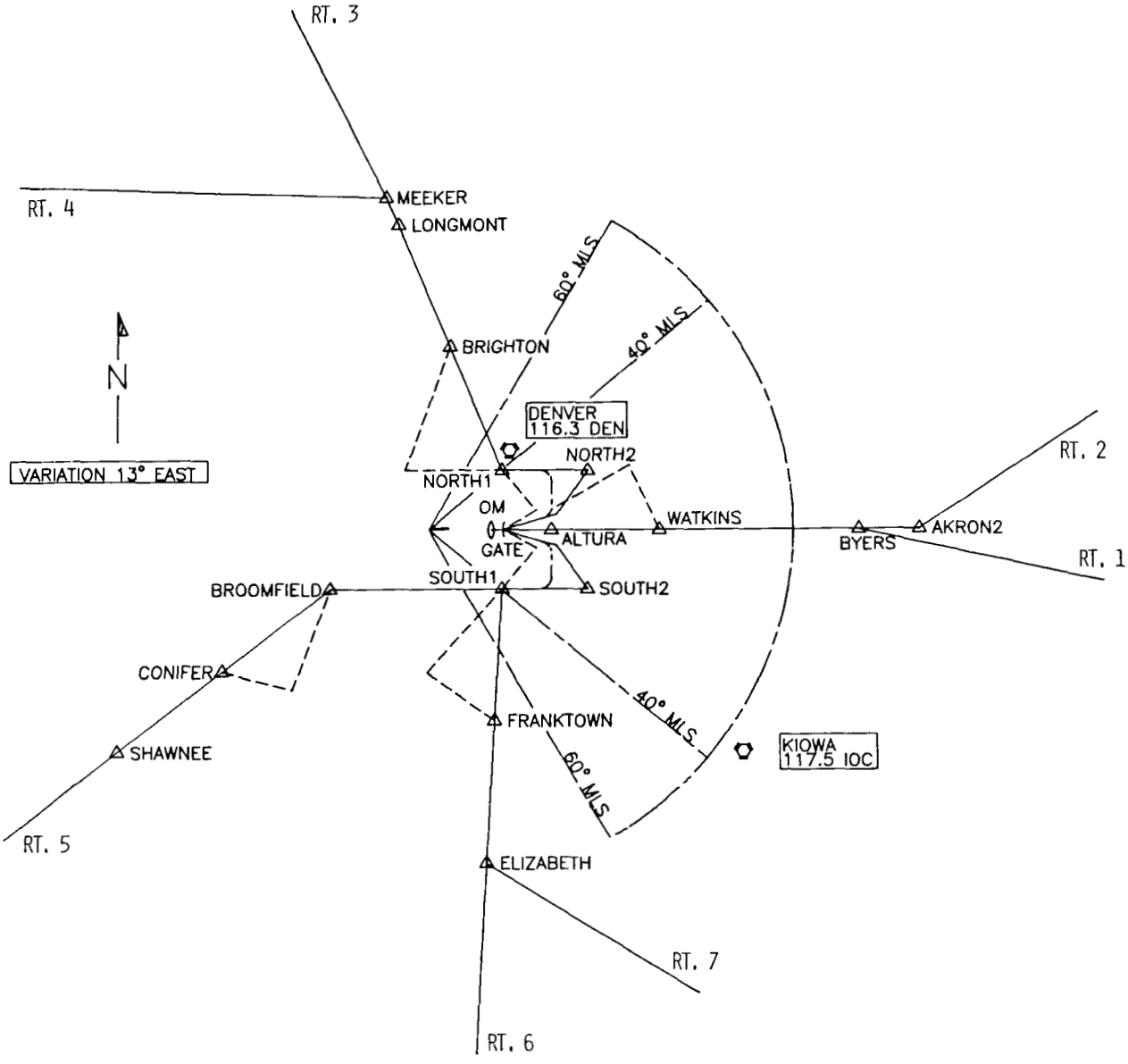

Figure 1. Fixed-path metering and spacing/MLS configuration for runway 26 arrival routes at Stapleton International Airport, Denver, Colorado.

However, if a holding stack is in use at the IAF, the next available stack altitude is assigned followed by a 210-knot speed command delivered at the appropriate computed time. All holding stacks consist of four levels starting at the IAF altitude and incremented by 305 m (1000 ft) upward.

To maintain the future controllability that would be lost by the 210-knot constraint in the holding pattern, a speed increase is usually requested by the speed-control routine (depending on existing conditions) upon departure from the IAF. This is an exception to the normal practice of issuing speed reductions only and is not objectionable from a pilotage viewpoint because of the potential-to-kinetic energy transfer available during the ensuing descent.

The following sections describe the particular regions of application of the M & S control concept discussed in detail in section 3.0. Typical delay times attainable with speed control only are shown for a Boeing 737-class aircraft in the following list:

BYERS arrival	66 sec
LONGMONT arrival	61 sec
SHAWNEE arrival	104 sec
ELIZABETH arrival	65 sec

2.1 BYERS Approach

The straight-in BYERS approach navigation plate is shown in figure 2. Due to the limited speed-control delay capability and heavy utilization of this path

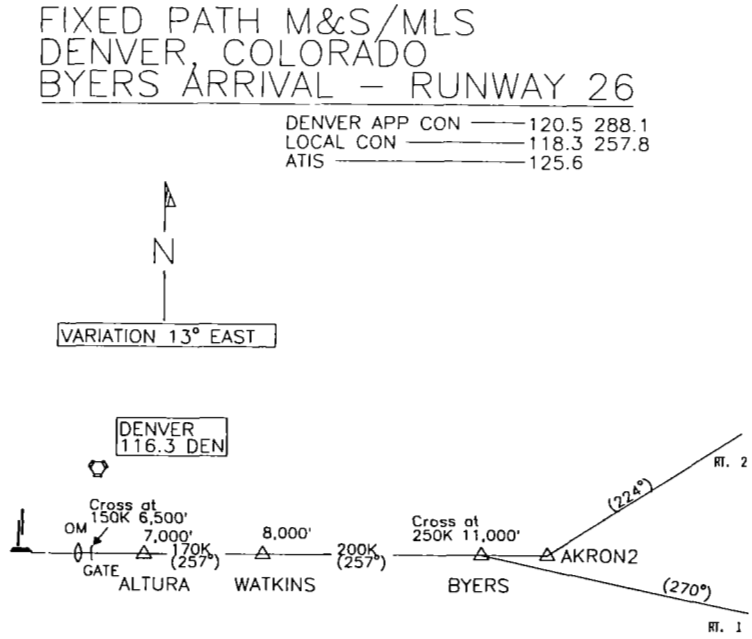

Figure 2.- BYERS STAR navigation plate.

(40 percent of the arrival traffic), the aircraft on routes 1 and 2 are given landing priority over those on the other three approach paths. Thus, holding stacks at BYERS are required much less frequently than at the other IAF's. The remainder of the path contains two speed-control regions (BYERS to WATKINS and WATKINS to GATE) with firm sequencing and possible path stretching occurring at WATKINS.

2.2 LONGMONT Approach

Arrival routes 3 and 4, carrying 35 percent of the traffic, merge at the MEEKER intersection before reaching the LONGMONT IAF as shown in figure 3.

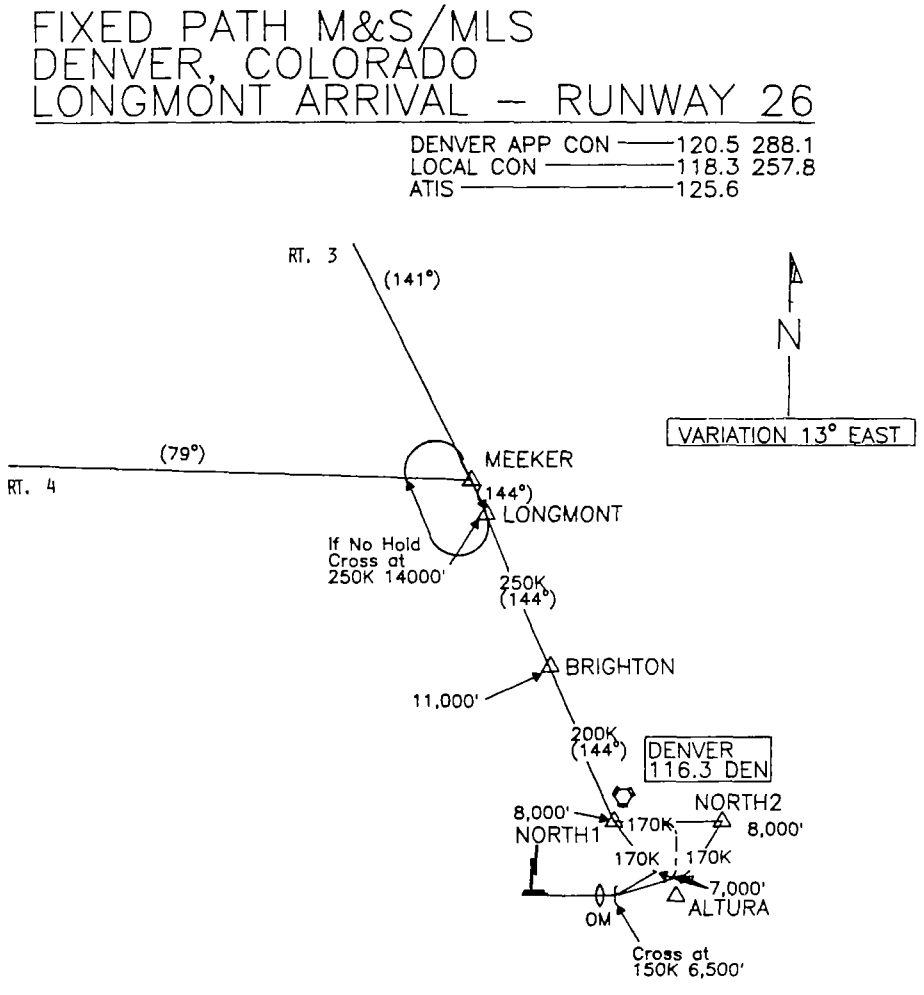

Figure 3.- LONGMONT STAR navigation plate.

Speed control may be applied in two regions (LONGMONT to BRIGHTON and BRIGHTON to NORTH1), with possible path stretching at BRIGHTON.

Firm sequencing takes place just prior to reaching NORTH1, at which point the minimum path direct to ALTURA is assigned if preceding traffic permits. Otherwise, the conventional downwind leg is assigned from which the initial DICE countdown to ALTURA is computed. Final DICE turns to GATE are computed from the minimum path or base (crosswind) leg along with a speed command such that final-approach speed reduction is completed at the gate.

2.3 SHAWNEE Approach

The lightest route loading (10 percent) occurs on arrival route 5 (SHAWNEE, fig. 4). Ironically, this path has the greatest speed-control capability, with three regions between SHAWNEE and SOUTH1. In addition, path stretching may be applied at CONIFER. Firm sequencing is done just prior to SOUTH1 and employs the same options as described for the LONGMONT approach.

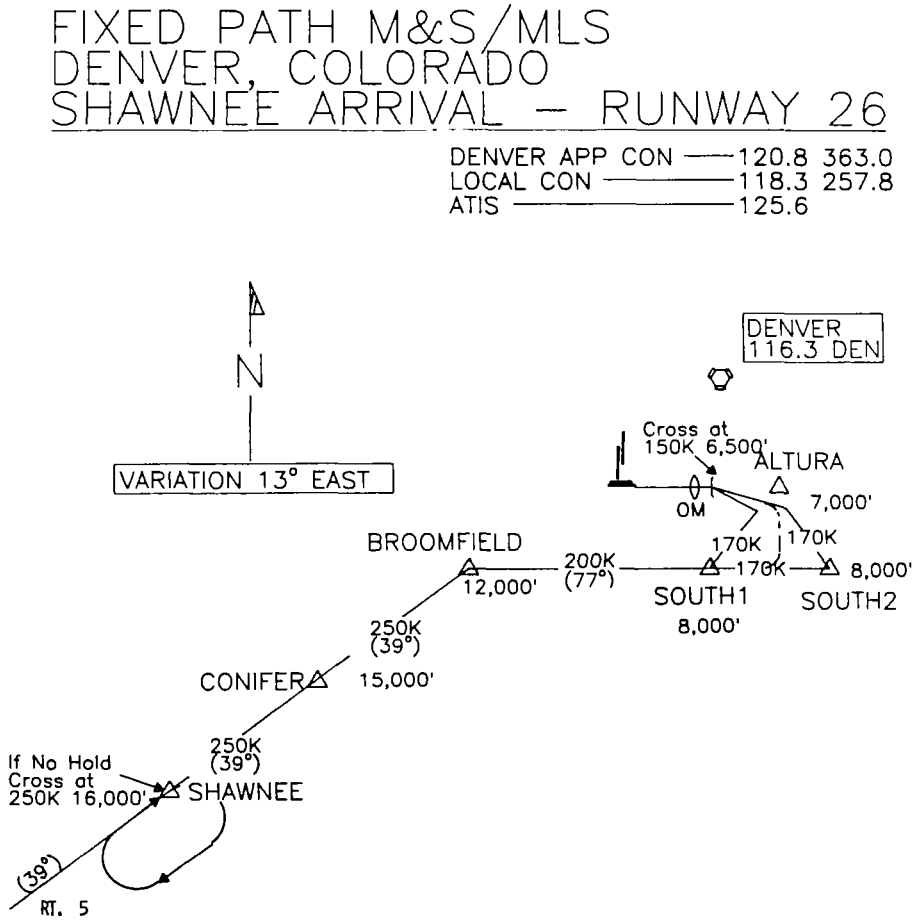

Figure 4.- SHAWNEE STAR navigation plate.

2.4 ELIZABETH Approach

Arrival routes 6 and 7, with 15 percent of the traffic, merge at the IAF (ELIZABETH, fig. 5). Beyond ELIZABETH, the control regions are essentially the same as on the LONGMONT approach.

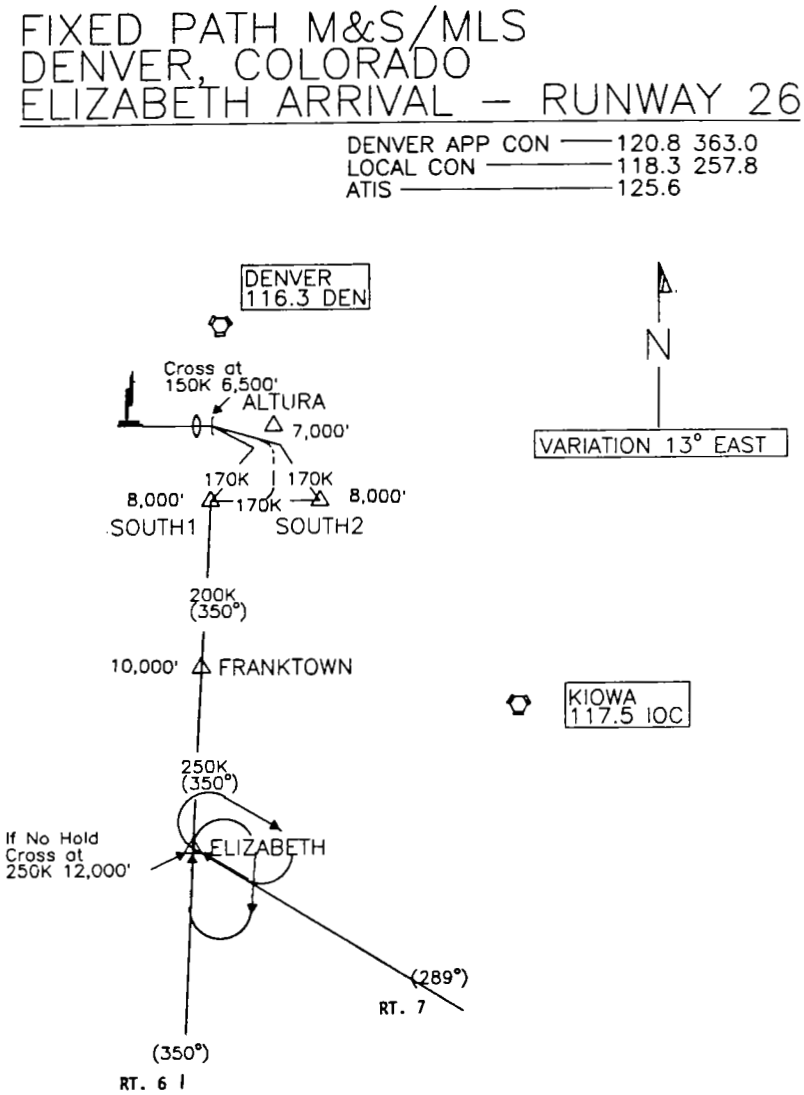

Figure 5.- ELIZABETH STAR navigation plate.

2.5 Controller Sector Allocation

For the real-time M & S studies described in section 7.0, the Denver terminal area is divided into four controller sectors. The North Approach Control is responsible for aircraft on the BYERS and LONGMONT paths between the perimeter and firm-sequencing points. Likewise, South Approach Control

is responsible for the same areas on the SHAWNEE and ELIZABETH approaches. All control for the DICE areas from the firm-sequencing points of each route to the outer marker is allocated to Local Approach Control. Finally, the landing clearance and associated information is issued by Stapleton Tower Control.

3.0 DESCRIPTION OF THE FIXED-PATH METERING AND SPACING (M & S) CONTROL CONCEPT

3.1 Overall View of the Fixed-Path M & S System

The basic functions of the M & S system are to establish a desired aircraft landing sequence, to assign scheduled times of arrival at the outer marker (OM) which provide adequate interarrival spacing between aircraft, and to offer control commands in order to realize these scheduled times of arrival. In order to accomplish these functions the system utilizes three levels of control: Metering, delay spacing, and precise final spacing. The particular control algorithms used in this study are an adaptation of the procedures described in references 1 to 4 for the Denver terminal area. These algorithms are described in greater detail in sections 3.2 and 3.3. Flow charts that accompany the discussion in these sections can be found in appendix D.

As seen in figure 6, the three levels of M & S control are performed on an arriving aircraft depending on its position relative to the runway. In the figure, the perimeter entry line represents the transition position from en route control to terminal control at terminal radar acquisition. The solid line from perimeter entry to the runway represents the desired fixed flight path of the aircraft within the terminal control region. The initial arrival fix (IAF) is denoted by a triangle on the flight path and is the point within the terminal area toward which en route control is responsible for feeding aircraft. The dashed lines in the figure represent the initiation of particular control actions which define the boundaries of the M & S control levels. Beginning at perimeter entry and moving toward the outer marker (OM), the dotted lines represent the holding delay region, a backup delay vector region, and the fine-tuning direct-course-error (DICE) delay area, respectively.

Metering is responsible for controlling the flow rate of aircraft into the terminal area. The metering region is bounded by the 20-min flight-plan-message and the 5-min flight-plan-message M & S control actions. This region falls within the en route control region where controllers are responsible for feeding aircraft to a terminal area IAF with adequate separation. The 20-min flight-plan message is issued by an en route controller to the M & S system when a particular aircraft under the controller's jurisdiction is estimated to arrive at an IAF in 20 minutes. This message identifies the aircraft to the M & S system and triggers the metering control logic. This logic is responsible for calculating needed en route delay when the flow rate toward the IAF or into the terminal area reaches some threshold above capacity. If no delay is requested by the system the en route controller permits the aircraft to proceed. If delay is needed, the M & S system issues to the en route controller a target time to deliver the aircraft at the IAF. The controller is then responsible for the aircraft achieving its target time.

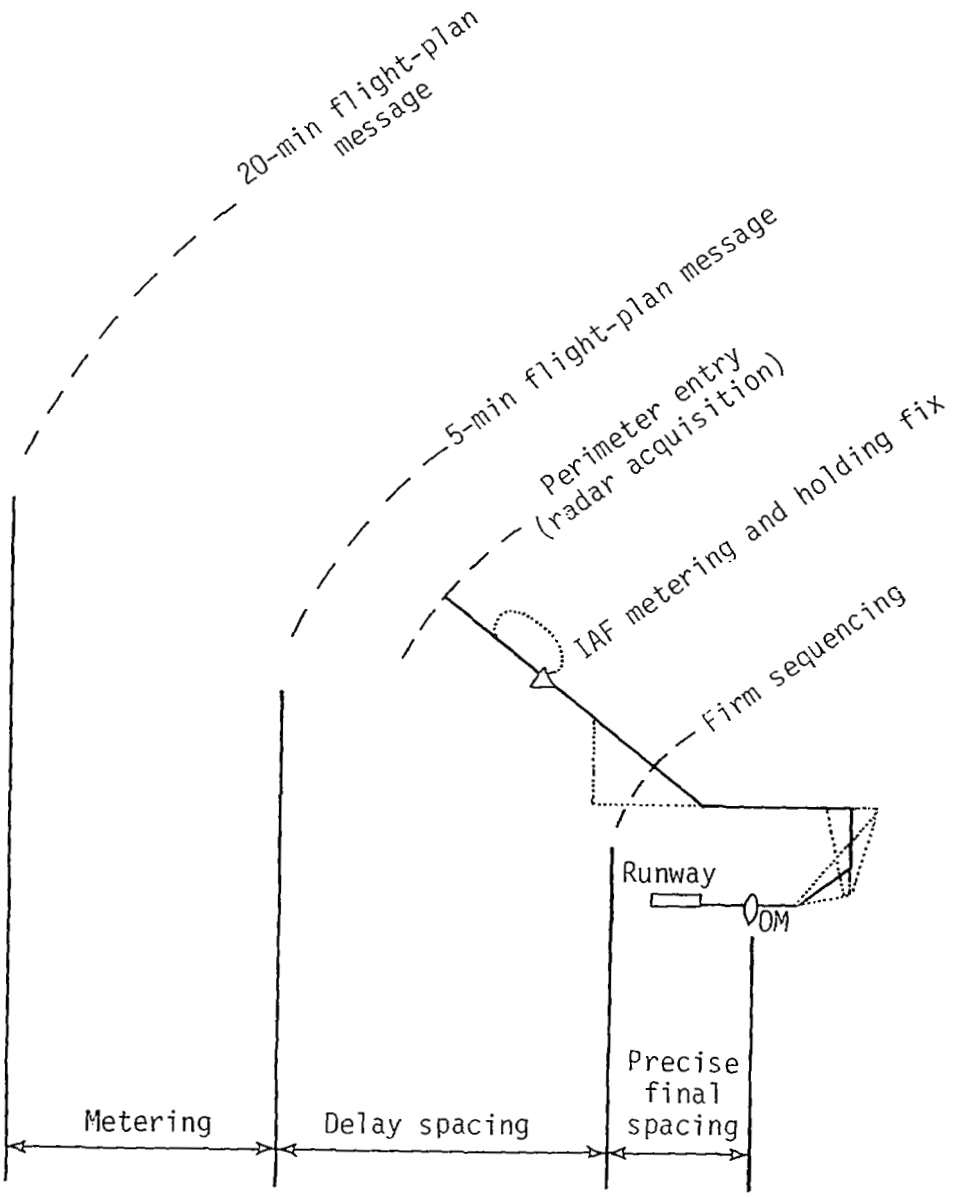

Figure 6.- Metering and spacing control philosophy.

Delay spacing is responsible for dynamically assigning and adjusting the landing sequence and scheduled outer-marker arrival times (SMT) and for issuing control commands in an attempt to match an aircraft's actual arrival time at the outer marker (OM) with its planned SMT. The delay-spacing region is bounded by the 5-min flight-plan message and the firm-sequencing M & S control actions. This region covers a portion of both the en route and terminal control regions. The 5-min flight-plan message from the en route controller to the M & S system represents an update of the estimated time of arrival (ETA) at the IAF for an aircraft. This update occurs after any required metering delay has been accomplished.

Upon receiving a 5-min message for a particular aircraft, the M & S system assigns to the aircraft an initial scheduled outer-marker arrival time (SMT), which allows for adequate separation from previously scheduled traffic and which is based on a projected first-arrival-at-the-runway criteria. As the aircraft proceeds along its flight path, its ETA at the OM is periodically updated. Based on updated ETA's, the SMT's of all aircraft within the delay spacing region are dynamically adjusted in order to account for errors and maintain separation. This dynamic adjustment consists of scheduling modification and resequencing.

At predefined points on the flight path within the delay-spacing region, attempts are made to match an aircraft's arrival time to its planned SMT by generating optional speed control, holding delay, and backup vector commands. Prior to the IAF, if a longer terminal delay is anticipated than can be accommodated by speed control alone, then a holding delay is used at the IAF. Between the IAF and the firm-sequencing point, delay is accomplished through speed control with vectoring as a backup if longer delay is required. Speed control is accomplished by indicated-airspeed commands within a performance range for a particular aircraft type and are calculated for the estimated wind and the known remaining distance along the approach path.

Nearer the runway, precise final spacing is used to correct for errors in aircraft performance during delay-spacing maneuvers in trying to meet SMT's. The firm-sequencing control action establishes a landing sequence which cannot be modified for aircraft within the precise final-spacing region. The SMT's within this region can only be modified by schedule slippage, which adjusts the spacing between aircraft by increasing their separation or closing unnecessary gaps. There are also normally two dynamic path-adjustment commands given in this region in order for an aircraft to achieve its SMT. These adjustments are accomplished using a direct-course-error (DICE) technique which determines the error at the OM which will occur if an aircraft immediately initiates a turn to a predetermined point on the path.

3.2 En Route Functions

3.2.1 General description.- En route control is responsible for feeding aircraft to the IAF's within the terminal area. The M & S system affects this control, however, by monitoring the flow rate of aircraft into the terminal area and limiting this flow, when necessary, by giving to the en route controllers target times for the aircraft to arrive at the IAF's. The en route controller

is responsible for maintaining separation between aircraft headed toward the same IAF, identifying aircraft to the M & S system, and determining the delay maneuvers required to achieve any target times requested by the M & S system.

The TAATM simulation of the M & S system includes a statistical modeling of the en route control region from the time an aircraft is identified to the M & S system until terminal area perimeter entry time. For each of the four IAF's modeled for the Denver terminal area, an arrival queue of aircraft is maintained. Each queue is divided into two lists of aircraft, (1) aircraft for which 20-min flight-plan messages are pending and which have not yet been entered into the M & S control environment, and (2) aircraft which have been identified to the M & S system but for which the 5-min flight-plan message has not been delivered. Each list contains aircraft identification information, predicted control-function times at which an en route control action should be performed for each aircraft, and information concerning the control function desired for each aircraft. The control logic within TAATM is responsible for monitoring the queues, executing the desired function for an aircraft at the time specified within its queue, and placing aircraft in the appropriate queue list. Each queue represents a set of aircraft for which a single en route controller maintains responsibility.

The traffic sample presented to the TAATM represents a desired set of aircraft to fly in the terminal area. The information associated with each aircraft in the sample includes its initial conditions (i.e., position, speed, and altitude), its performance type, desired route, and an offer time. For this study, the traffic sample was generated using a statistical model of arrival traffic in the Denver area. When the offer time for a given aircraft is reached, the model places the aircraft in the appropriate queue, dependent on the IAF toward which it will be flying. The control-function time associated with the aircraft in the queue is its offer time. The list within the queue, into which the aircraft is placed, contains aircraft waiting for a 20-min flight-plan-message control action. Aircraft for which a 20-min flight-plan-message control action has been successfully completed are moved within their queue into the list of aircraft waiting for a 5-min flight-plan-message control action. The control-function times associated with aircraft in this list are the predicted 5-min flight-plan-message times calculated for the particular aircraft within the 20-min flight-plan control-action logic. Details of how these times are calculated are found in the following sections.

The control logic which monitors the queues places highest priority on performing control actions for aircraft needing a 5-min flight-plan message. The assumption is made that the en route controller, responsible for all of the aircraft headed toward a particular IAF, would place highest priority on identifying to the M & S system those aircraft closest to the IAF. When the control-function time for a particular aircraft is equal to or less than the model's current clock time, the aircraft is flagged for the needed control action. If more than one aircraft within a queue needs a control action performed on a particular simulated 4-sec radar scan, only the aircraft with the highest priority and also the earliest desired control-function time receives the control during that scan. Necessary control for other aircraft must therefore be delayed for at least one scan depending on the number of aircraft needing a control action performed during the given scan.

3.2.2 Twenty-minute flight-plan message.- The 20-min flight-plan message is defined as the message which identifies an aircraft to the M & S system when the aircraft is predicted to arrive at its IAF in 20 min. This message is delivered by an en route controller to the M & S system with the assumption that the controller has provided for adequate separation between this aircraft and the aircraft ahead flying to the same IAF. Since the offer times within the traffic sample are statistically generated and do not automatically insure this separation, the determination of the 20-min flight-plan-message time for a given aircraft requires simulated en route control logic to provide this separation.

The aircraft having the earliest 20-min control-function time is considered by the control logic for a 20-min flight-plan message if there is no other aircraft in the same queue being considered for or receiving a 5-min flight-plan message. For an aircraft being considered for the 20-min message, the en route control logic determines if adequate separation at the particular IAF would exist between this aircraft and the previous aircraft accepted on the same route. If the aircraft cannot proceed and arrive at the fix conflict free, then the associated control-function time is rejected as a 20-min flight-plan-message time. Under this condition, the aircraft is left in its queue within the list of aircraft waiting for 20-min messages. The control-function times of all aircraft within this particular list, however, are then incremented by 4 sec (equivalent to one scan) and no further control is performed during this scan on any of the aircraft in this queue. If adequate separation exists between the aircraft pair, the control-function time associated with the aircraft is accepted as the 20-min flight-plan-message time T_{20}. The M & S system then proceeds to determine the impact of the terminal traffic flow on this aircraft.

The M & S system is responsible for calculating an estimated time of arrival (ETA) at the outer marker (OM) and for determining a metering scheduled marker time (MSMT). For the purpose of metering the arrival of aircraft into the terminal area, the MSMT assigned to an aircraft is computed based on the MSMT assigned to the last aircraft accepted into the M & S system plus separation time. This MSMT is used only to obtain a gross initial estimate of the flow of traffic and is not used by the system except during the 20-min flight-plan control action. No provision is made for a metering schedule or sequence update of the previous aircraft as it proceeds into the terminal area.

The following equation is used to calculate the MSMT for the nth aircraft accepted into the system:

$$MSMT_n = \max(MSMT_{n-1} + t_{sep} + t_{comp} + 15,\ ETA_n)$$

The value t_{sep} is the required time separation at the OM between aircraft n and $n-1$ and is dependent on the performance and weight classes of the two aircraft. The value t_{comp} provides additional separation at the OM, if necessary, in order to compensate for the loss of separation due to speed differences along the common path on final approach. The 15-sec buffer is added to the required separation to compensate for the delivery errors of the system at the OM. For a normal error distribution and a separation violation rate of 5 percent, the value used would be 1.65 times the actual delivery interarrival-error standard

deviation. However, the interarrival error is the very quantity which this study is measuring. Since the measure is not throughput rate, assuming some approximate value for the experiment yields a reasonable flow performance. The discussion in a later section on fast-time performance criteria indicates that interarrival-error standard deviation is independent of the time interval between scheduled arrival times. Since the buffer value only affects the scheduled separation times, the interarrival-error standard deviation is independent of the buffer value assumed. The 15 sec used implies an assumed interarrival-error standard deviation of 9.1 sec, which the data show is reasonable.

Metering the flow of aircraft into the terminal area is accomplished by calculating the required time delay $t_{R\Delta}$ in order for an aircraft to attain its MSMT and assigning an en route delay $t_{E\Delta}$ equal to $t_{R\Delta}$ if $t_{R\Delta}$ exceeds an input threshold E_Δ:

$$t_{E\Delta} = t_{R\Delta} \qquad (t_{R\Delta} > E_\Delta)$$

or

$$t_{E\Delta} = 0 \qquad (t_{R\Delta} \leq E_\Delta)$$

where

$$t_{R\Delta} = MSMT_n - ETA_n$$

If the value $t_{E\Delta}$ is greater than zero, the M & S system is responsible for requesting the appropriate en route controller to delay the aircraft by that amount. The M & S system does not, however, suggest a maneuver to achieve this delay.

Completion of the 20-min flight-plan control action includes moving the aircraft within its queue to the list of aircraft waiting for the 5-min flight-plan message. The new control-function time associated with the aircraft is the time to deliver the 5-min message. The equation for computing this time is described in the next section.

3.2.3 Five-minute flight-plan message.- The 5-min flight-plan message is defined as the message which identifies an aircraft to the M & S system when the aircraft is predicted to arrive at its IAF in 5 min. The time T_5 to deliver this message is computed within the 20-min flight-plan logic and is stored as the control-function time in the appropriate queue. This time reflects any assigned en route delay, any errors which account for delivery accuracy between T_{20} and T_5, and any necessary additional time to insure separation between aircraft pairs at the fix. The following equations are used to calculate T_5:

$$T_5 = T \qquad (T > T_{5_{sep}})$$

or

$$T_5 = T_{5_{sep}} + t_{sep_\Delta} \qquad (T \leq T_{5_{sep}})$$

where

$$T = T_{20} + 900 + t_{20_\Delta} + t_{E\Delta}$$

where t_{20_Δ} is a delivery error between T_{20} and T_5, $T_{5_{sep}}$ is the predicted time at the IAF for the preceding aircraft on the same route plus separation time at the fix, t_{sep_Δ} is a separation error at the fix, and 900 indicates a time value (15 min). The units in all of the preceding equations are seconds. The values of t_{20_Δ} and t_{sep_Δ} are random numbers based on a normal distribution. The mean and standard deviation for t_{20_Δ} are, respectively, 0 and 30 sec. The mean and standard deviation for t_{sep_Δ} are, respectively, 0 and 2.5 sec.

Simulation of the en route control region between the initial 20-min flight-plan message and the calculated 5-min flight-plan message time is restricted to maintaining the aircraft in its particular en route queue. The T_5 control-function times are maintained in en route queues depending on the IAF's toward which the aircraft are flying, and are ordered on increasing time within the appropriate list in the particular queue. No flight dynamics are simulated for an aircraft in the system until the terminal area perimeter entry time for the aircraft has been reached. This time is calculated during the 5-min flight-plan message control action associated with T_5.

When the time for an aircraft to receive a 5-min flight-plan message has been reached, the model logic first determines whether or not there is room in the holding stack for the aircraft if it was to proceed to its IAF. If the stack is full, the aircraft is left in its en route queue list and all queue times within the list are incremented by 4 sec, the equivalent of a radar sweep (scan) time. This logic simulates the responsibility of an en route controller for maintaining a reasonable flow of aircraft to the IAF. If there is an available altitude in the holding stack at the fix, the control-function time associated with the aircraft in its queue is accepted as T_5 and the control logic for a 5-min flight-plan message is executed.

The 5-min flight-plan logic in the M & S simulation is responsible for updating the sequence of aircraft presently in the system and performing an initial scheduling of the new aircraft being accepted into the terminal area by the M & S system. The sequencing and scheduling algorithms used are the same as those described in section 3.3.2 for the terminal model. The only

delay option made available to the control logic at this time, however, is a hold at the initial fix.

Transition of an aircraft from its en route queue to an active aircraft in the terminal area is accomplished by calculating a perimeter-entry time T_p, which corresponds to a radar-acquisition time for the terminal area. At time T_p, the aircraft is located at its initial terminal-entry point provided by the traffic sample, and flight dynamics are initiated which update the position of the aircraft at 4-sec intervals, simulating the radar scan time. The elapsed time required to fly from the perimeter to the fix Δt_{pf} is calculated based on flight-path data input to the model. Time T_p is then calculated by using the equation

$$T_p = T_5 + \frac{(300 - \Delta t_{pf})}{300}(300 + t_{5_\Delta})$$

where t_{5_Δ} is a delivery error between T_5 and the fix and 300 is a time value equal to 5 min. The value t_{5_Δ} is a normally distributed random number with a mean of 0 and a standard deviation of 15 sec. The elapsed time to fly between the perimeter and the fix is calculated by the ETA computation routine in TAATM described in reference 7.

3.3 Terminal Functions

3.3.1 General description.- The TAATM provides a realistic terminal area environment in which to test the M & S concept. In order to incorporate the M & S concept, modifications were made to the TAATM control logic and real-time simulated radar display. The RNAV and MLS navigational models were also added. The logic, which was retained basically intact from the original version of TAATM, includes the following: The flight dynamics of the aircraft whose positions are updated every 4 sec, the logic for assigning flight-path descriptions to an aircraft, the holding-stack maintenance logic, the communication logic, the logic for determining when a control action should be performed for an aircraft, and the wind-model algorithms. Detailed descriptions of these logic components can be found in references 7 and 8.

The M & S concept incorporated in TAATM is a modification of the system in reference 4. Where possible, the logic described in reference 4 was adapted directly. Initial test runs, however, indicated that these procedures required modifications to handle problems generated by realistic traffic samples, holding procedures, flight dynamics, and errors which the TAATM model provides. The control philosophy implemented in TAATM follows the basic plan in reference 4 of examining aircraft at discrete points within the terminal area in order to perform dynamic sequence and schedule updates and in order to determine whether a delay maneuver should be executed by an aircraft. Expansion of the sequencing concept, however, was necessary in order to avoid giving some aircraft unrealistic priority over holding aircraft. This modification will be described in detail later. The determination was also made that precalculated estimated times

of arrival, prestored delay times associated with given delay maneuvers, and fixed time separations at the OM cannot adequately handle arbitrary wind conditions and variability of arrival times because of the performance differences of the classes of commercial aircraft considered in our model.

The M & S system establishes at fixed points, or at fixed times relative to fixed points, procedures which must be executed for a given aircraft as it proceeds to the runway. The basic philosophy assumes a single fixed point at the OM where the M & S system must maintain separation between aircraft. All control procedures prior to the OM must assist in maintaining this separation. The control procedures specified include updates of the landing sequence and scheduled outer-marker arrival times (SMT's) as well as dynamic adjustment of the speed and, if absolutely necessary, the path of the aircraft. Figure 7 represents the LONGMONT approach to runway 26 at Denver and shows the types and relative positions of the control points which were implemented for this route. The perimeter-entry line represents the position at which the aircraft first appears to the tracking model following a "hand-off" from en route to terminal control at time T_p. The position of the aircraft is then updated every 4 sec (simulating a radar scan rate) as it moves along this path. Control actions are triggered as it proceeds to the runway. The terminal control elements in figure 7 are discussed in the following sections.

3.3.2 Sequencing and scheduling.- The sequencing and scheduling algorithms of the M & S system incorporated in TAATM allow for the dynamic adjustment of the landing order and landing times of the aircraft in the terminal area as they proceed toward the OM. These adjustments are necessary when navigation, performance, surveillance, and wind errors cause the original assigned SMT's to fall outside the capabilities of an aircraft on a given route. The schedule and sequence adjustment algorithms include the nominal schedule and sequence update algorithm, a resequencing algorithm, and a schedule slippage algorithm. An update of the landing sequence and SMT assignments occurs for all aircraft in the system which have not been firmly sequenced when any one of these aircraft passes a control action point that requires rescheduling. These control action points include the 5-min flight-plan message, radar acquisition (perimeter entry), exit determination for a hold, and firm sequencing. (See fig. 7, elements 2, 3, 5, and 7, respectively.) Resequencing of aircraft occurs when the normal sequence cannot be maintained because adequate separation does not exist between a pair of aircraft. Resequencing alters the normal sequence and permits an aircraft which has reached the limits of its delay capability to receive a higher landing priority. The system does not permit a change in the landing order of aircraft which have been firmly sequenced, but does permit these aircraft to initiate a fine tuning of their SMT's in the form of forward or backward slippage.

3.3.2.1 Scheduled outer-marker arrival time (SMT) computation: For each aircraft in the system from the 5-min flight-plan-message acquisition point to the runway, a set of parameters is stored in an array which describes the relationship of that aircraft to the rest of the aircraft in the system, its delay capabilities in terms of bounds on possible times of arrival, and any delay

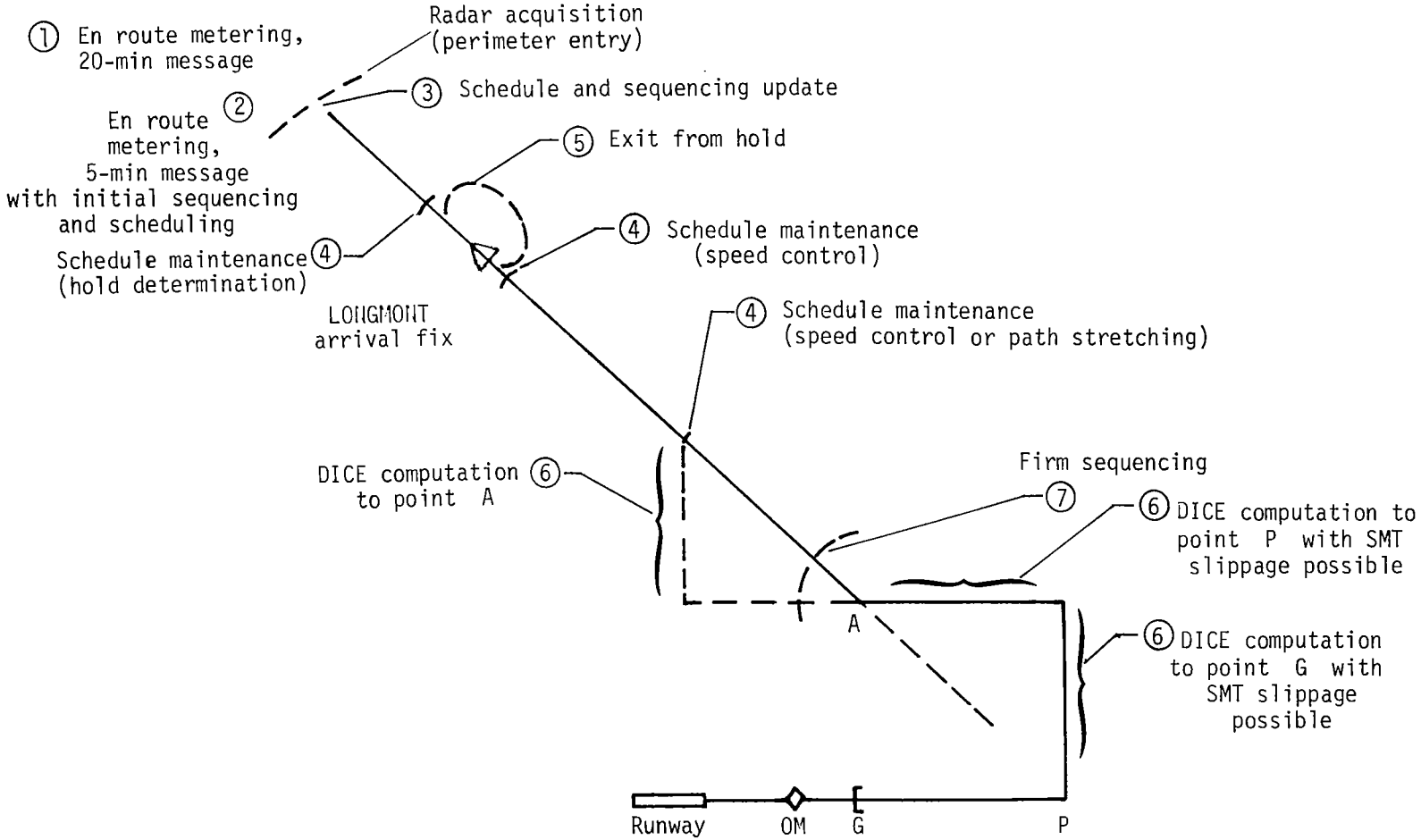

Figure 7.- Control actions performed on LONGMONT approach.

which has already been assigned to the aircraft. The array is ordered on assigned SMT's and at all times represents the latest update of the desired landing sequence and SMT assignments. The parameters stored in this SMT array which are used for SMT computation include the following:

ETA_{min_n} earliest estimated time of arrival at the OM of aircraft n, considering any delays assigned to the aircraft

ETA_{max_n} latest estimated time of arrival at the OM of aircraft n, considering the maximum delay capability which the system desires to use as an SMT bound

SMT_n assigned SMT for aircraft n

$Delay_n$ required delay needed to realize the assigned SMT ($Delay_n = SMT_n - ETA_n$, where ETA_n is the earliest estimated time of arrival at the OM excluding any hold delays assigned to the aircraft; if holds are assigned to aircraft n, ETA_n remains static until the aircraft is cleared out of the holding pattern)

Initialization of an aircraft into the SMT array is accomplished during the 5-min flight-plan-message control action. The aircraft is simply placed at the end of the landing sequence and assigned an SMT which provides for adequate separation with the aircraft ahead in the sequence. (The separation criteria are discussed later in the section.) The SMT computation logic then redetermines the overall desired landing sequence and set of SMT's based on the delay capabilities of the aircraft within the array, including the newly entered aircraft.

The procedure for determining the desired landing sequence is a modification of the logic described in reference 4. For the purpose of sequencing the aircraft, the terminal area is divided into three distinct regions instead of the two regions described in this reference. These three regions consist of the following: (1) All aircraft which have been accepted into the system from the 5-min flight-plan message to the holding fix, including all aircraft which have not yet received clearance past the fix; (2) aircraft which have received clearance past the fix but have not been firmly sequenced; and (3) all firmly sequenced aircraft. In reference 4, regions 1 and 2 are combined.

On entry into the sequencing logic all aircraft are sorted into the three regions. Those aircraft which have not been cleared past the fix (region 1) are assigned a sequence ordered on the last ETA_n which excludes assigned holding delays. This establishes a first-come-first-serve sequencing order. For region 2 aircraft, the previously assigned sequence is maintained unless the control action being performed is the firm sequencing of an aircraft. If firm sequencing is anticipated for an aircraft, ETA_{min_n} is used to reorder up to three aircraft in region 2 behind that aircraft and all aircraft in front of it which have not been firmly sequenced. The order of those aircraft already firmly sequenced remains unchanged.

The establishment of a desired landing sequence within regions 1 and 2 prior to determining the overall landing sequence provides some stability between successive attempts to determine this sequence. If the separate ordering within regions 1 and 2 is not first performed, two problems are generated: (1) The holding stacks create a discontinuity when attempting to order the aircraft on a projected first-come-first-serve (FCFS) principle. Aircraft on routes where no holding is being performed are then capable of receiving excessive priority over aircraft on other routes where holding is taking place, and this can create excessive holds for the holding aircraft. (2) The aircraft not yet to the fix are ordered on an FCFS principle based on ETA_{min_n} which includes hold assignments. Under this condition, it is possible for aircraft headed for the same stack to have their landing sequence swapped back and forth, depending on when hold times are updated and the delay times assigned.

The development of a desired overall landing sequence is accomplished by merging the aircraft from the ordered lists of aircraft from regions 1 and 2. While maintaining the order of these two lists, the ETA_{min_n} value for each aircraft is used to merge the two lists on an FCFS principle. This enables the system to maintain a landing-sequence continuity within the regions while providing a means to handle the merging of aircraft on a short route with those on a long route and the merging of faster aircraft with slower aircraft which are making a transition from region 1 to 2.

Once the desired landing sequence has been developed, new SMT's are computed for all aircraft after the last firmly sequenced aircraft such that for an aircraft in order position n,

$$SMT_n \geqq SMT_{n-1} + Sep_{n/n-1}$$

where

$$ETA_{max_n} \geqq SMT_n \geqq ETA_{min_n}$$

and $Sep_{n/n-1}$ is the time separation required between aircraft n-1 and n. The value $Sep_{n/n-1}$ is computed by

$$Sep_{n/n-1} = t_{sep} + t_{comp} + 15$$

where t_{sep} is the minimum required time separation at the OM between aircraft n and n-1, t_{comp} is a separation at the OM to compensate for speed differences along the common path on final approach, and the additional 15-sec buffer is a separation to compensate for delivery errors of the system at the OM. These separation factors are identical to those used in en route metering as described in section 3.2.2. If an SMT cannot be assigned so that it does not violate the preceding criteria, then the desired landing order must be

modified in an attempt to develop a sequence and schedule which can be realized by all aircraft in the terminal area. This modification is referred to as resequencing.

3.3.2.2 Resequencing: Due to the limitations on the delay capability of some aircraft and dependent on the traffic interactions, the desired sequence of aircraft may not be realizable. If SMT's cannot be assigned under the criteria in section 3.3.2.1 for regions 1 and 2, resequencing is attempted. As SMT's are being assigned beginning with the aircraft behind the last firmly sequenced aircraft, the first aircraft encountered which cannot be assigned an SMT within its ETA bounds is swapped in sequence with the aircraft ahead of it. In other words, if aircraft n cannot fit behind aircraft $n-1$, then the SMT for aircraft $n-1$ is ignored and an attempt is made to fit aircraft n behind aircraft $n-2$. If this second attempt is unsuccessful, then aircraft n continues to move ahead in sequence until it can be successfully assigned an SMT. Once a successful assignment is made, then the last aircraft which was passed in sequence by aircraft n becomes the next aircraft for which an SMT assignment is attempted. Priority is thus given to aircraft with limited delay capability.

Under certain ETA boundary constraints, a resequencing attempt may still result in a failure to assign realizable SMT's to all aircraft under consideration. A failure mode is assumed during the resequencing process if more than six unsuccessful swaps are attempted or if no SMT can be successfully assigned to a given aircraft. Under either of these conditions, the updating of schedules is discontinued and the previously assigned SMT's are retained. Because at least one of these SMT's is unrealizable, the potential for a separation violation can then exist. Following each control action, however, a check is made to determine the magnitude in time of any potential interarrival separation violation. This time error is displayed on the simulated radar display and the assumption is made that the problem will be resolved either by human intervention or by a later control action.

3.3.2.3 Schedule slippage: For those aircraft which have been firmly sequenced, schedule slippage is initiated in order to fine tune the SMT's to account for minor errors as the aircraft are making their last turns to final approach and to close unnecessary gaps between aircraft. Schedule slippage is initiated prior to each direct-course-error (DICE) calculation performed for an aircraft. During schedule slippage no change in the landing sequence occurs and only those aircraft behind the aircraft initiating slippage are also considered for slippage.

Initially a desired SMT (DSMT) is calculated for the aircraft in sequence position n:

$$DSMT_n = \max(SMT_{n-1} + Sep_{n/n-1}, ETA_{min_n})$$

where SMT_{n-1} is the SMT assigned to the aircraft ahead, $Sep_{n/n-1}$ is the time separation required between aircraft n and $n-1$, and ETA_{min_n} is the earliest time of arrival for aircraft n. If

$$DSMT_n = SMT_n$$

where SMT_n is the previously assigned SMT for aircraft n, then no slippage occurs. If

$$DSMT_n > SMT_n$$

then backward slippage is required. Given that ETA_{max_n} is the latest possible arrival time stored for aircraft n, if

$$DSMT_n \leqq ETA_{max_n}$$

then the SMT can be and is slipped back to $DSMT_n$. If

$$DSMT_n > ETA_{max_n}$$

then the SMT is slipped back to $DSMT_n$, even though it is not attainable.

Beginning with the first aircraft under consideration for schedule slippage, each aircraft in turn behind this aircraft is tested to see if backward slippage is required. Backward slippage ceases when, for aircraft n, the $DSMT_n$ is less than or equal to the previously assigned SMT_n. If

$$DSMT_n < SMT_n$$

then forward slippage is possible. If

$$DSMT_n > ETA_{max_n}$$

then the aircraft cannot attain the $DSMT_n$, but the SMT is still slipped forward to $DSMT_n$. If

$$DSMT_n \leqq ETA_{max_n}$$

then a new SMT (SMT_{new}) is assigned to aircraft n:

$$SMT_{new} = \min(DSMT_n + Slack, ETA_{max_n}, SMT_n)$$

The min function is used to prevent backward slippage if adding slack time to $DSMT_n$ results in a greater time than either ETA_{max_n} or SMT_n. The term

Slack is a buffer (normally 10 sec) used during the direct-course-error (DICE) calculations on the backup-delay vector paths and on the downwind leg to prevent slipping an aircraft schedule forward and then having to slip it backward. This slack is removed during the final DICE turn on base. Each firmly sequenced aircraft behind the aircraft under consideration is tested in turn to see if forward slippage is possible for the aircraft. If an aircraft is encountered which is not in a DICE region or for which forward slippage is impossible, the testing of aircraft for forward slippage ceases. If forward slippage is possible for an aircraft behind the initially considered aircraft, a DICE calculation is triggered for that aircraft on the next 4-sec radar-scan update.

3.3.3 Schedule maintenance.- Realization of a desired sequence and scheduled OM time is accomplished by determining necessary modifications to the flight profiles of the aircraft. Two types of schedule-maintenance logic are available within TAATM. Coarse schedule maintenance is performed by assigning speed changes, holding patterns, or backup-delay paths to the aircraft to achieve a desired SMT. Fine-tuning schedule maintenance is performed with calculated DICE maneuvers.

The need for coarse schedule maintenance is determined at prespecified geometric points along the flight path or at calculated times during the flight for a particular aircraft. Control actions are performed which calculate estimated times of arrival at the OM and compare them to the aircraft's scheduled time of arrival. In addition, future delay capability for the aircraft is calculated and 70 percent of this capability is compared with the delay needed by the aircraft in order for it to achieve the scheduled time of arrival. No action is taken to modify the current flight-path segment if the delay needed can be realized at a future control-action point while retaining 30 percent of the future delay capability for subsequent accumulation of errors or schedule slippage. If the delay needed exceeds 70 percent of the future delay capability, however, an action must be taken as soon as possible to modify the flight profile to achieve the necessary delay.

Given that a delay action is necessary, an option is chosen from an array of possible options for coarse schedule maintenance associated with the particular control action. Prior to the initial arrival fixes, no immediate delay option is available, but delay can be achieved by holding the aircraft at the fix. On the paths from the holding fixes to the final sequencing area the highest priority option is a speed change. In this same region delay paths can be specified to achieve additional delay if a speed change alone is not adequate. The specification of options and the logic for determining which option to use, however, favors the utilizaton of speed-change delays over other delay manuevers. If there is no option available which is capable of achieving the needed delay, the aircraft is given the lowest speed profile and is permitted to proceed. If a conflict is produced because the delay problem cannot be resolved, a conflict alert will be generated and displayed on the real-time simulated radar display as described in section 3.4.

The fine-tuning DICE calculation is handled as a separate control action type which is different from the coarse schedule-maintenance actions. Calculations are performed to determine if an aircraft will arrive early or late at the OM if a turn to an RNAV waypoint is initiated immediately. Results of the DICE computation consist of a DICE value and a yes or no decision to initiate the turn. If the DICE value is 2 sec or less, an immediate, direct-engage turn message is developed. This message is delivered by the communications logic to the aircraft during the next TAATM position update. DICE computations are performed in two basic regions. These are the path-stretching regions between the holding fix and the firm-sequencing points and the final-sequencing area between the firm-sequencing points and the gate for routes from the north or south. DICE is calculated in the path-stretching regions to determine when the aircraft should return to its nominal approach route if a delay path has been assigned to the aircraft.

3.3.3.1 Speed option: When an arrival aircraft is entering a path segment with a speed-control option, the speed-control algorithm (SPDOPT) may be called upon by the control logic to determine the desired indicated airspeed for the aircraft to fly that segment. This determination involves calculating the estimated time of arrival at the outer marker and comparing it to the aircraft's scheduled outer-marker arrival time (SMT). If the delay required for the aircraft to achieve its SMT is greater than 70 percent of the future delay capability, then some speed modification will be applied on the current path segment. Otherwise, action is deferred to a future control-action point.

All the velocities relating to the aircraft and path-segment speed specifications are given in indicated airspeeds. However, in calculating times to fly, indicated-airspeed values are converted to equivalent ground speeds for the altitudes and wind speeds encountered by the aircraft. From this point in the speed-option discussion, the references to segment velocities will refer to the ground-speed equivalents. Once a segment ground speed is determined, then it is inversely transformed to desired indicated airspeed for the aircraft.

Consider the events an aircraft goes through upon entering a single segment of length S_1 of an arrival route with initial ground speed V_{i_1}. The arrival route is made up of an arbitrary number of n segments. The aircraft decelerates at a constant rate to some segment velocity V_{S_1} which is within the speed range allowed for that aircraft type on the segment ($V_{H_1} \geqq V_{S_1} \geqq V_{L_1}$). For the balance of the segment in question the aircraft maintains the velocity V_{S_1}. The purpose of the speed-control algorithm, if speed control is to be applied, is to determine the value of V_{S_1} which meets the necessary criteria. Once V_{S_1} is chosen, it then becomes the initial velocity for segment 2. The following sketch illustrates the segment-velocity relationship for a representative route with n segments.

For the sake of discussion the initial assumption will be that there are no speed overlaps in successive segments, that is, $V_{L_1} \geqq V_{H_2}$. The more general

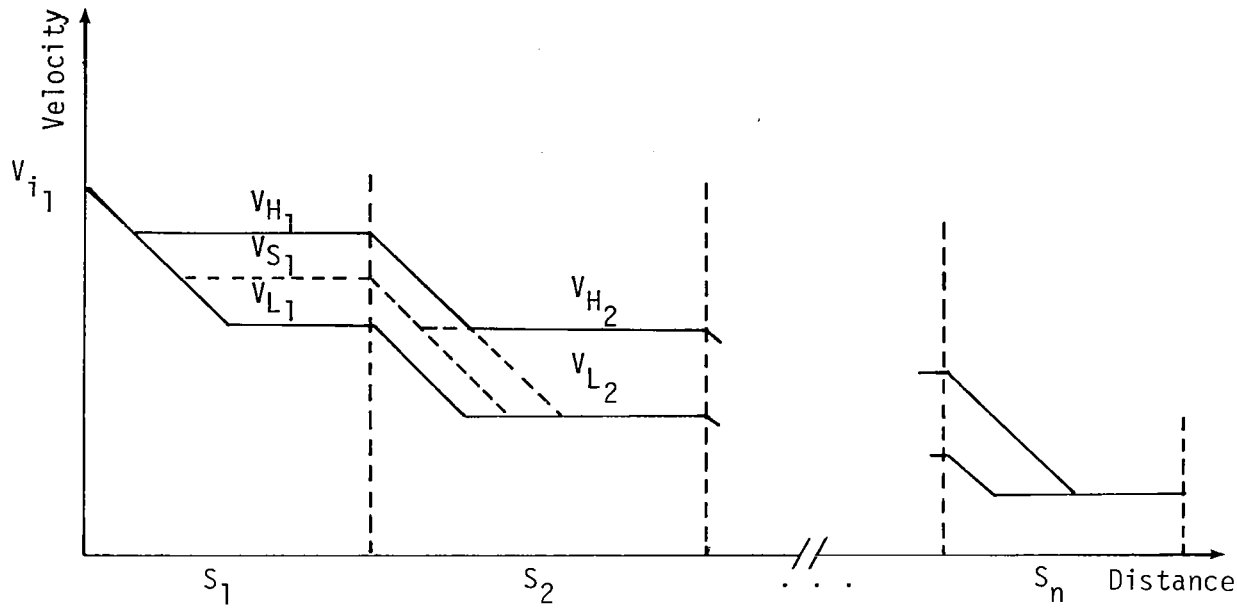

case will be covered later. Given V_{i_1}, three estimated times of arrival at the outer marker are calculated external to SPDOPT for the value V_{S_1}. These times are defined as follows:

ETAR(V_{S_1}) outer-marker arrival time using V_{S_1} on S_1 and the highest velocities on the remaining segments

XLLT(V_{S_1}) outer-marker arrival time using V_{S_1} on S_1 and the lowest velocities on the remaining segments

XMLLT outer-marker arrival time using the lowest velocities on all segments

With the estimated times of arrival defined previously and $V_{S_1} = V_{H_1}$, the following can be determined:

PDELAY present delay capability, XMLLT - ETAR(V_{H_1})

FDELAY future delay capability, XLLT(V_{H_1}) - ETAR(V_{H_1})

XLLT'(V_{H_1}) outer-marker arrival time by assuming no delay on S_1 and by using 70 percent of future delay capability, ETAR(V_{H_1}) + 0.7FDELAY

The following diagram illustrates these quantities on a time-of-day axis. Also shown are the possible relative positions of these quantities to an assigned SMT for the aircraft.

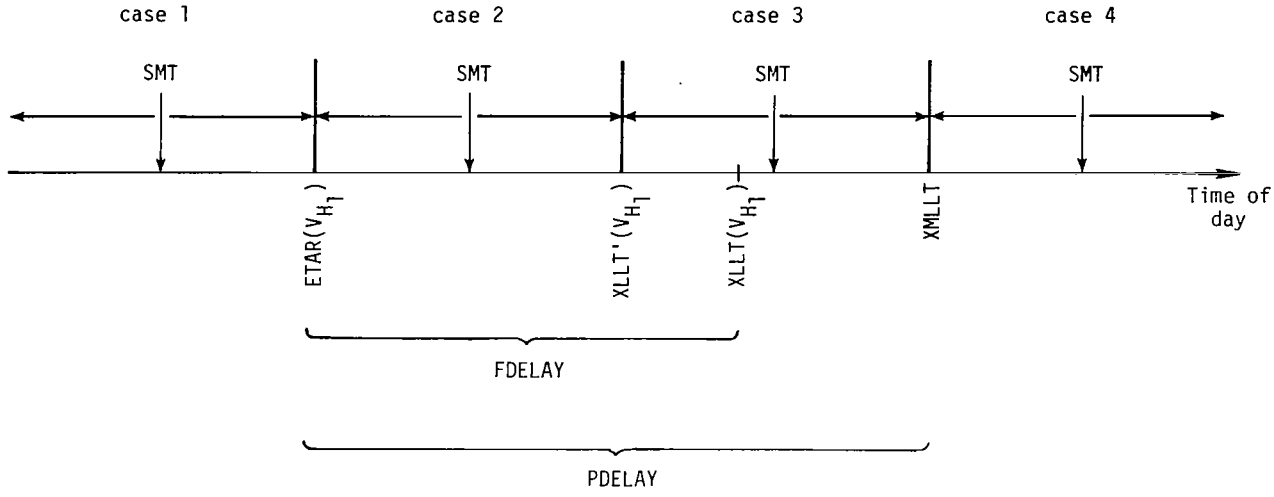

There are four major cases which need to be considered depending on when the SMT occurs. These are as follows:

Case 1: SMT < ETAR(V_{H_1}). The aircraft is too slow to attain the assigned SMT, even though the highest velocities are assumed. Rescheduling is therefore required to resolve the problem. (No speed-option delay is utilized for S_1.)

Case 2: ETAR(V_{H_1}) ≦ SMT ≦ XLLT'(V_{H_1}). In this case the aircraft will be assigned a V_{H_1} to fly S_1 since there is enough delay capability on the following segments to achieve the required delay. (No speed-option delay is utilized for S_1.)

Case 3: XLLT'(V_{H_1}) < SMT ≦ XMLLT. In this case the speed needs to be determined in order to meet the SMT since there is not enough delay capability in the future. (Speed-option delay is necessary.)

Case 4: XMLLT < SMT. The aircraft has insufficient delay capability to make its desired SMT. Under normal flight-error conditions, some action should have occurred before reaching S_1 to prevent this case. This case could occur, however, with the accumulation of severe flight errors. (Other delay options are examined to resolve the problem, e.g., backup-delay vectoring.)

For case 3, the criteria used to determine the segment velocty V_{S_1} used to meet the aircraft's SMT are:

$$SMT = XLLT'(V_{S_1})$$

and

$$SMT = ETAR(V_{S_1}) + k'[FDELAY(V_{S_1})]$$

where

$$FDELAY(V_{S_1}) = XLLT(V_{S_1}) - ETAR(V_{S_1})$$

and

$$k' = k + (1 - k)\left(\frac{V_{H_1} - V_{S_1}}{V_{H_1} - V_{L_1}}\right)$$

for $k = 0.7$. The speed-control algorithm determines V_{S_1} with the assumption that a portion of the delay required will be achieved on future segments. The value k defines the percentage (70 percent here) of the future delay capability which must be used in the future to help achieve the required delay if V_{H_1} is assigned for S_1. The value k' is determined by a function which defines this percentage for the full range of possible speeds over S_1 (i.e., V_{H_1} to V_{L_1}). For V_{H_1} the value of k' is 0.7 and for V_{L_1} the value is 1.0. The inclusion of k' forces the highest reasonable V_{S_1} to be chosen and decreases the future delay capability held in reserve as V_{S_1} approaches V_{L_1}.

In order to determine the value of V_{S_1}, it is necessary to solve the preceding equations with $XLLT(V_{S_1})$ and $ETAR(V_{S_1})$ as explicit functions of V_{S_1}. These relations are contained in appendix B. The value V_{S_1} obtained in this manner with the function k' will reserve some delay capability for schedule slippage. The previous time-of-day diagram only showed the relationship of ETAR, XLLT', and XLLT for the value of $V_{S_1} = V_{H_1}$. A more general representation as a function of V_{S_1} is shown in the following drawing:

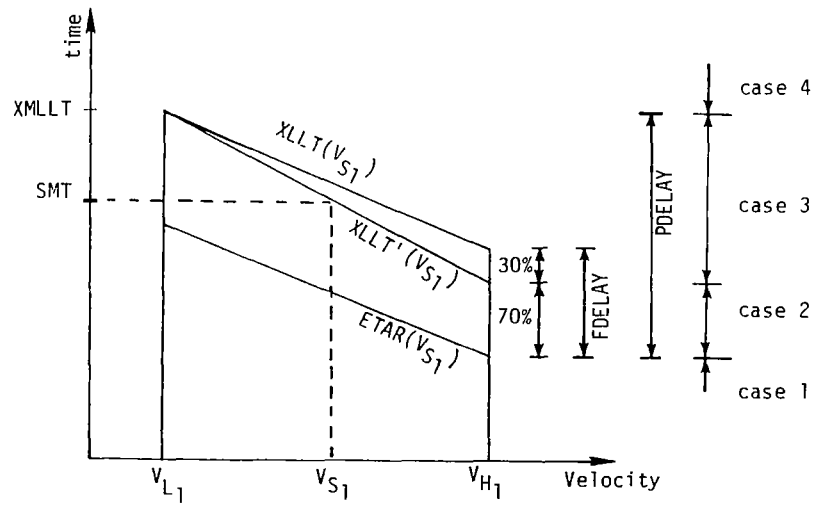

Thus far in the discussion there has been no speed overlap on adjacent segments, that is, $V_{L_1} \geq V_{H_2}$. A more general procedure to handle the overlap situation ($V_{H_1} \geq V_{H_2} \geq V_{L_1} \geq V_{L_2}$) must be considered. It is possible that a V_{S_1} can be determined such that $V_{S_1} \leq V_{H_2}$. The M & S system normally either maintains or reduces velocity for arrival aircraft. Whenever $V_{S_1} \leq V_{H_2}$, the highest velocity permitted on segment 2 must be equal to V_{S_1} ($V_{H_2} = V_{S_1}$).

Bounding V_{H_2} affects $ETAR(V_{S_1})$ since it is defined as the time to fly to the outer marker using V_{S_1} on S_1 and the highest segment velocities on all remaining segments. Since the calculation for $XLLT'(V_{S_1})$ involves using $ETAR(V_{S_1})$, it is also affected. The relationships previously defined are adequate once the explicit function of $XLLT(V_{S_1})$ and $ETAR(V_{S_1})$ in terms of V_{S_1} for the overlap case are used. These relationships are contained in appendix B.

3.3.3.2 Delay path stretching: The M & S system under evaluation in this report is based on a fixed-path speed-control concept with contingency delay path stretching. Prior to the aircraft reaching a holding fix, excessive delays which cannot be realized with speed control alone are handled by holding the aircraft at the fix. For aircraft which have passed the holding fixes, contingency delay path stretching is provided as an option to absorb excessive delay needed beyond the speed-control capability.

Delay path stretching is accomplished by providing an alternate control-action description at specific points on the routes. In this case, the control logic returns to the main control routine and the new action is attempted from the top of the control logic with a new path description and a new set of control options. For the Denver M & S configuration this action is specified as an alternate path which provides a vector off the nominal path. A return to the nominal path is accomplished by DICE calculations after the aircraft has established itself on the vector.

3.3.3.3 Hold: Prior to an initial arrival fix (IAF), the need for excessive delays can be resolved by holding aircraft at the fix. Holding stacks are provided at each of the four IAF's so that up to four aircraft can execute holding patterns simultaneously at each fix. The rules for holding an aircraft consist of the following: (1) Any aircraft which has previously been advised to anticipate a hold will in fact be required to hold, even if the traffic environment changes prior to the aircraft reaching the fix; (2) an automatic hold is assigned to an aircraft if the aircraft ahead (assigned to same IAF) is holding or anticipating a hold; and (3) a hold is assigned if the delay required is in excess of 70 percent of the speed-control delay capability.

Once the determination has been made that an aircraft will hold, a desired holding time is calculated based on the amount of delay needed minus 30 percent of the delay attainable with speed control in the future. This permits some forward slippage once the aircraft has left the hold. This desired holding time is then used to compute an actual assigned holding time. If the desired time is less than a minimum hold time, the minimum hold is assigned.

Hold assignments can be initiated by the 5-min flight-plan message, at the radar-acquisition point, or by the schedule-maintenance control action prior to the holding fix. Once the hold has been assigned, an update of the holding time can occur on subsequent control actions prior to the aircraft reaching the fix. Once the aircraft has initiated a hold, a holding-time update is possible only on the hold-exit-determination control action. This action occurs 50 sec prior to the aircraft's predicted time of departure from the holding fix.

For the purpose of scheduling and sequencing aircraft, a possible holding delay time is included under certain conditions in the calculation of the maximum estimated time of arrival. The inclusion of this delay time is dependent on the route being used by the aircraft and whether or not holds have already been assigned to the aircraft. For the straight-in BYERS route, this possible delay time is included only when the aircraft has already been assigned a hold. On all other routes, this time is included if the aircraft has not yet reached the holding fix, whether or not a hold has been assigned. This distinction is made between the BYERS route and all other routes in order to give BYERS aircraft a sequencing and scheduling priority. The result is that resequencing is attempted for a BYERS aircraft before a hold is considered. The reason for this priority is that the straight-in BYERS route has limited speed-control delay capability and is heavily used (40 percent of arrival traffic). If a BYERS aircraft cannot be resequenced ahead of another aircraft, it may be forced to hold. Once it is assigned a hold, the route priority is removed by the inclusion of the maximum possible holding delay in the maximum ETA calculation of the aircraft. While BYERS aircraft are holding, all routes have equal priority.

3.3.3.4 Direct-course-error (DICE): A DICE computation is performed to determine how late or how early an aircraft will arrive at the OM if a direct-engage turn to a new RNAV waypoint is initiated immediately. This direct-engage procedure uses the capability of a two-dimensional RNAV system (discussed in appendix C) to make a smooth turn from the present position and then fly directly to the next prespecified waypoint rather than continue toward the currently specified waypoint. A DICE control action can be initially triggered after an elapsed time following another control-action type or by a forward-slippage calculation performed on another aircraft. Once the calculation has been initiated the value returned from the DICE algorithm controls when the next computation is performed. The following conditions define how often the algorithm is called:

DICE value, sec	Time before next computation, sec
≥100	28
≥50	8
<50	4

The data used to determine these values was obtained from reference 4 and rounded to the nearest 4-sec radar scan.

The DICE computation can consist of an ETA calculation which assumes either a single immediate turn to a waypoint or an immediate turn towards a waypoint followed by a nominal second turn to the next waypoint. In either case the algorithm is responsible for determining the path to be flown, calculating the estimated time of arrival at the OM, and comparing this estimate with the scheduled time of arrival (SMT) of the aircraft at the outer marker. Initial input variables to the algorithm consist of the following:

V_1 initial true airspeed

X_o north radar coordinate for aircraft

Y_o east radar coordinate for aircraft

h_1 initial track heading of aircraft

T_M time required to deliver direct engage message

T_R roll-in time for turn

All angles and headings used in this discussion are in degrees. In reference to figure 8, the predicted flight path of the aircraft is computed with the following equations:

$$D_i = V_1 (T_M + T_R)$$

$$\theta = \text{mod } (450 - h_1, 360)$$

$$X_1 = X_o + D_i \sin \theta$$

$$Y_1 = Y_o + D_i \cos \theta$$

where D_i is the distance traveled before the turn, θ is the angle measured counterclockwise from east to the heading vector, and (X_1,Y_1) is the initial position of the aircraft before the turn. If the turn direction Q_1 to waypoint (X_p,Y_p) is known, where $Q_1 = 1$ indicates a right-hand turn and $Q_1 = -1$ indicates a left-hand turn, the position (X_2,Y_2) at the end of the turn is calculated as follows:

$$X_2 = X_1 + \Delta X_1$$

$$Y_2 = Y_1 + \Delta Y_1$$

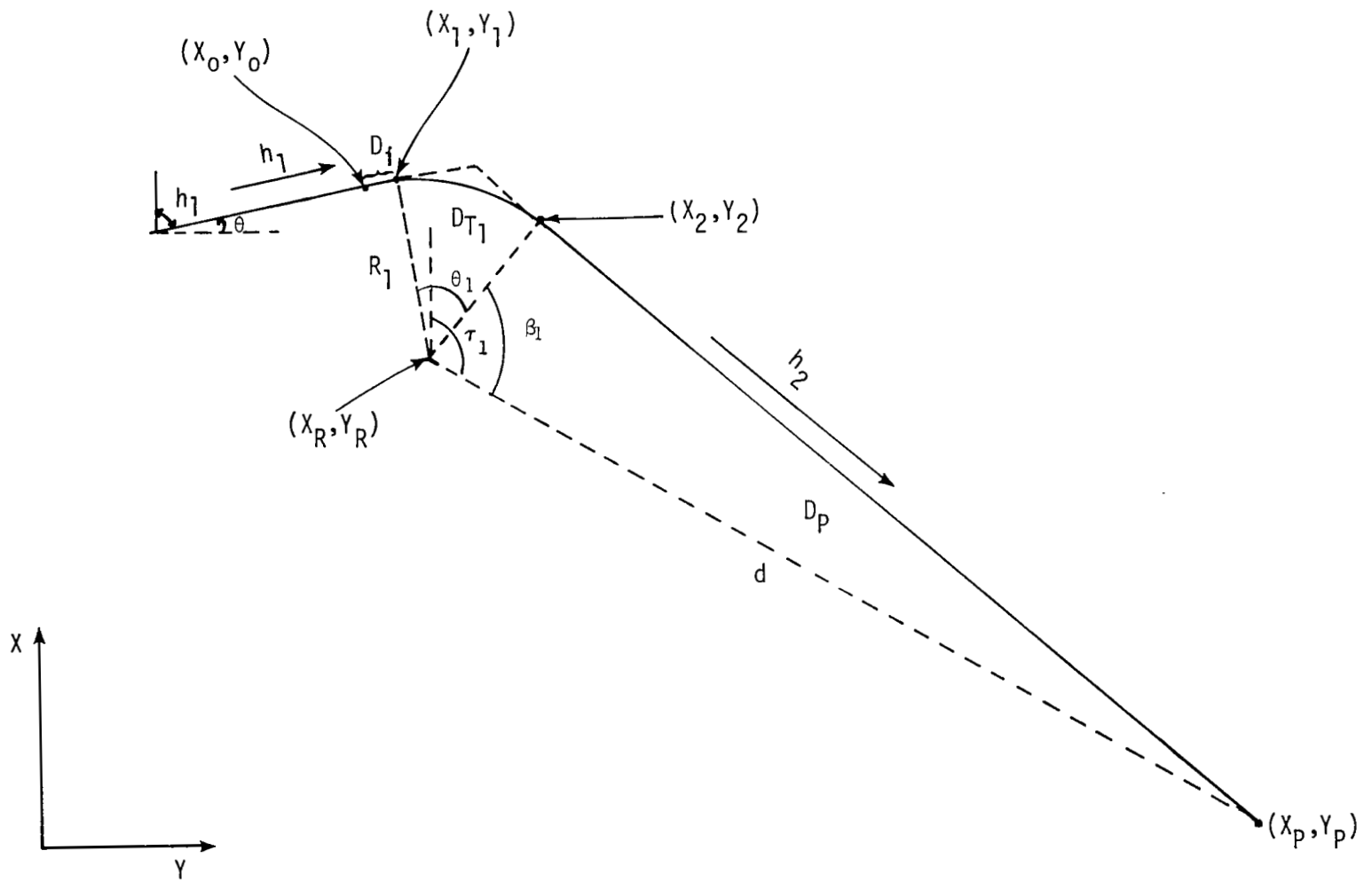

Figure 8.- One-turn DICE geometry.

where

$$\Delta X_1 = R_1 Q_1 (\sin h_2 - \sin h_1)$$

$$\Delta Y_1 = R_1 Q_1 (\cos h_1 - \cos h_2)$$

The following equations relate to figure 8:

$$R_1 = V_1^2/(g \tan \Phi_{NOM})$$

where

g gravity

Φ_{NOM} nominal bank angle assumed for an RNAV direct-engage turn

$$X_R = X_1 - R_1 Q_1 \sin h_1$$

$$Y_R = Y_1 + R_1 Q_1 \cos h_1$$

$$\tau_1 = \tan^{-1}\left(\frac{Y_R - Y_P}{X_R - X_P}\right) + 180$$

$$d = \sqrt{(X_P - X_R)^2 + (Y_P - Y_R)^2}$$

$$\beta_1 = \cos^{-1}\left(\frac{R_1}{d}\right)$$

$$\theta_1 = 90 - Q_1 (h_1 - \tau_1) - \beta_1$$

$$h_2 = h_1 + \theta_1 Q_1$$

If h_2 is negative, then $h_2 = h_2 + 360$. The distance traveled in the turn D_{T_1} is

$$D_{T_1} = R_1 \theta_1 C_R$$

where C_R is a conversion factor from degrees to radians.

If a single DICE turn is specified, the distance D_P to travel from the end of the turn (X_2,Y_2) to the waypoint (X_P,Y_P) is

$$D_P = \sqrt{(X_2 - X_P)^2 + (Y_2 - Y_P)^2}$$

The total distance D_1 to be flown from the aircraft's present position to the waypoint is

$$D_1 = D_i + D_{T_1} + D_P$$

For a two-turn DICE computation, shown in figure 9, the algorithm calculates a point (X_3,Y_3) where the turn to intercept the nominal path to waypoint G begins. This calculation is accomplished by determining the offset to begin a turn from point (X_2,Y_2) with initial heading h_2 and terminating tangent to a line parallel to the nominal path to point G. The nominal-path heading to point G is denoted h_3. By assuming a true airspeed V_2, associated with the second turn, the radius of turn R_2 is

$$R_2 = V_2^2/(g \tan \Phi_{NOM})$$

If the turn direction Q_2 to waypoint G is known, where $Q_2 = 1$ indicates a right-hand turn and $Q_2 = -1$ indicates a left-hand turn, the position (X_b,Y_b) is

$$X_b = X_2 + \Delta X_2$$

and

$$Y_b = Y_2 + \Delta Y_2$$

where

$$\Delta X_2 = R_2 Q_2 (\sin h_3 - \sin h_2)$$

$$\Delta Y_2 = R_2 Q_2 (\cos h_2 - \cos h_3)$$

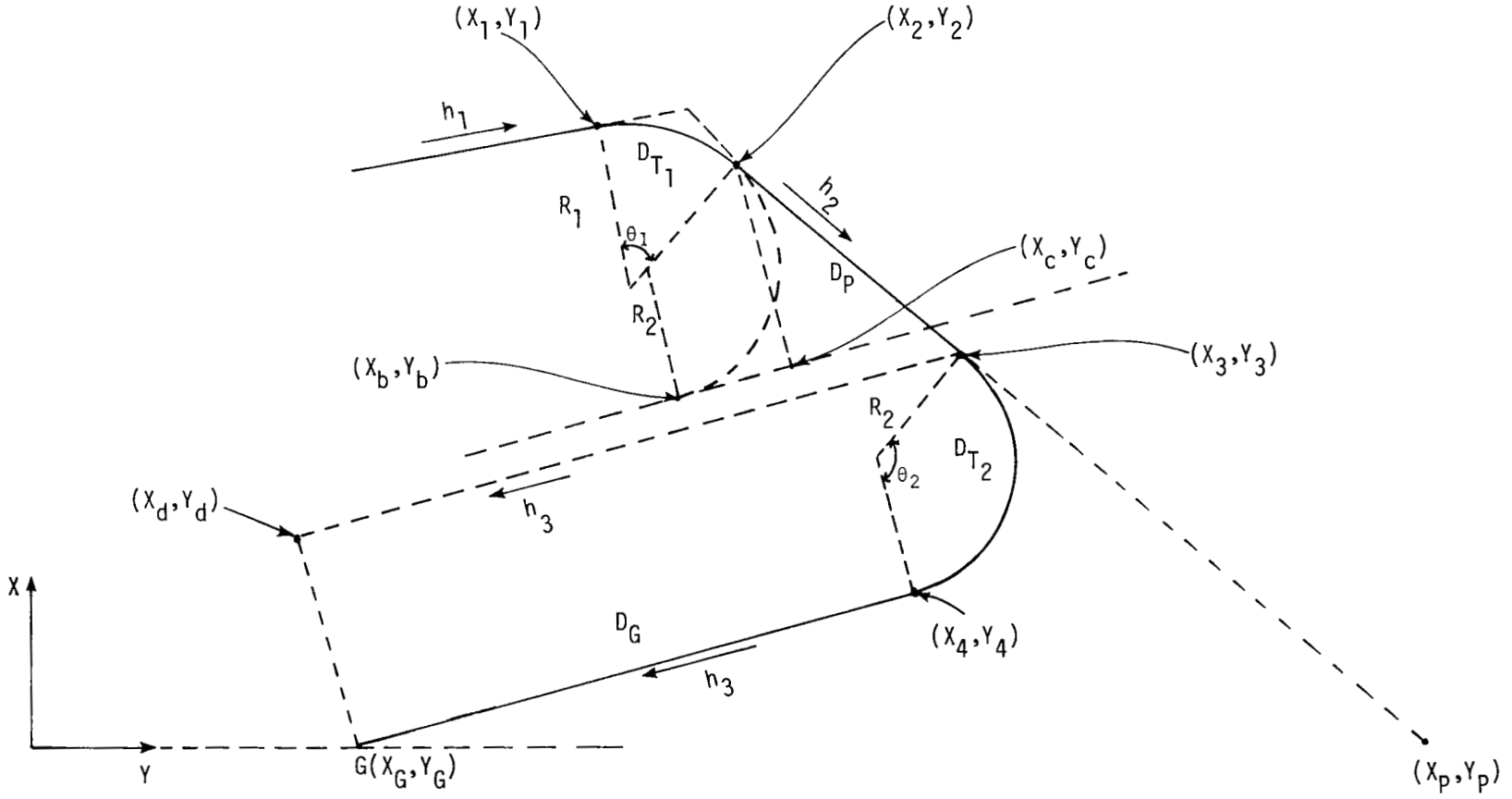

Figure 9.- Two-turn DICE geometry.

Point (X_c,Y_c) is the intersection of the line through (X_b,Y_b) with heading h_3 and the line through (X_2,Y_2) with heading $h_3 + 90$. Point (X_d,Y_d) is

$$X_d = X_G + X_2 - X_c$$

$$Y_d = Y_G + Y_2 - Y_c$$

The offset location (X_d,Y_d) is used to define a line parallel to the nominal path to point G with heading h_3 and intersecting the path to point (X_p,Y_p) with heading h_2. The intersection point is point (X_3,Y_3).

The distance traveled in the turn D_{T_2} is

$$D_{T_2} = R_2\theta_2C_R$$

where

$$\theta_2 = |\Delta h'| \qquad (-180 \leqq \Delta h' < 180)$$

$$\theta_2 = 360 - \Delta h' \qquad (\Delta h' \geqq 180)$$

$$\theta_2 = 360 + \Delta h' \qquad (\Delta h' < -180)$$

for

$$\Delta h' = h_3 - h_2$$

Point (X_4,Y_4) is

$$X_4 = X_3 + \Delta X_2$$

$$Y_4 = Y_3 + \Delta Y_2$$

The distance D_P flown on heading h_2 is

$$D_P = \sqrt{(X_3 - X_2)^2 + (Y_3 - Y_2)^2}$$

The distance D_G flown from (X_4,Y_4) to point G is

$$D_G = \sqrt{(X_G - X_4)^2 + (Y_G - Y_4)^2}$$

The total distance flown D_1 from the aircraft's position to (X_3,Y_3) for the first turn is

$$D_1 = D_i + D_{T_1} + D_P$$

The total distance flown D_2 from (X_3,Y_3) to point G for the second turn is

$$D_2 = D_{T_2} + D_G$$

These calculations provide the distances and headings necessary to calculate an estimated time of arrival (ETA) at the outer marker. A detailed explanation of ETA calculations in TAATM can be found in reference 7. The DICE value (in seconds) is calculated by DICE = SMT - ETA and indicates how early (if positive) or how late (if negative) the aircraft will arrive at the OM. The DICE value is then presented in the aircraft tag on the display. When this value is less than or equal to 2 sec, a message is generated and delivered to the aircraft to perform a direct engage to the next waypoint.

3.4 System Output and Display

Commands and other information generated by the TAATM M & S control logic are output by alphanumeric display at the controller console in the form of tabular lists and aircraft tag components. It is envisioned that in a real system the controller would use the tag information to formulate the desired ATC commands. It should be noted that the display format adopted for TAATM does not necessarily replicate any existing or proposed actual air traffic controller's display but was developed for the intended uses of the TAATM program in an experimental environment.

The TAATM simulation has the feature of displaying abbreviated command messages in ATC phraseology for a period of time dependent on message length. These messages and their delivery times are generated in accordance with the schedule-maintenance algorithms described in section 3.3.3.

Two other types of lists are displayed as long as the information is applicable. One of these is a list for each holding stack of desired fix departure times of aircraft which have been assigned delays at the arrival (metering) fixes. The other is a conflict-alert list containing the aircraft flight numbers and predicted time errors for which conflicts are not currently resolved. This list and the data tags of the aircraft involved are displayed in a flashing mode for emphasis.

In close proximity to each aircraft position symbol, a data tag containing both conventional status and M & S control-directive information is written. The status data include the airline flight number, a heavy performance-class-aircraft indicator, a controller hand-off symbol, and radar altitude and ground speed. The control directives may include assigned holding times, a left- or right-turn vector instruction with a desired heading, a desired indicated-airspeed objective, and a DICE countdown value and an associated waypoint symbol and name. The name of the waypoint toward which the aircraft should be directed to turn as a DICE value approaches zero is displayed continuously when the value is less than 30 sec and flashing for values less than 15 sec. If the control logic determines that a waypoint should be entirely skipped by the aircraft, a leader line is flashed from the aircraft symbol to the desired waypoint.

Figure 10 shows a representative TAATM display and figure 11 describes the aircraft-tag nomenclature based on the data-block organization in reference 4.

3.5 Interaction of the TCV B-737 Aft Flight Deck Simulator and the M & S Terminal-Area Simulation

The TAATM real-time simulation program and a fixed-base cockpit simulator form the basis of an overall mission simulator for real-time pilot-in-the-loop experiments. The cockpit simulator used in the experiments is a replica of the aft flight deck of the TCV B-737-100 aircraft described in reference 9. The computer program for the aerodynamics, displays, and controls of the cockpit is programmed for the Control Data CYBER computer systems and Adage Graphics Systems. This simulation package includes a nonlinear mathematical model of the B-737-100 aircraft with the addition of landing-gear dynamics, gust/wind models, nonlinear actuator models, and instrument landing system (ILS) and microwave landing system (MLS) sensor models.

Initialization of the cockpit takes place through a prescribed procedure in which the data for a selected TAATM aircraft is used to set the proper state values in the TCV program. Mode control for the TCV program is then slaved to the TAATM program for the ensuing operation in synchronized real time (SRT). The TAATM program and the cockpit simulation are run simultaneously on separate Control Data CYBER 175 computer systems under the direct communication capabilities and constraints provided by the Langley Real-Time Simulation System. Reference 10 is a guide for the basic operation of the TAATM program and reference 11 contains documentation of the interface and operation procedure in the mission simulator mode. A block diagram of the real-time experimental configuration is shown in figure 12. Data transmitted between the programs consist of aircraft initialization parameters and mode-control signals from the TAATM and updated aircraft parameters from the cockpit simulation to TAATM during SRT operation. Data transfer of the updated aircraft parameters occurs at a rate of 32 times per second while operating. The TAATM, however, only examines the data lines at 4-sec intervals as if the inputs were from an automated radar terminal system (ARTS) radar. Tables 1 and 2 present the parameters involved in the mission-simulator data exchange.

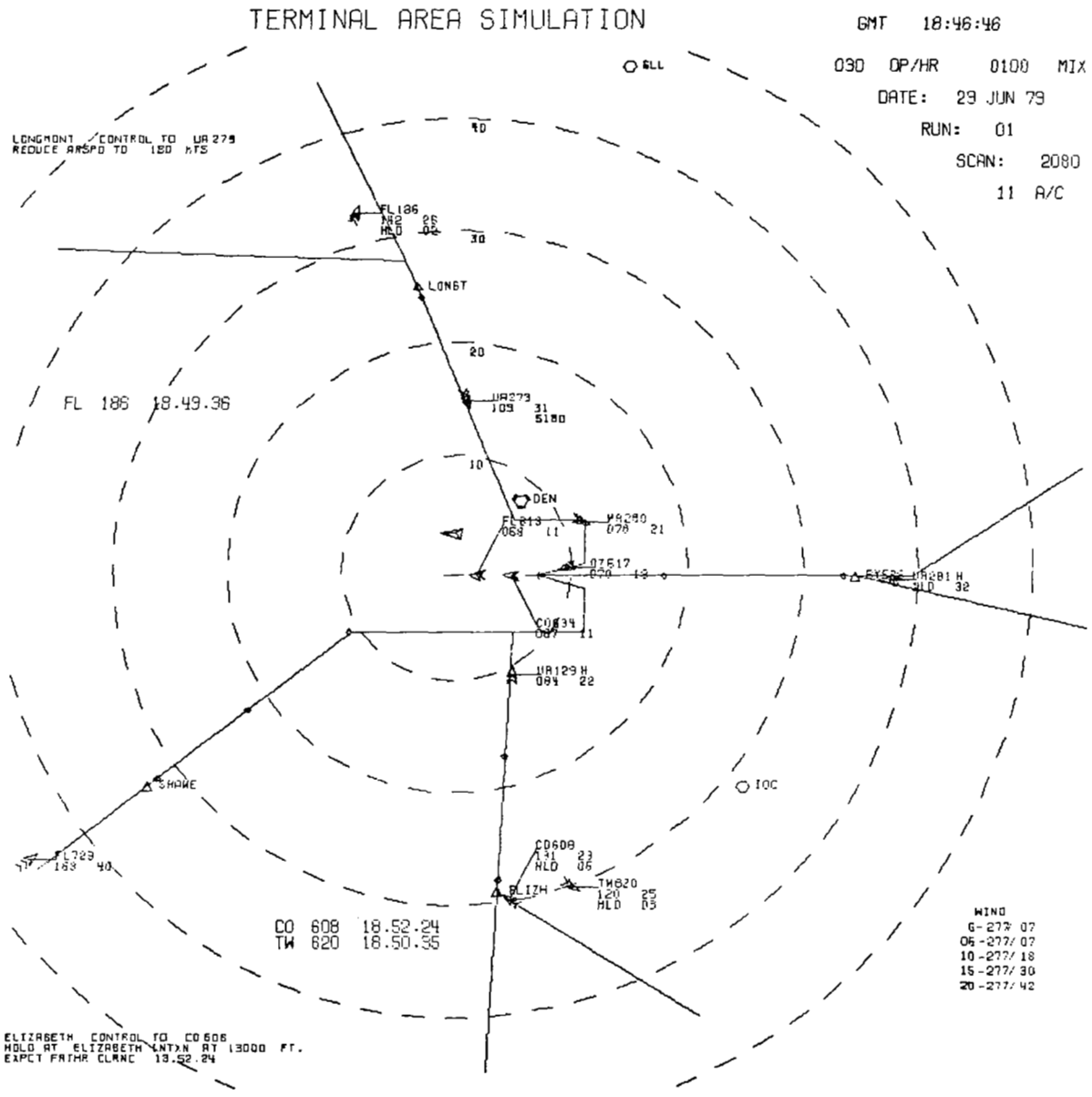

Figure 10.- Example of TAATM simulated controller display.

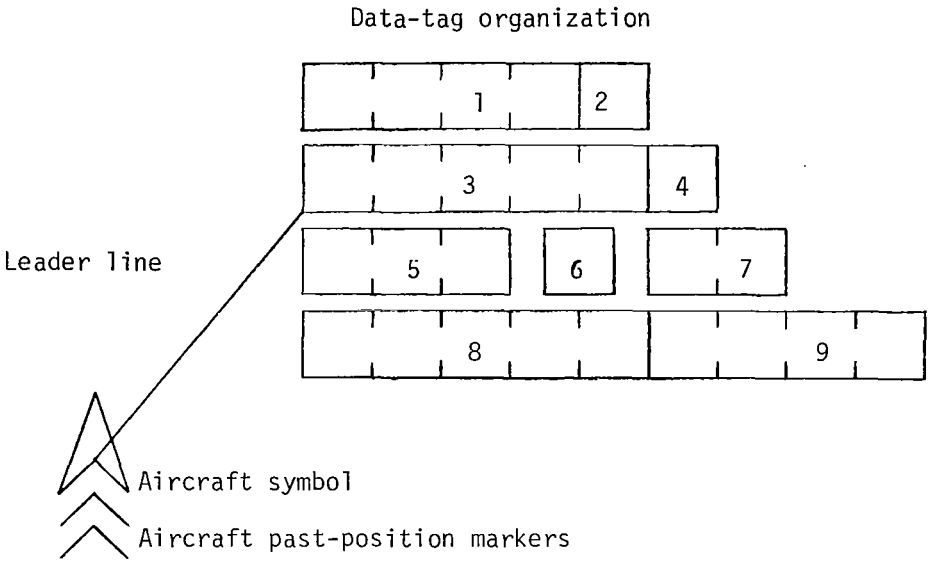

Data-tag fields

Field 1	DICE countdown	(e.g., +75 → 75 sec early at waypoint -5 → 5 sec late at waypoint)
Field 2	Waypoint symbol associated with DICE	(e.g., G → Waypoint at point G)
Field 3	Aircraft flight identification	
Field 4	Symbol (H) for heavy aircraft	
Field 5	Altitude/100	
Field 6	Hand-off symbol	
Field 7	Ground speed/10	
Field 8	Vector command Hold command Waypoint name	(e.g., L210 → Turn left to 210°) (e.g., HLD) (e.g., GATE → Turn to gate)
Field 9	Speed command Holding time	(e.g., S210 → Speed 210 knots) (e.g., 04 → Hold for 4 min)

NOTE: Waypoint name in Field 8 can extend into Field 9

Figure 11.- Aircraft data-tag information for TAATM display.

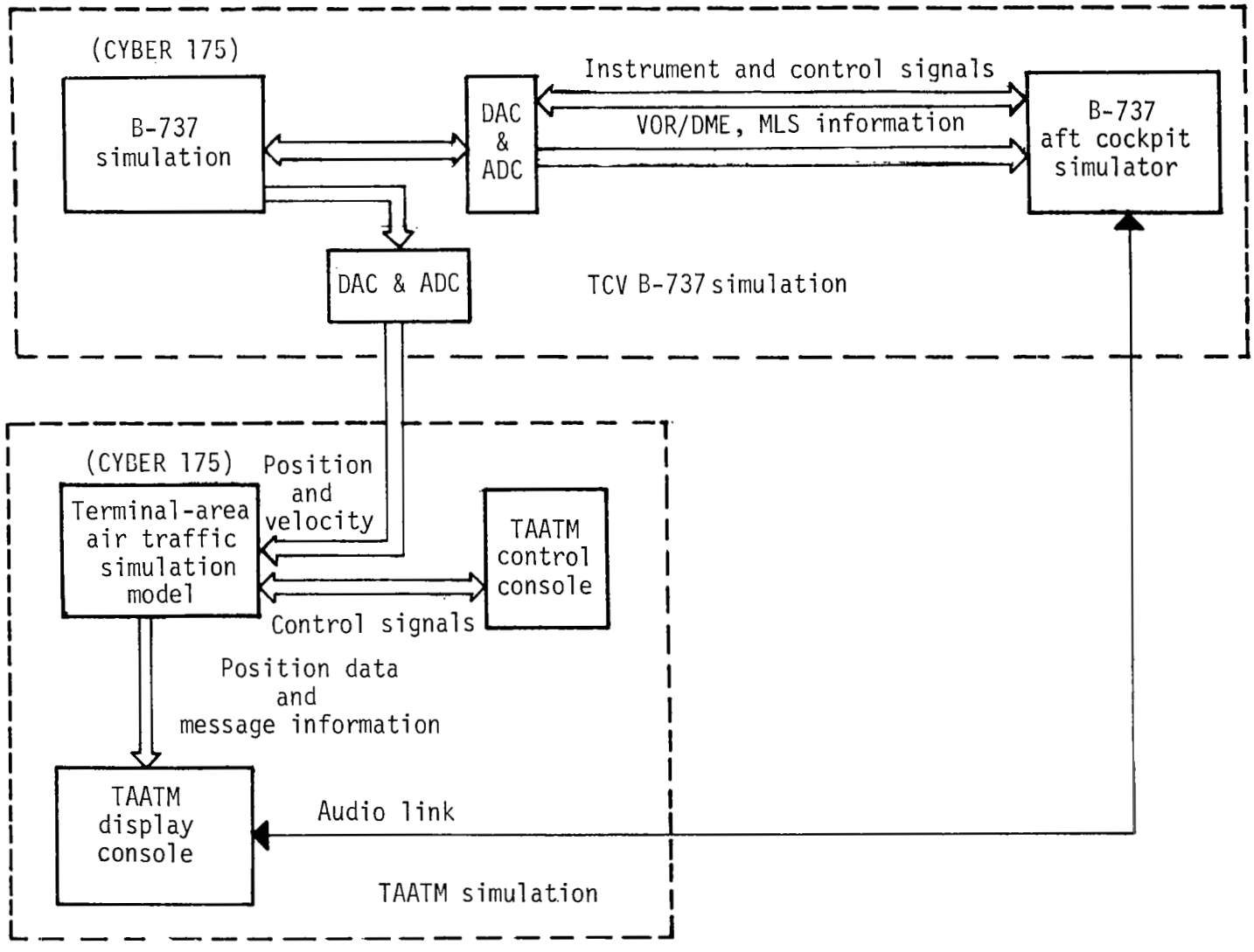

Figure 12.- Block diagram of the real-time experimental configuration.

The TAATM simulation treats the cockpit as if it were part of the internally generated traffic and will resolve conflicts and/or take advantage of situations created by controller/pilot actions. However, gross errors by either party can exceed the controllability of the system which will, of course, result in unresolved conflicts.

In addition to the computer data transfer, voice communication is maintained between the flight crew and the person acting in the role of the air traffic controller at the TAATM simulated radar display. During the mission simulation experiments, the TAATM controller and the cockpit crew interact in the manner described in section 3.6.

TABLE 1.- INITIAL CONDITIONS TRANSMITTED FROM TAATM TO THE TCV SIMULATION

Data description	Data range	Resolution
X-position, ft (m)	±501 000 (±152 705)	±0.06 (±0.02)
Y-position, ft (m)	±501 000 (±152 705)	±0.06 (±0.02)
Altitude, ft (m)	0 to 30 000 (0 to 9144)	±0.90 (±0.27)
Heading, deg	0 to 360	±0.0108
Indicated airspeed (IAS), knots	0 to 500	±0.015
RNAV bias errors:		
Azimuth, deg	±5	$\pm 3 \times 10^{-4}$
Range, n.mi.	±1	$\pm 6 \times 10^{-5}$

TABLE 2.- AIRPLANE-STATE PARAMETERS TRANSMITTED FROM TCV SIMULATION TO TAATM

Data description	Data range	Resolution
X-position, ft (m)	±501 000 (±152 705)	±0.06 (±0.02)
Y-position, ft (m)	±501 000 (±152 705)	±0.06 (±0.02)
Altitude, ft (m)	0 to 30 000 (0 to 9144)	±0.90 (±0.27)
Heading, deg	0 to 360	±0.0108
IAS, knots	0 to 500	±0.015
Ground speed, knots	0 to 500	±0.015
Bank angle, deg	±90	±0.0054

3.6 Procedural Description of Human Interaction

For the computer-assisted M & S system to operate smoothly, both the controller(s) and the pilot(s) must respond to the computer-generated requests within time ranges assumed by the ground computer. Although minor discrepancies are unavoidable due to human and mechanical factors, extreme navigation errors and/or ignored instructions can create circumstances to which the control logic may be unable to adjust. The model will then generate excessive resequencing and delays in its attempt to control the traffic.

3.6.1 Controller responsibilities.- The primary responsibilities of the controller with respect to the computer-assisted M & S system are to interpret and relay the generated requests to the aircraft under his control, to monitor the traffic flow for safety, and to resort to alternative ATC procedures in the event of computer failure or catastrophic errors. In general, there are three types of control areas for each arrival route or STAR. These are: (1) Altitude, speed, and fix departure-time clearances (possibly including holding-stack delays) for the area between the terminal area perimeter and initial arrival fix (IAF); (2) fixed-path speed requests with possible delay vectoring between the IAF and firm-sequencing point; and (3) direct-engage and final-speed reduction requests for fine tuning between the firm-sequencing point and the outer marker. The direct-engage requests to specified waypoints are issued in response to the computer-generated DICE-procedure countdown in the final control area and also for an imposed delay vector. Of course, other information such as traffic advisories, airport conditions, and radio-frequency changes (handoffs) is issued as required.

3.6.2 Flight-crew responsibilities.- The nominal flight path, waypoint altitudes, and speeds are depicted on the navigation plate (STAR) for each approach path. An example procedure for the SHAWNEE STAR is shown in figure 13. The normal flight-crew procedure in flying an approach is to adhere to the STAR specifications except in response to deviations such as speed changes and holds or delay vectors requested by the controller (i.e., "control by exception"). To the best of their ability, the crew must determine the holding-pattern leg geometry necessary to meet the desired fix departure time for an assigned hold. Speed changes should be initiated immediately upon passing the points indicated on the approach plate or in response to a controller request. Altitude objectives should be met at or prior to passing the specified waypoint but generally have second priority to meeting speed objectives.

Other time-critical responses include altitude changes within a holding stack, delay vector initiation, and direct-engage turns to waypoints in the DICE control areas. A direct-engage turn consists of simply breaking off from the current flight path and turning to a heading that will take the aircraft directly over the navigation waypoint specified in the controller request. Deceleration and descent rates should be consistent with those values modeled in the M & S computer for ETA computations.

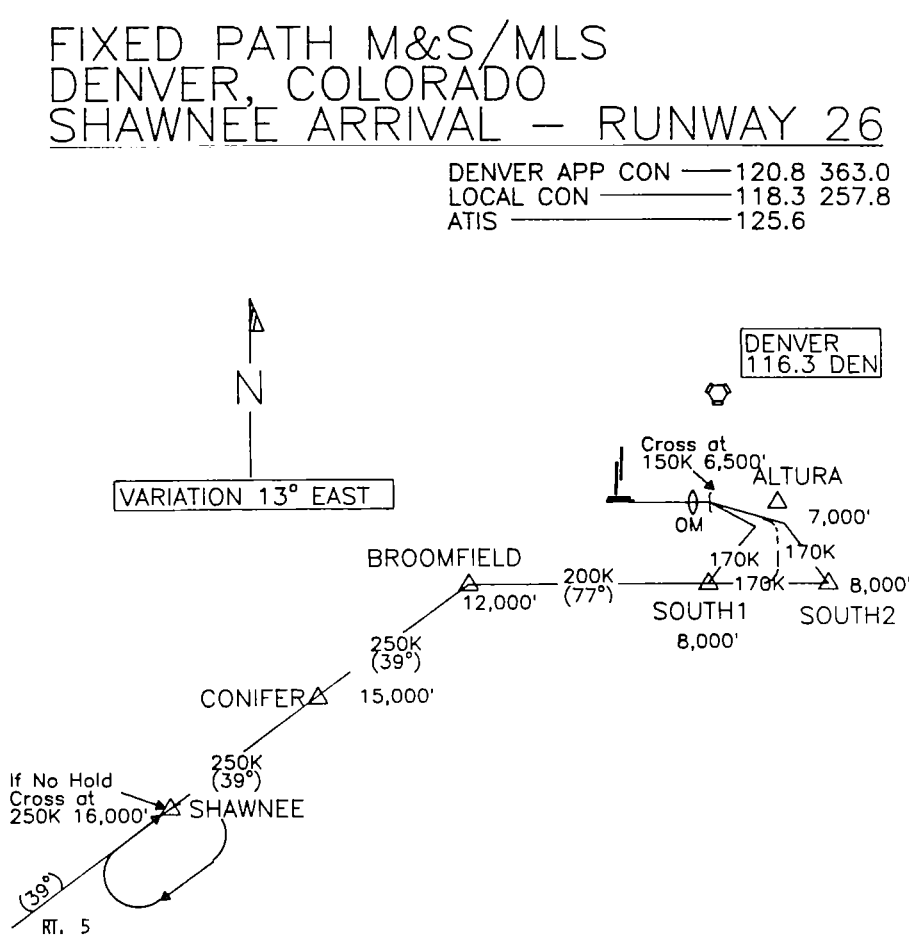

Figure 13.- Navigation plate for SHAWNEE STAR.

4.0 ERROR MODELS

The errors used in the study are a combination of the Terminal Area Air Traffic Model (TAATM) system and aircraft errors together with errors for the RNAV model supplied by the MITRE Corporation. The significant navigation models used for the M & S study are VOR/DME RNAV and MLS. The RNAV bias errors presented in table 3 include angle and range errors associated with both the airborne equipment ($\Delta\theta_a$ and $\Delta\rho_a$) and the ground station ($\Delta\theta_g$ and $\Delta\rho_g$). They are combined in accordance with the equations

$$\Delta\theta_{RNAV} = \Delta\theta_g + \Delta\theta_a$$

$$\Delta\rho_{RNAV} = \Delta\rho_g + \Delta\rho_a$$

where $\Delta\theta_{RNAV}$ is the bearing-angle error and $\Delta\rho_{RNAV}$ is the DME range error. The airborne-equipment errors are applied as a constant for a particular air-

craft and the ground-station errors are applied as a constant for a particular station site. The values $\Delta\theta_{RNAV}$ and $\Delta\rho_{RNAV}$ are applied to the exact position of the aircraft on a given scan in order to simulate the position measured by the airborne navigation system.

TABLE 3.- RNAV BIAS-ERROR MODEL

Error	Symbol	1σ value	Application
Airborne equipment:			
VOR	$\Delta\theta_a$	0.75°	Determined once for each aircraft and kept constant during flight
DME	$\Delta\rho_a$	0.3 n.mi.	Determined once for each aircraft and kept constant during flight
Ground station:			
VOR	$\Delta\theta_g$	1.0°	Determined once for each ground station and kept constant
DME	$\Delta\rho_g$	0.05 n.mi.	Determined once for each ground station and kept constant

The MLS errors presented in table 4 include signal noise ($\Delta\theta_n$ and $\Delta\rho_n$) and bias errors ($\Delta\theta_b$ and $\Delta\rho_b$) which are applied depending on the range of the aircraft from the station. The errors were chosen to model the basic wide-aperture, high-resolution MLS system intended for high-density terminal areas. For this system two MLS coverage configurations, ±40° and ±60° coverage, were used in the experiments. Within this coverage the range errors for both bias and noise vary as a function of distance from the MLS station site. The errors are combined in accordance with the equations

$$\Delta\theta_{MLS} = \Delta\theta_b + \Delta\theta_n$$

$$\Delta\rho_{MLS} = \Delta\rho_b + \Delta\rho_n$$

where $\Delta\theta_{MLS}$ is the angle error and $\Delta\rho_{MLS}$ is the range error. The values $\Delta\theta_{MLS}$ and $\Delta\rho_{MLS}$ are applied to the exact position of the aircraft on a given scan in order to simulate the position measured by the airborne navigation system.

TABLE 4.- MLS ERROR MODEL

Error	Symbol	1σ value	Application
Bias:			
Azimuth	$\Delta\theta_b$	0.066°	Determined once for each aircraft and kept constant during flight
Range	$\Delta\rho_b$	[a]14.3 m (46.8 ft) [b]88.7 m (291.0 ft)	Determined once for each range for each aircraft and kept constant for the balance of that range
Noise:			
Azimuth	$\Delta\theta_n$	0.091°	Redetermined every 4 sec for each aircraft
Range	$\Delta\rho_n$	[a]3.7 m (12.2 ft) [b]6.8 m (22.3 ft)	Redetermined every 4 sec for each aircraft and applied dependent on range of aircraft from station

[a]For range ≤4.5 n.mi.
[b]For range >4.5 n.mi.

The aircraft-performance deviation errors presented in table 5 are used to simulate the precise achieved values as opposed to the exact desired values. The first four deviation errors in the table are redetermined for each aircraft whenever a speed or altitude change is initiated. The application of speed and altitude deviation is discontinued once the aircraft is on final approach. The application of a descent-rate deviation is discontinued once the aircraft is between the outer marker and the runway. The last deviation included in the table is the time-delay flight technical error. This error simulates pilot variability in initiating a DICE turn. The assumption is that the pilot will respond to a direct-engage message from the controller with a mean time of 4 sec and a standard deviation of 3.5 sec.

TABLE 5.- AIRCRAFT-PERFORMANCE DEVIATION ERRORS

Error	1σ value	Application
Altitude, m (ft)	30.5 (100.0)	Determined each time altitude change is initiated
Speed, knots	5	Determined each time speed change is initiated
Descent rate, percent	5	Determined each time a descent is initiated
Deceleration rate, knots/min . . .	5	Determined each time a deceleration is initiated
Flight technical time deviation in initiating a turn, sec . . .	3.5	Determined each time a DICE turn is calculated

The wind-speed and direction bias errors are applied as straight percentages of the wind values which affect an aircraft's position on a given scan. The wind model and its associated errors consist of the following:

$$W_S = [\omega + \Delta s_a(h - h_o)](1 + B_s)$$

$$W_D = [\Psi + \gamma(h - h_o)](1 + B_d)$$

where

W_S actual wind speed

ω assumed wind speed at ground level

Δs_a assumed change in speed with change in altitude

h aircraft altitude, MSL

h_o airport altitude, MSL

B_s wind-speed bias

W_D actual wind direction, deg true

Ψ assumed wind direction at ground level, deg true

γ assumed change in wind direction with change in altitude

B_d wind-direction bias

The nominal values for Denver consist of the following:

ω = 7.918 knots

Δs_a = 0.007769 knots/m (0.002368 knots/ft)

Ψ = 277°

γ = 0 deg/m (0 deg/ft)

h_o = 1625 m (5330 ft)

B_s = 10 percent

B_d = 5 percent

The en route metering errors presented in table 6 are used in the determination of the 20-min and 5-min flight-plan-message times. The first two errors correspond to the uncertainties in the estimated times of arrival. When a minimum separation is called for between the 20-min and 5-min flight-plan messages, the en route separation-time error corresponds to a variation in the interarrival separation time compared to the minimum required.

TABLE 6.- EN ROUTE METERING ERRORS

Error[a]	1σ value, sec
Arrival-time error 20 min from fix	30
Arrival-time error 5 min from fix	15
En route entrail separation error	2.5

[a]Determined once for each aircraft.

The surveillance errors presented in table 7 are used to simulate the difference between the actual position of an aircraft and the radar measurement of the position. The error values are redetermined for each aircraft on each simulated radar scan.

The determination of an aircraft's actual final-approach and touchdown speeds is based on the aircraft's gross landing weight. Since weight is related to the load factor of the aircraft, there exists a functional relation between final speeds and load factor. By using this relation, the TAATM aircraft final-approach and touchdown speeds are determined using a mean load factor of 50 percent and a standard deviation of 15 percent. The load factor for a particular aircraft is determined based on a normal distribution which is bounded by 10 and 100 percent. If a load factor is computed outside these bounds a new load factor is recomputed. The factor chosen for a particular aircraft remains constant over the duration of its flight. For the purpose of estimating times of arrival, the control logic assumes a constant 50-percent load factor for all aircraft.

TABLE 7.- SURVEILLANCE ERRORS

Error[a]	1 σ value
Range	79.2 m (260.0 ft)
Azimuth	0.25°
Mode C altitude	12.5 m (41.0 ft)

[a]Determined each scan for each aircraft position update.

5.0 IDENTIFIED LIMITATIONS AND CONSTRAINTS OF THE TESTED FIXED-PATH M & S SYSTEM

During the M & S study several limitations and constraints on the system were identified which are functions of the terminal geometry used, the procedures for separating aircraft, and the sequencing and scheduling control algorithm. The following discussion analyzes the effects of these limitations and constraints on the operation of the experimentally tested M & S system. Within the bounds of this study, however, no attempt was made to remove them from the system.

5.1 Geometry Constraints

The terminal geometry described in section 2.0 includes the straight-in BYERS approach route. Unlike the remaining routes, the controllability available on this route does not include the two-turn DICE prior to final approach. The two-turn DICE provides the advantages of path shortening and path stretching to adjust to an assigned SMT close-in to the OM. It is also capable of accommodating SMT schedule slippages. In contrast, the controllability on the BYERS approach includes a path-stretching vector which is only used as a back-up to its speed-control capability. The decision to initiate

the vector occurs only once on the approach route, at the final speed-control point. If an aircraft passes this speed-control point without initiating a vector, further controllability is not available for the aircraft and schedule slippages cannot be accommodated. To lessen the impact of this constraint, the BYERS approach is handled as a priority route. For this route, hold assignments are applied prior to the fix only after resequencing has failed to resolve a separation problem. For all other routes, hold assignments have priority over resequencing. Additionally, the en route delay threshold for this route is set at 60 sec instead of the nominal 240 sec applied to the other routes. The impact of these differences in handling BYERS' aircraft is to smooth the flow of aircraft on this approach by forcing larger and more frequent en route delays and by minimizing holds.

5.2 Separation-Procedure Limits

The limitations and constraints with respect to the procedures for separating aircraft consist of the following: (1) Separation is insured only on initial arrival at the IAF's and on final approach; (2) the schedule-slippage procedure can shift a separation problem from an aircraft which has generated the need for backward slippage to an aircraft behind with limited delay capability; (3) the ground rules for the assignment of holds can generate a cascade of holds resulting in excessive separations; and (4) the accumulation of aircraft flight errors can generate a schedule-maintenance problem which cannot be resolved by the system. The result is that not all separation violations and gaps can be resolved by the M & S system studied.

5.2.1 Common-path separation violations.- Because separation is insured only on an aircraft's initial arrival at the IAF and then again on final approach, separation violations due to speed differences can occur between a pair of aircraft on a common path. These violations are possible but are rare because they occur only under certain circumstances for aircraft pairs exiting from holding patterns and for aircraft pairs with large speed errors. Because separation is insured on initial arrival at an IAF and on final approach and because the speeds of the aircraft are decreasing as they approach the OM, aircraft normally have excess separation upon leaving the IAF. The separation distance then closes gradually to the minimum required separation distance at the OM due to decreases in speeds.

If a pair of aircraft are holding at the fix, it is possible for the schedule-maintenance logic to release the first aircraft assuming no speed-control delay will be used in the future to realize the SMT. The second aircraft can then be released from the hold assuming speed-control delay will be required. The result is a loss of separation just past the fix until the second aircraft receives its speed-control delay so that the separation distance is increased.

Consider, for example, the LONGMONT approach. (See fig. 3.) Assume that a minimum required 3-n.mi. separation distance between a pair of aircraft at the OM results in a time separation of 82 sec. Assume also that the delay achievable by using speed control is 62 sec (i.e., the speed delay for a B-737 on LONGMONT approach). The schedule-maintenance logic for hold-exit determi-

nation will permit the second aircraft to proceed past the fix if its needed delay can be achieved by using 70 percent or less of its speed-control delay capability in the future. In other words, the second aircraft can exit the fix needing to delay for 43 sec in order to meet its SMT. If the first aircraft exited from the hold needing no delay, then the pair of aircraft is separated at the fix by approximately 39 sec. If both aircraft leave the fix at an indicated airspeed of 210 knots and an altitude of 4267 m (14 000 ft), the ground speed of each aircraft is approximately 257 knots, assuming no winds are present. With a separation time of 39 sec, the separation distance would be about 2.8 n.mi. The condition can therefore exist where the minimum 3.0-n.mi. separation is not maintained over the entire route.

A loss of separation between a pair of aircraft can also occur on a route because of large speed errors. The speed-error model computes actual speeds attained by aircraft which can be faster or slower than the M & S requested speeds. The possibility exists that a pair of aircraft on the same approach route have large speed errors and are scheduled to land consecutively. Depending on the magnitude of the errors, and if the speed of the first aircraft is slower than desired and the speed of the second aircraft is faster than desired, a loss of separation can occur before the control logic is capable of recognizing and resolving the problem.

5.2.2 Schedule-slippage-procedure limitations.- Another type of problem can exist due to the schedule-slippage procedure. This procedure is designed to close gaps between aircraft and resolve possible separation violations at the OM by adjusting SMT's without performing any resequencing of aircraft. This adjustment can consist of either a forward or backward slippage of the SMT's to resolve accumulated flight errors. Assume that an aircraft has accumulated flight errors such that SMT backward slippage is required because of the aircraft's late estimated time of arrival at the OM. Once backward slippage has been accomplished for this aircraft, all aircraft behind must be examined in turn and schedules must be slipped backward until slippage is no longer necessary or cannot be realized for a particular aircraft. If the second case occurs, the possibility can exist that an aircraft behind is penalized because of errors accumulated by the aircraft initiating the slippage. Separation violations occur then between a pair of aircraft which did not generate the flight error requiring the slippage. This occurs particularly when one of the aircraft behind is on the BYERS approach and has already used up its limited delay capability.

5.2.3 Holding-procedure constraints.- In contrast to the separation problems mentioned previously, the holding logic is capable of generating separation gaps in the traffic flow on a single approach route. This occurs because of the severe constraints of the ground rules associated with the assignment of holds. As stated previously, the ground rules consist of the following:

1. Any aircraft which has previously been advised to anticipate a hold will in fact be required to hold, even if the traffic environment changes prior to the aircraft reaching the fix.

2. Hold assignments can occur during the 5-min flight-plan message action, at radar acquisition, at the control action just prior to the holding fix, and during the hold-exit determination.

3. An automatic hold is assigned to an aircraft if the aircraft ahead (assigned to the same holding fix) is holding or anticipating a hold.

4. A hold is assigned if the delay required is in excess of 70 percent of the speed-control delay capability.

Values for 70 percent of the speed-control delay capability for the four arrival routes for a B-737 are presented in the following list:

BYERS arrival	~46 sec
LONGMONT arrival	~43 sec
SHAWNEE arrival	~73 sec
ELIZABETH arrival	~46 sec

Therefore, if a B-737 on the LONGMONT approach requires a delay of greater than 43 sec prior to the holding fix, the aircraft will be required to hold. A single hold for one aircraft can then generate a cascade of holds for all aircraft behind it which are proceeding to the fix. Resolution of the holds requires a sufficient break in the traffic flow to the fix such that the holding stack is cleared before another aircraft is offered into the active traffic for that same fix. A minimum hold for a B-737 requires approximately 3 min depending on the altitude at which the hold is executed. If the aircraft requires a delay of 50 sec, an excess delay of approximately 130 sec is actually achieved. It should be noted, however, that resequencing can occur such that the gaps can be used by aircraft on other approach routes.

5.2.4 Limited-delay-option specification.- Another limitation exists within the experimentally implemented M & S system because the specified delay options are finite. Depending on the magnitude of the flight errors, the traffic load, and the delay capability, the possibility exists that an aircraft at a control-action point after the holding fix does not have adequate delay capability remaining to achieve its SMT. The resulting individual-aircraft error may or may not, however, result in separation error depending on the relative error between aircraft pairs. Following each control action performed, a separation error predicted at the OM is calculated for all aircraft pairs within the terminal area. If an aircraft's SMT is either early with respect to its calculated minimum ETA or late with respect to its calculated maximum ETA, a potential separation error for the aircraft exists. By comparing the potential separation errors between an aircraft pair, a predicted separation error can be calculated. If the predicted error indicates a potential loss of separation, the desired aircraft delay to resolve the problem is displayed on the simulated radar display. The simulation run, however, proceeds and the assumption is made that the problem will be resolved by human intervention or by M & S resequencing or rescheduling in the future.

5.3 Limitations of the Scheduling Algorithms

Two important limitations have been identified within the control algorithms concerning scheduling. The first is that the knowledge of the delay capability used by the scheduling and sequencing logic is limited to a single pair of minimum and maximum anticipated ETA's at the OM for a given aircraft. The second is that the en route metering function is performed independent of the terminal sequencing and scheduling algorithm.

The first control limitation is a result of the types of ETA information made available to the scheduling algorithm. The algorithm for assigning an SMT attempts to bound the SMT by a minimum and maxium possible ETA at the OM for a given aircraft. These bounds represent the SMT limitations which are assumed at a given control-action point for the realization of an SMT. The time difference between the two ETA's, however, does not necessarily reflect the total controllability available for the aircraft on the entire path. No additional information is presented to the scheduling algorithm that describes achievable ETA's with path shortening or stretching. The result is that sequencing and resequencing decisions are made for the aircraft without a complete knowledge of the controllability of the aircraft. If SMT assignments cannot be made within the nominal ETA bounds, this additional information could be used to more realistically resolve the problem.

Within the constraints of a fixed-path speed-control M & S philosophy, this scheduling procedure places highest priority on the realization of SMT's by speed control with a secondary priority on holding aircraft and resequencing SMT's. Vectoring is used by the schedule-maintenance algorithm only as a backup option to realize an SMT, but the scheduler does not assign SMT's with the assumption that vectoring will be used. If the scheduler was given more knowledge of the controllability which could be achieved by path shortening and stretching, speed control could still be given highest priority but the secondary priority would be placed on path changes rather than holding and resequencing. With this change, the problems generated by holding aircraft could be reduced, but more vectoring would occur within the terminal area.

A severe constraint of the studied M & S control philosophy is that the scheduling algorithm for performing en route metering is not coupled to the terminal scheduling algorithm. The en route metering function is designed to regulate the flow of aircraft into the terminal area but does not recognize the dynamically changing environment within the terminal area. En route delays are assigned based on a scheduling algorithm which differs from the terminal scheduler in the following two ways: (1) The terminal scheduler performs sequencing based on a projected first-come-first-serve-at-the-runway principle whereas the en route scheduler simply assigns a first-in-first-out order, and (2) the en route scheduler does not use the dynamically updated ETA information available to the terminal scheduler. The result is that large delays in the form of holds or vectoring are still necessary within the terminal area even though en route delays have been assigned. If, however, the en route scheduling algorithm was coupled with the terminal algorithm, potential problems within the terminal area could be anticipated more accurately in the en route area and

en route delays could be assigned accordingly. Gross delays could therefore be absorbed at the higher, more fuel-efficient altitudes. Results discussed in section 6.2 support this view.

6.0 FAST-TIME STUDIES

The primary goals of this study were to evaluate a particular fixed-path metering and spacing (M & S) system, described in section 2.0, and to determine if the M & S's delivery performance was improved by using the microwave landing system (MLS) instead of the VOR/DME as the RNAV data source during approach, fine-tuning, and DICE directed maneuvers. Both $\pm 40^{\circ}$ and $\pm 60^{\circ}$ MLS were evaluated. Each aircraft was assumed to be equipped with a skip-waypoint, two-dimensional RNAV system operated as discussed in sections 3.3.3.4 and 3.6.2. Data collected from fast-time (batch) runs of the computerized Terminal Area Air Traffic Model (TAATM) were used as a basis for evaluation. The data are analyzed and plotted in this section.

6.1 Performance Criterion and Data Combination

The aircraft interarrival-error standard deviation at the outer marker is the primary criterion of performance evaluation and indicates the variation in interarrival error achieved by a system. Interarrival error is the difference between realized aircraft interarrival time and that of the expected interarrival time obtained from the scheduled times between succeeding aircraft pairs. (See eq. (A11) in appendix A.) This measure translates the errors of the M & S system in meeting its time objective into an indication of system separation performance, which is more closely related to ATC safety than the actual arrival errors. For instance, if all aircraft were to arrive with sizable time errors, but of the same magnitude and direction, then interarrival separation is still maintained. Another attractive feature of the measure is that it is theoretically independent of arrival rate. Time errors are determined from each aircraft's own specific schedule time to which the system is working to meet. Within limits, as the arrival rate increases, the interval between scheduled times decreases but the dynamics of meeting each aircraft's time objective remains the same. Therefore, results of separate data runs of the same system, even with different arrival rates, can be combined to obtain an improved pooled estimate of the variance of the system under study.

Arrival-only traffic was used to increase the number of interarrival times for data analysis purposes. An estimate of the system interarrival-error standard deviation was obtained from a set of data runs with all parameters except arrival rate held constant. A data set consisted of 2 separate runs for each of the arrival-rate samples of 25, 30, 35, and 40 aircraft per hour. Each of the 8 runs in a data set contained 2 hr of steady-state, outer-marker interarrival data. A combined pooled estimate for the data-set variance was used to measure the system interarrival-error variance. If k samples from a population having a common variance are available for estimating the variance, the pooled estimate s_o^2 is defined by the following:

$$s_o^2 = \frac{(n_1 - 1)s_1^2 + (n_2 - 1)s_2^2 + \ldots + (n_k - 1)s_k^2}{n_1 + n_2 + \ldots + n_k - k}$$

where s_k^2 is the sample-run variance and n_k is the number of data points for the kth sample. The pooled estimate of standard deviation is simply s_o.

6.2 Approach Navigation

6.2.1 General M & S performance.- Figure 14 shows the fast-time values of the interarrival-error standard deviation for various final-approach navigation systems. The figure shows a standard deviation in the range of 7.5 to 10 sec depending on the particular approach navigation used. Current manual ATC procedures normally achieve values in the order of 18 to 21 sec (ref. 12). Thus the relatively fixed-path, speed-control M & S system studied gave reduced instrument flight rule (IFR) delivery dispersions in comparison with today's manual vectoring and yielded results comparable to M & S systems employing only vectoring.

6.2.2 Total-geometry performance.- For the terminal route geometry studied, figure 14 shows comparison of the overall delivery performance of the M & S system using various approach navigation systems. There is no statistically significant difference between the performance of the $\pm 40^\circ$ MLS system and that of the $\pm 60^\circ$ MLS system. Use of the equal-tails F-test at the 1-percent level of significance indicates there is a difference in the delivery performances between using VOR/DME and ILS and using MLS as the final-approach navigation system. Although statistically different, the standard-deviation decrease from 9.2 to 7.9 sec shows that MLS offers only a slight improvement in system delivery precision over VOR/DME and ILS for the particular M & S and terminal route geometry used.

6.2.3 Route effect.- The total-geometry system performance discussed previously is due to the interaction of two types of approach routes. It is desirable to separate and assess the individual performances of the straight-in routes as well as the other three routes, all of which use two DICE turns to supplement the time-control-by-speed instructions. Figures 15 and 16 illustrate two types of traffic samples which were run with that end in mind. One sample contains only straight-in traffic and the other contains no straight-in traffic. Figure 17 indicates the interarrival-error standard deviation delivery performance for the final-approach navigation system evaluated for the two types of traffic samples. The F-test at the 1-percent level of significance shows that the two-DICE-turn route is worse than that for the all straight-in traffic when the VOR/DME and ILS system is used for approach navigation. When the MLS system is used, the DICE-turn routes yield a reduction of about 1.5 sec in the interarrival-error standard deviation compared with that from the all straight-in route.

Figure 17 also indicates that if there had not been a straight-in route in the geometry but instead only routes using two DICE turns, then the VOR/DME and ILS and MLS delivery-performance difference would be larger than that for

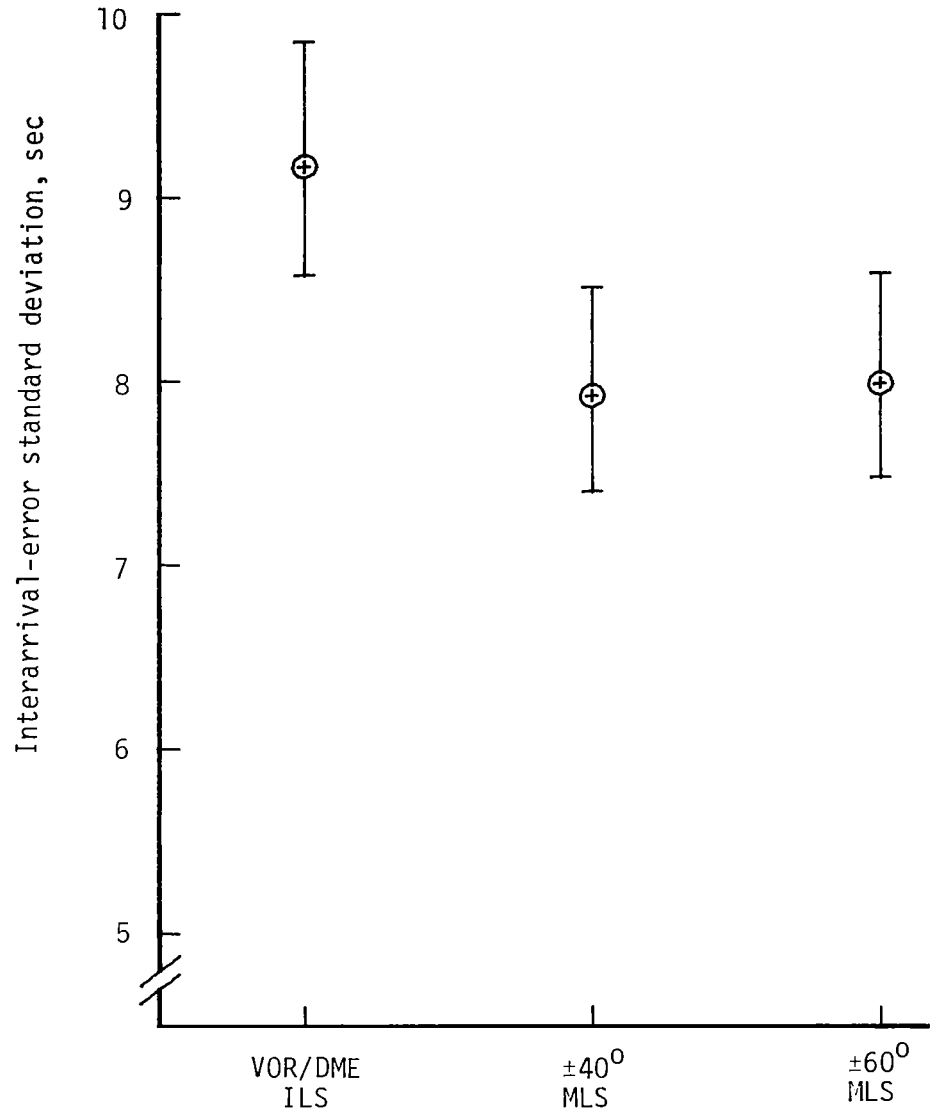

Figure 14.- Interarrival delivery precision for various final-approach navigation systems. Wind error of 10-percent strength and 5-percent direction. Confidence interval of 95 percent for values shown.

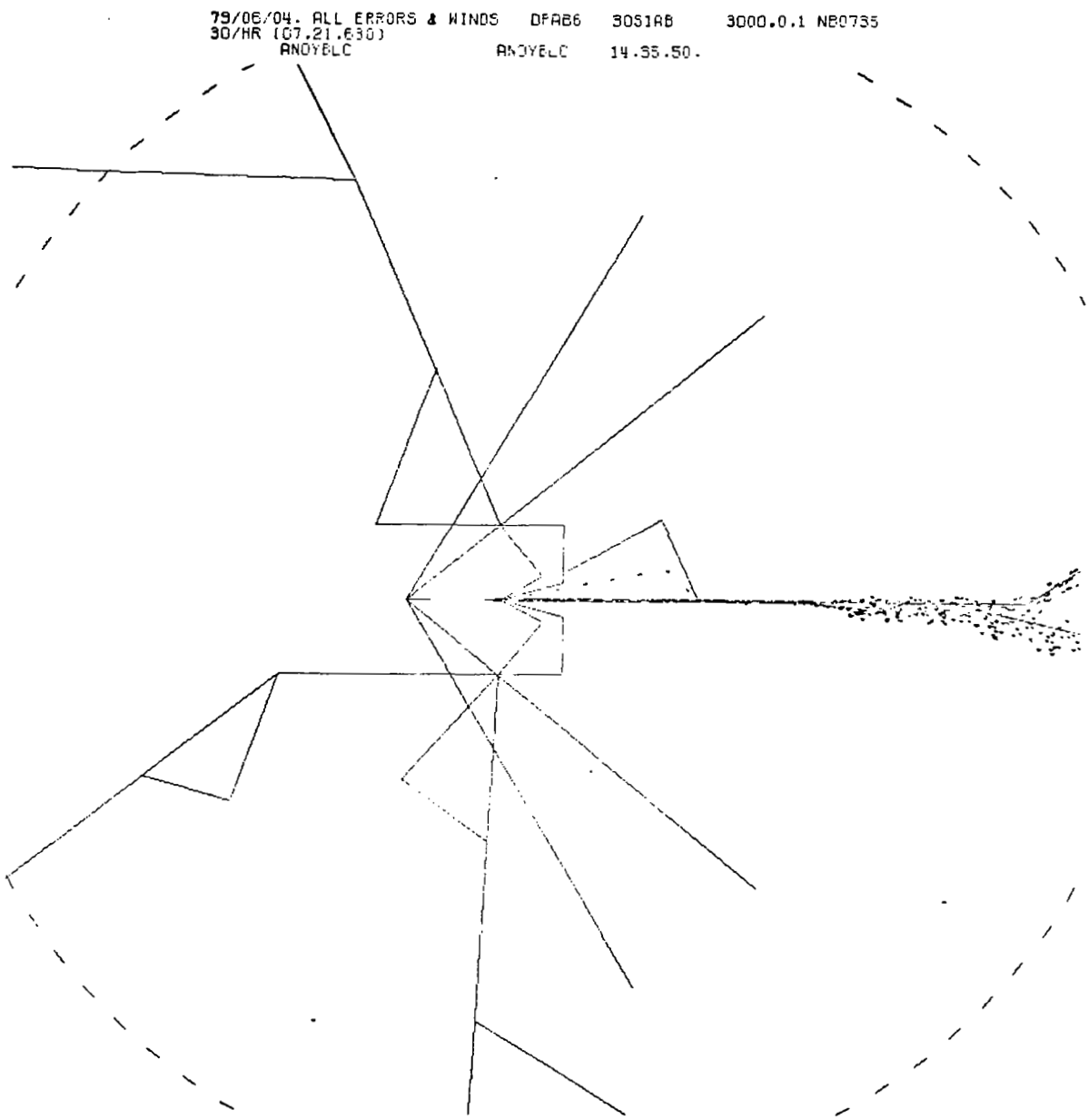

Figure 15.- Traffic flow for 30 aircraft per hour data sample with all traffic on straight-in route. Final-approach navigation with ±60° MLS.

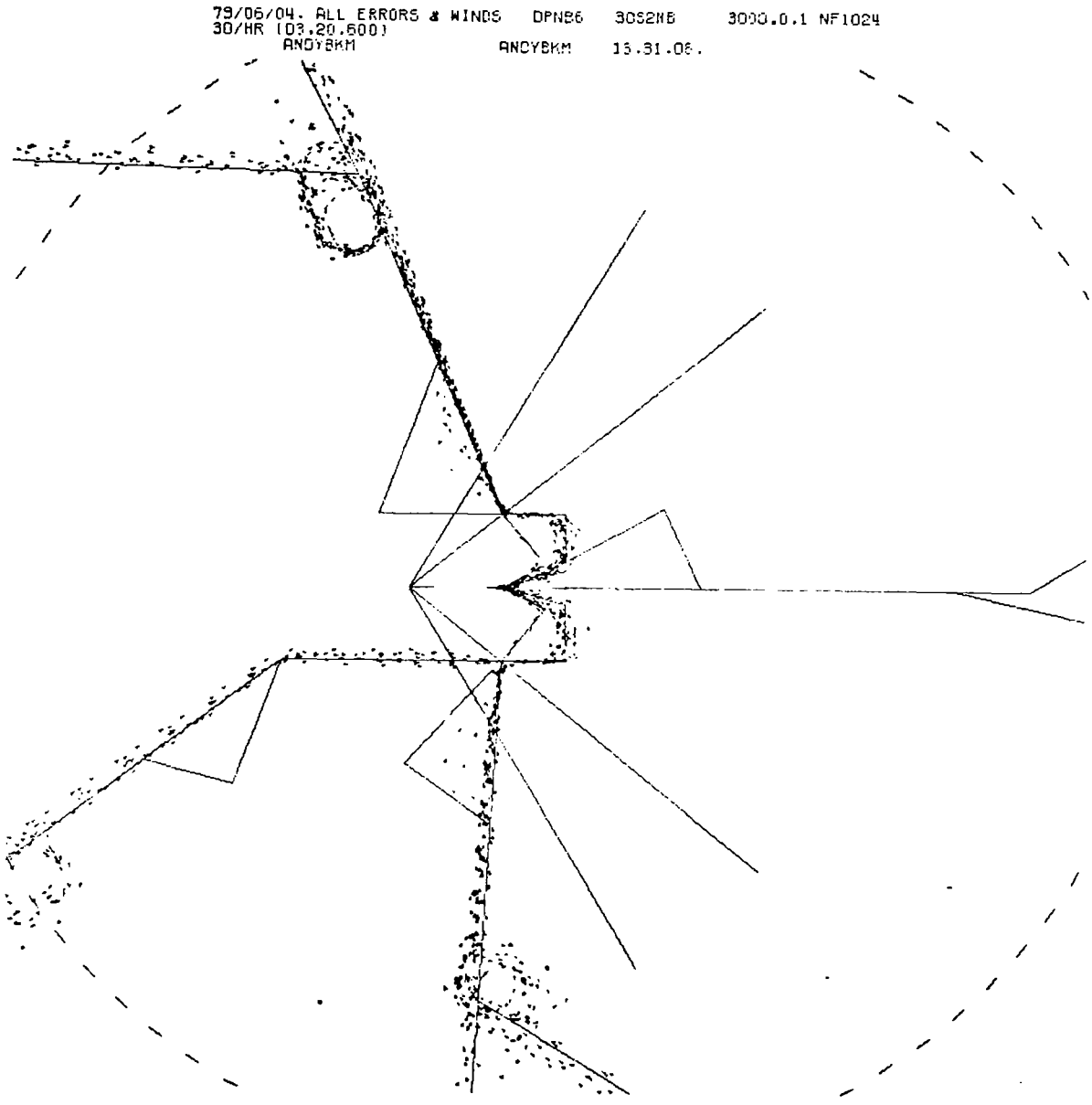

Figure 16.- Traffic flow for 30 aircraft per hour data sample with all traffic on DICE-turn routes. Final approach navigation with ±60° MLS.

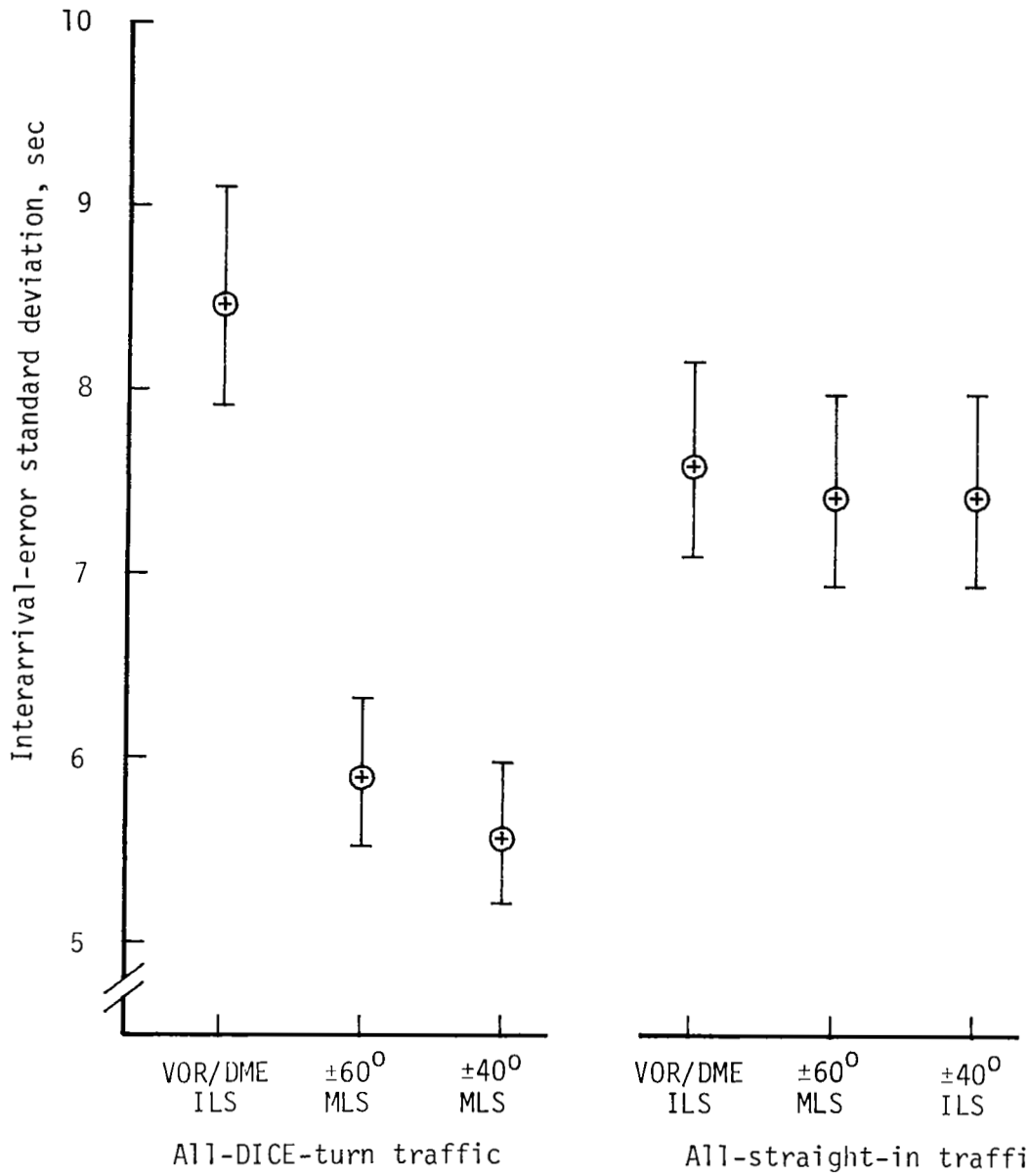

Figure 17.- Route delivery characteristics. Interarrival delivery precision for all-DICE-turn traffic and for all-straight-in traffic. No wind error; 95 percent confidence interval for values shown.

the total-geometry case. With all-DICE-turn routes, the VOR/DME and ILS interarrival-error standard deviation is 8.5 sec, whereas the MLS is 5.9 sec. So for the all-DICE-turn case, the improved path-following capability of the MLS system enables the M & S system to make better use of the fine-tuning potential of DICE maneuvers.

As would be expected, there was no significant difference among the approach navigation systems studied when the traffic was all straight-in. Also, there was no significant difference between the ±60° and ±40° MLS systems for either the all-straight-in or the all-DICE-turn traffic sample.

6.2.4 Summary of final-approach navigation comparison.- In general, for the particular ground-based, fixed-path speed-control M & S system evaluated, if the route structure contains a mixture of DICE-turn routes and straight-in routes, then MLS offers only a slight improvement over VOR/DME and ILS in the interarrival-error standard deviation performance. If the routes all contain two DICE turns, then the VOR/DME and MLS improvement over VOR/DME and ILS is more substantial, taking 2.6 sec off of the already fairly low 8.5-sec interarrival-error standard deviation for the combined VOR/DME and ILS M & S system. For a geometry with only two-DICE-turn final-approach routes, the improved path-following capability of the MLS system over that of a conventional VOR/DME and ILS system enables the M & S control system to utilize some of the fine-tuning potential of the two DICE turns. For the M & S system studied, we can also say that wider coverage ±60° MLS system appears to offer no time-delivery precision over the basic ±40° MLS system regardless of the arrival-route geometry.

6.3 Wind-Error Effects

With the ±60° MLS final-approach navigation system as a basis for comparison, runs were made using three wind conditions to evaluate wind-error influence on this particular fixed-path M & S system. The three steady-state wind conditions were: (1) 10-percent error in wind strength and 5 percent error in direction; (2) no error in strength or direction; and (3) -10 percent error in wind strength and -5 percent error in direction. The reference steady-state wind at ground level was 7.92 knots at 277° (true north) with a linear increase in strength of 2.37 knots per 305 m (1000 ft). Figure 18 shows that for the range of wind errors considered, the interarrival error standard deviation is not significantly changed. The dynamic schedule adjustment, which works to eliminate interarrival spacing violations, is responsible for keeping wind effects from building up.

6.4 Tentative-Schedule Point

The metering time used to determine if en route delay will be applied to regulate the traffic flow is actually not used by the terminal scheduler of the M & S system studied. Thus the metering is effectively uncoupled from the terminal sequencing and spacing. The ±60° MLS system was used as a basis of comparison to determine the effect of moving the terminal tentative-schedule time from its normal 5 min to arrival fix. There appears to be no discernable

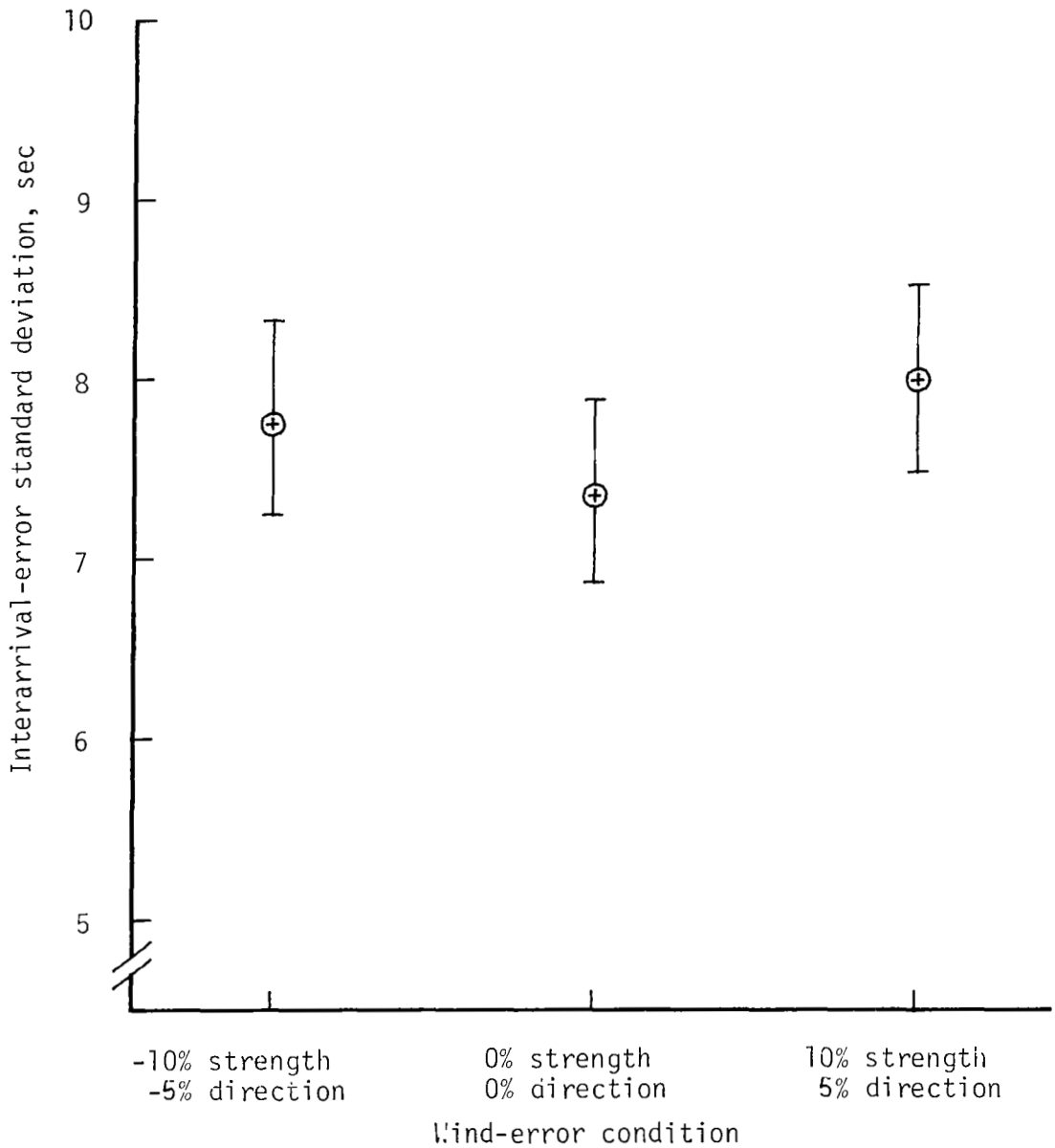

Figure 18.- Interarrival delivery precision for various wind-error conditions. Final-approach navigation with ±60° MLS; confidence interval of 95 percent for values shown.

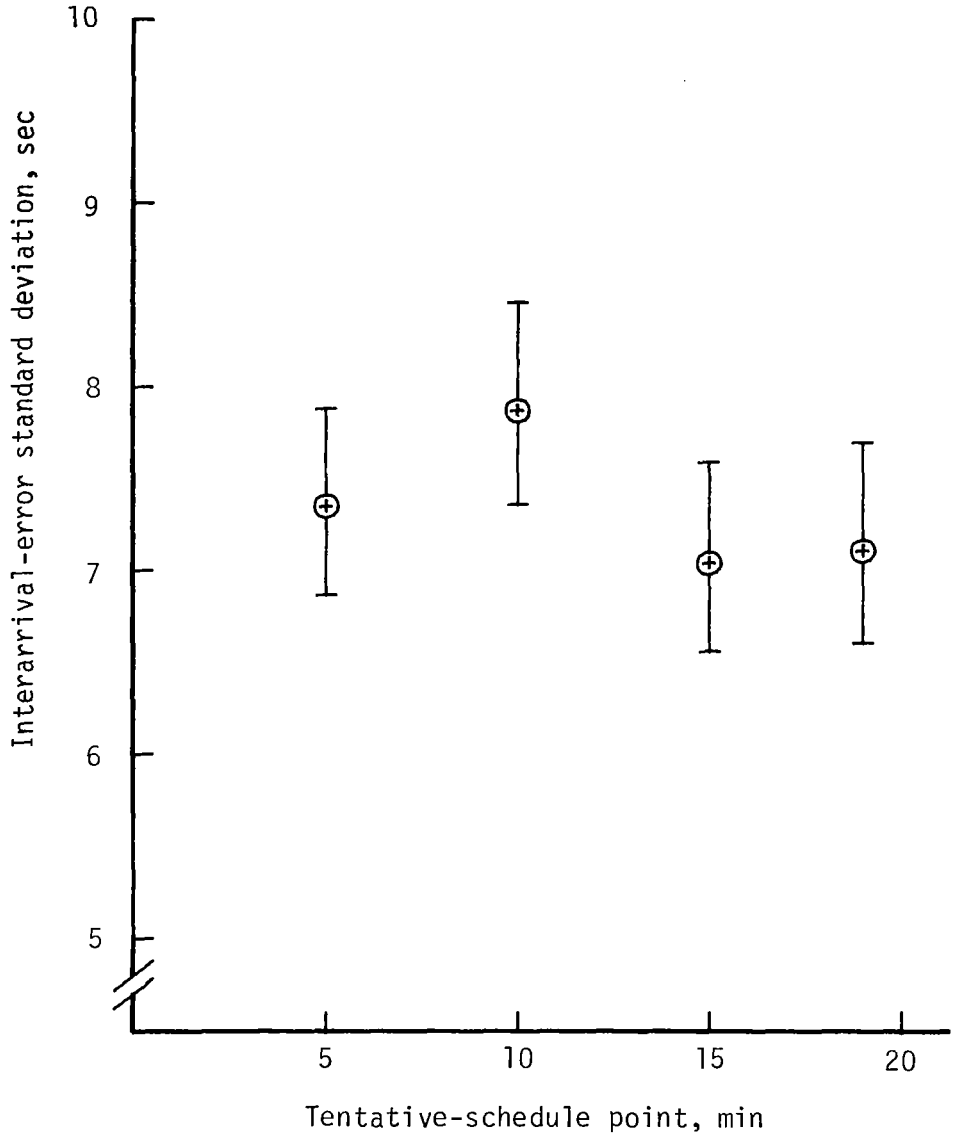

Figure 19.- Interarrival delivery precision for various tentative-schedule times from arrival fix. Final-approach navigation with ±60° MLS; no wind error; confidence interval of 95 percent for values shown.

effect on the delivery precision, as shown by figure 19. This is because of the resequencing capability and the dynamic schedule adjustment which are trying to eliminate interarrival spacing violations.

Although final delivery performance is not affected, the impact on the average flight time from the perimeter of the terminal to the outer marker is significant. Figure 20 shows that the average time of flight from the terminal perimeter is reduced from 29.1 min to 19.4 min by moving the tentative sequencing time from 5 min from the projected arrival (metering) fix time to 19 min. As figure 21 shows, the arrival-fix holding-stack delay time decreases as the time interval between the terminal tentative-schedule time and the metering fix is increased. Figures 22 and 23 illustrate this effect on the holding stack for identical traffic samples.

Analysis indicates the average aircraft flight durations from the 20-min ETA at the metering fix to runway touchdown are all about equal for the various tentative-schedule point runs made. Clearly, the closer the tentative-schedule time is made to the en route metering time, the closer we approach a coupled metering and scheduling system. Therefore, we can conclude that more of the delay for a given traffic arrival rate is taken at the more fuel-efficient higher en route altitude and less is taken at the arrival-fix holding stack if the metering and scheduling are coupled when both are time-based systems. This coupling should definitely be incorporated in the design of a metering and spacing system using fuel-efficient profile descent paths.

In addition to saving fuel, further safety benefits are gained by reducing the average terminal flight time. If delays are taken en route, the result is reduced terminal area traffic congestion and conflict risk. Since the terminal is the flight area of heaviest pilot work load, any reduction in controller directed maneuvers to delay and sequence aircraft is welcomed in the cockpit. Reducing the traffic volume within the terminal allows more controller attention time per aircraft, thus reducing controller stress. Another consideration is that higher en route rather than terminal delay reduces the interaction of high performance traffic with lower flying general-aviation visual flight rules (VFR) traffic.

7.0 REAL-TIME STUDIES

The primary purpose of conducting real-time pilot-in-the-loop experiments was to verify and demonstrate the fast-time results under representative cockpit work-load conditions. A simultaneous joint experiment was conducted to also study the effects of flight-deck systems operating in the M & S environment (ref. 13). This situation subjected the pilot crew to a full range of cockpit tasks from cruise descent to runway touchdown. This prevented the crew, for example, from concentrating on meeting delivery times at the outer marker at the expense of runway alignment and landing preparation.

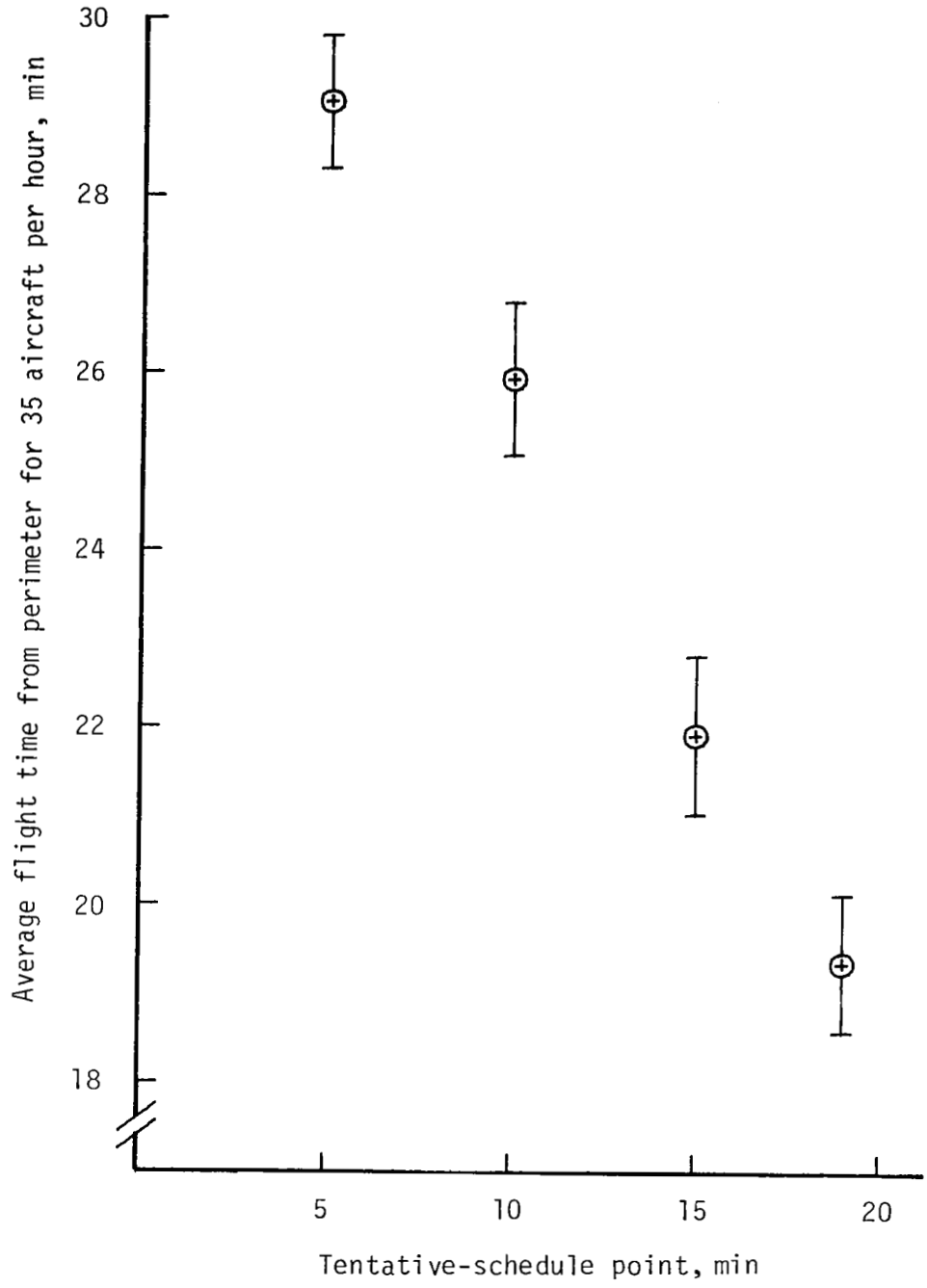

Figure 20.- Average flight time from terminal boundary for various tentative-schedule times from arrival fix. Final-approach navigation with ±60° MLS; no wind error; 35 aircraft per hour; confidence interval of 95 percent for values shown.

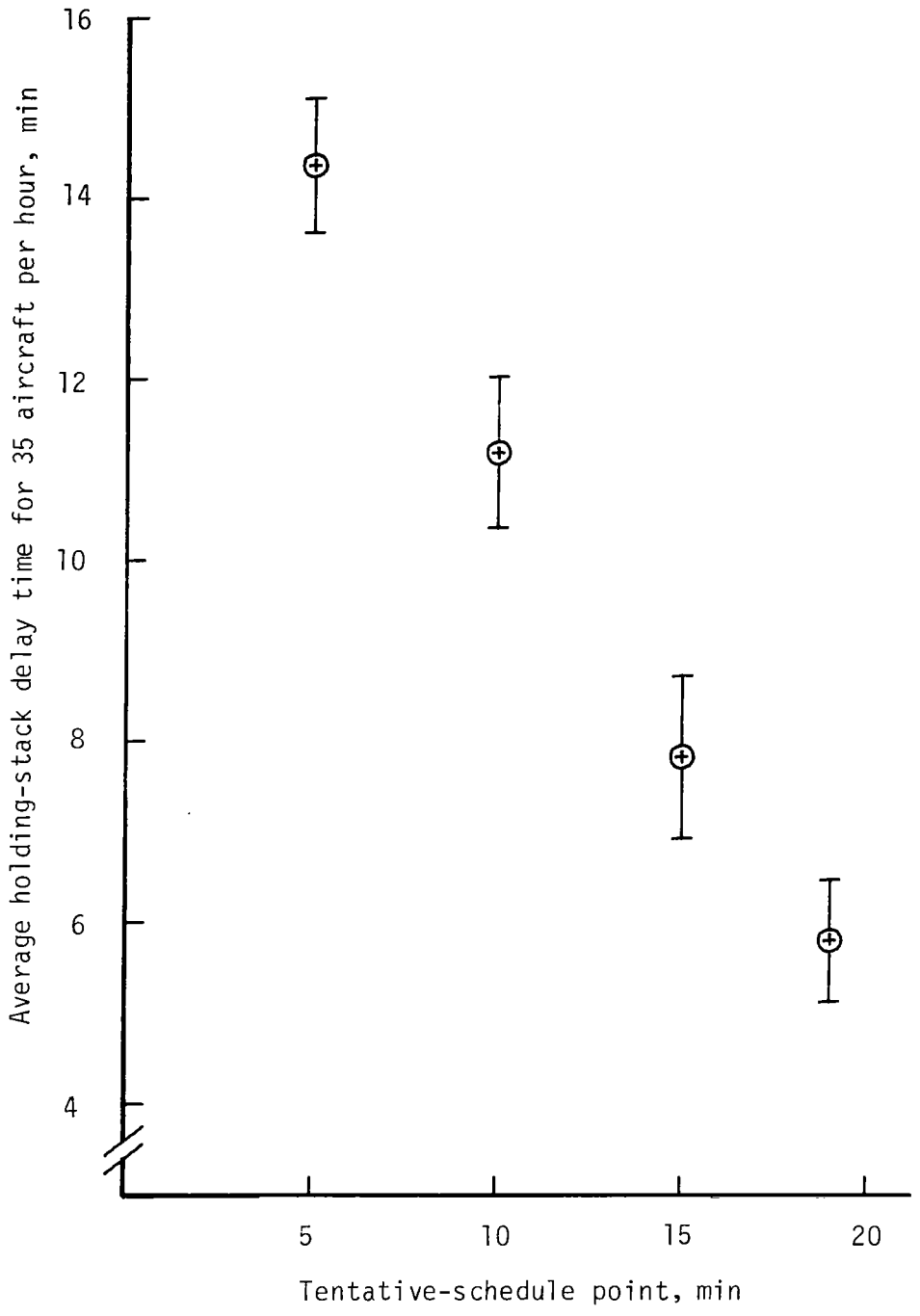

Figure 21.- Average holding-stack delay time for various tentative-schedule times from arrival fix. Final-approach navigation with ±60° MLS; no wind error; 35 aircraft per hour; confidence interval of 95 percent for values shown.

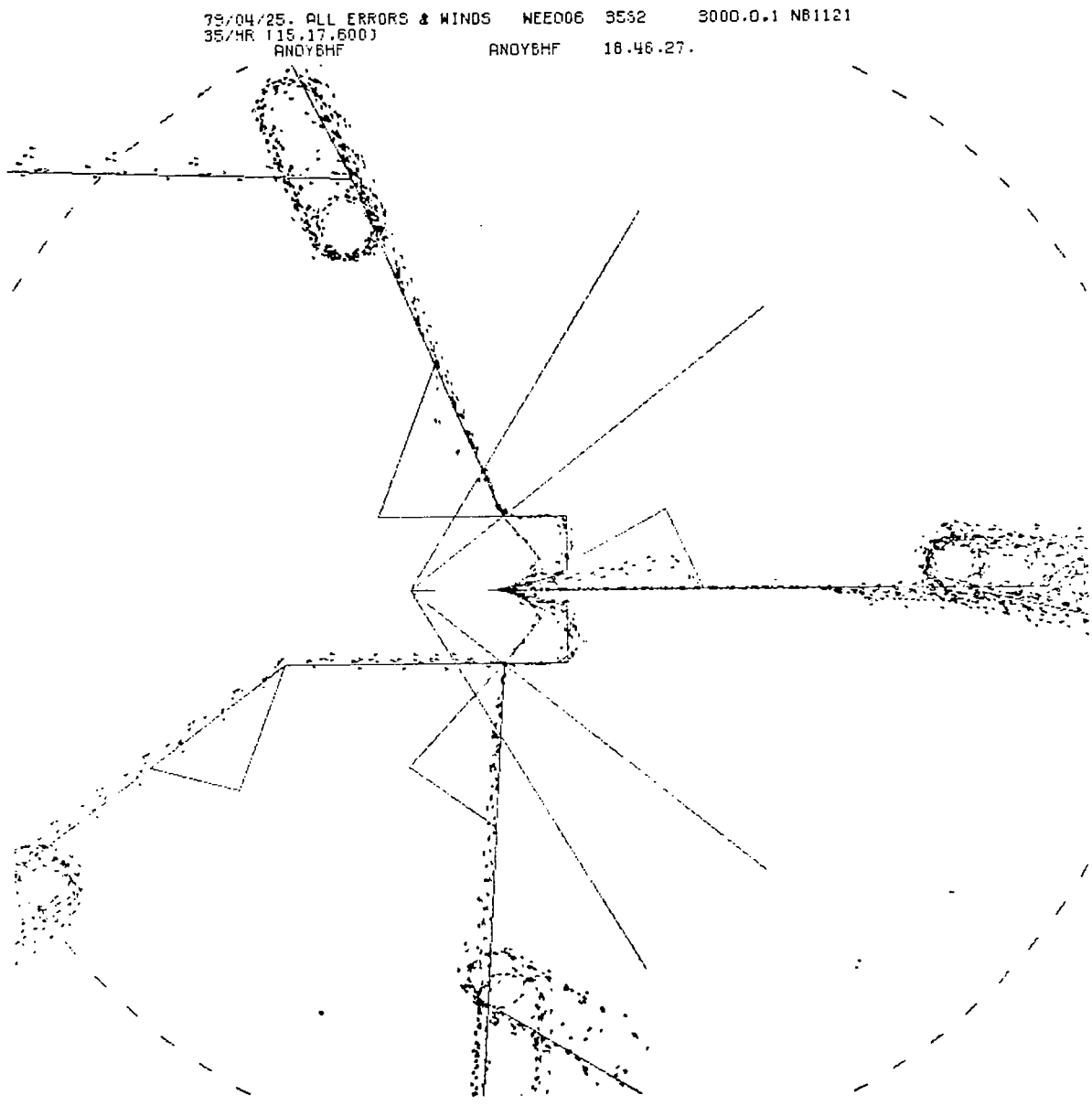

Figure 22.- Traffic flow for 35 aircraft per hour data sample with a 5-min-to-arrival-fix tentative-schedule time. Final-approach navigation with ±60° MLS.

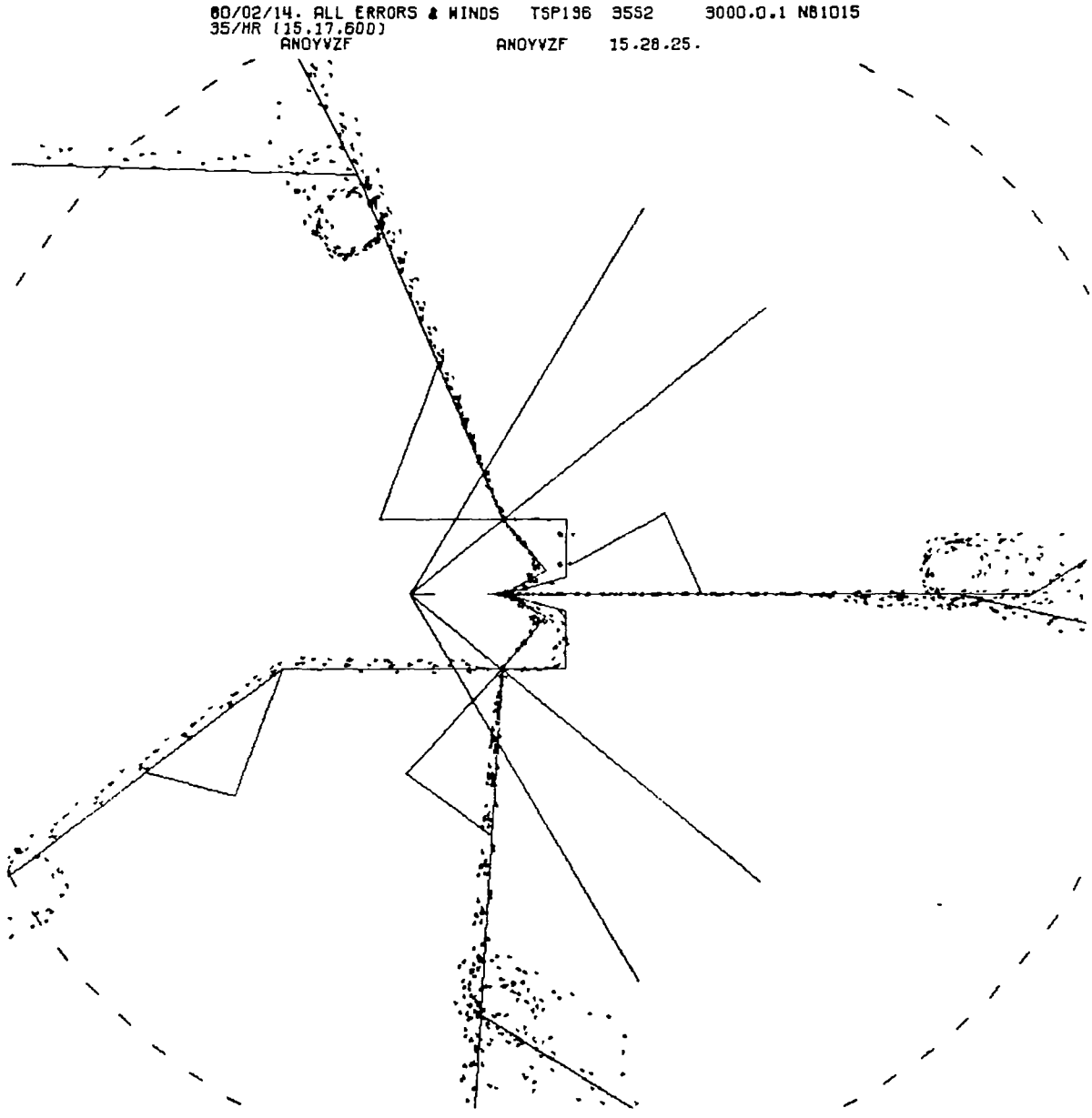

Figure 23.- Traffic flow for 35 aircraft per hour data sample with a 19-min-to-arrival-fix tentative-schedule time. Final-approach navigation with ±60° MLS.

7.1 Cockpit and Crew Considerations

The TCV Aft Flight Deck Simulator was integrated with the Terminal Area Air Traffic Model (TAATM) as described in section 3.5. A person acting as an air traffic controller working together with TAATM (see section 3.6) provided an environment and ATC commands to the simulated cockpit. The cockpit was treated by TAATM in the same way as software-generated aircraft controlled in the TAATM airspace. The task assigned to the research pilots was to fly an assigned STAR (described in section 3.6.2) into the simulated Denver terminal area with the onboard RNAV system. The control-system configuration used was a manual mode made up of the velocity control-wheel steering (VCWS) system and the autothrottle system with the pilot required to fly and land the aircraft manually. The cockpit is equipped with a set of electronic attitude director indicator (EADI) and electronic horizontal situation indicator (EHSI) displays (ref. 9) at both the pilot and copilot positions.

For each of the experimental conditions studied, the equivalent of three complete two-man professional pilot crews were used. Three NASA research pilots were rotated as captain and first officer. These pilots are the crew members normally used for TCV flight experiments and therefore have considerable flight and simulator experience with the TCV aft flight deck system.

7.2 Navigation and Route Factors

As in the fast-time studies, the delivery performance of the ground-based, fixed-path speed-control system using VOR/DME and MLS was compared with the performance of this same system using current VOR/DME and ILS. Both $\pm 40^{\circ}$ MLS and $\pm 60^{\circ}$ MLS coverage were tested in real time to verify fast-time results on the issue of whether wider coverage MLS provided any benefit. As noted in section 2.0, the outer marker was moved 2 n.mi. closer to the runway for the MLS runs. In theory, the MLS's navigation precision should allow close-in runway-centerline intercept thereby reducing the final-approach common path. Later discussion of experimental results will indicate that this gate relocation may lead to real-world problems not originally anticipated.

For the real-time case, time-of-arrival errors at the outer marker for the TCV Aft Flight Deck Simulator can be independently and directly measured but the interarrival-error measurement must use a TAATM (real-time version) generated aircraft as the "other" aircraft of a pair. Since verification is the goal, it would be desirable to isolate the real-time TCV simulator results from any TAATM fast-time effects. In addition, the aircraft interarrival-error distributions are not necessarily equal for the straight-in and DICE-turn routes of the geometry shown in figure 1. With this situation there is a route interaction effect in the interarrival-error measurement which, for the real-time single-aircraft case, cannot be directly measured in the same manner as was done in the all-TAATM, multiple-aircraft fast-time data runs.

Appendix A details a procedure to obtain a strictly real-time TCV simulator estimate of the interarrival system performance. The procedure uses the piloted-cockpit arrival-time-error variances at the outer marker for each type of route to calculate an equivalent-system interarrival delivery value. In addition to

the real-time arrival-error data, the procedure required knowledge of the relative route loadings, which for this study were 40 percent for the straight-in route and 60 percent for the DICE-turn route. This approach yields the interarrival delivery variance or standard deviation which would be expected if the entire traffic sample was comprised of aircraft having the same delivery-error distribution as that obtained from the piloted-cockpit real-time data runs. Consequently, direct comparison with the fast-time interarrival-error delivery precision is possible.

Table 8 gives the number of initial real-time TCV-simulator data runs made for each approach navigation system and type of approach route. Each of the three crews repeated a particular experimental condition three times for a total of nine real-time data runs for that situation.

TABLE 8.- INITIAL REAL-TIME TCV AFT FLIGHT DECK SIMULATOR DATA RUNS

Navigation system	Number of runs for -	
	DICE-turn routes	Straight-in routes
VOR/DME and ILS	9	9
VOR/DME and ±40° MLS	9	9
VOR/DME and ±60° MLS	9	9

7.3 Real-Time Results

7.3.1 Initial data runs.- Figure 24 gives a comparison of the fast-time and real-time interarrival-delivery-precision results. Each of the first three real-time cases shown represents a total of 18 real-time experimental runs, 9 of which were straight-in approaches and the other 9 were DICE-turn approaches. When the real-time results of the straight-in and DICE-turn runs are combined using equation (A20) of appendix A, one unfortunately gets 8 degrees of freedom for the resultant estimate of interarrival-error standard deviation. This produces a fairly large confidence interval and less discrimination between output results from the F-test than if the route results could be directly pooled with 16 degrees of freedom. Since there were no statistically significant differences between the fast-time ±40° MLS and ±60° MLS systems or between those systems in real time, the real-time ±40° MLS and ±60° MLS were combined to get a larger sample to represent the MLS system. The ±40° and ±60° MLS results were pooled at the route level and combined according to the procedure derived in appendix A. This combined MLS real-time result is shown on the far right of figure 24. Table 9 is a summarized comparison of the real-time and fast-time results.

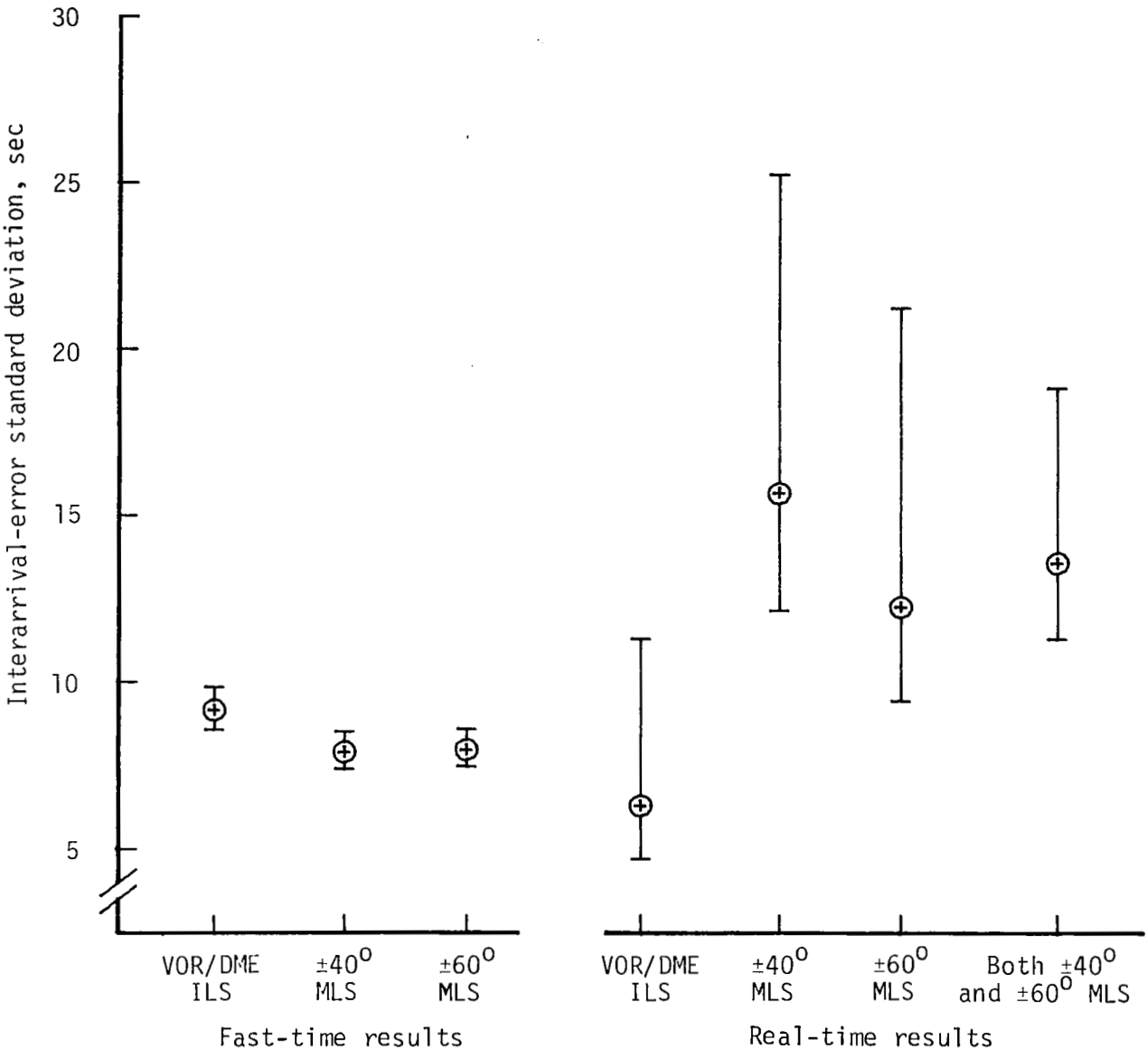

Figure 24.- Fast-time and real-time comparisons of interarrival delivery precision for various final-approach navigation systems. Confidence interval of 95 percent for fast-time data shown and of between 90.25 percent and 99.88 percent for real-time data.

TABLE 9.- SUMMARIZED COMPARISON OF FAST-TIME AND REAL-TIME RESULTS

Navigation system	Standard deviation of interarrival time error for -	
	Real-time runs, sec	Fast-time runs, sec
VOR/DME and ILS	6.3	9.2
VOR/DME and ±60° MLS	12.3	8.0
VOR/DME and ±40° MLS	15.7	7.9
Combined ±40° with ±60° MLS and VOR/DME	13.6	---

The equal-tails F-test was used to determine whether there was discernible difference between the real-time and fast-time interarrival time-error variances at the 5 percent level. The hypothesis tested is

$$H_0: \quad s^2 \text{ (fast time)} = s^2 \text{ (real time)}$$

against

$$H_1: \quad s^2 \text{ (fast time)} \neq s^2 \text{ (real time)}$$

where H_0 is the null hypothesis; H_1 is the alternate hypothesis, and s^2 is the variance. The number of degrees of freedom used were 400 for the fast-time data, 8 for the real-time VOR/DME and ILS, and 16 for the real-time combined ±40° and ±60° MLS. A comparison of the fast-time and real-time results follows with equality indicated when the null hypothesis is not rejected.

Fast-time VOR/DME and ILS = Real-time VOR/DME and ILS

Fast-time ±40° MLS ≠ Real-time combined ±40° and ±60° MLS

Fast-time ±60° MLS ≠ Real-time combined ±40° and ±60° MLS

The real-time VOR/DME and ILS data seem to meet the initial objective of verifying the fast-time results. However, a significant factor is that not only do the real-time MLS results not agree with the fast-time data for the F-test but they also show a worse delivery performance. A comparison of the real-time data with the F-test indicates that even the VOR/DME and ILS real-time interarrival time-error variance was less than that observed for the real-time combined ±40° and ±60° MLS data. This real-time data comparison indicates there is only a 0.032 probability that the interarrival time-error variance of the real-time VOR/DME and ILS is equal to that of the combined ±40° and ±60° MLS.

7.3.2 Gate location.- The question then is what factor is influencing the pilots' actions and overshadowing the accuracy of the MLS system? A check on the sequence of the real-time data runs eliminated a learning curve as the cause. The pilots themselves said they were not aware of a concious reaction to either the MLS or VOR/DME and ILS systems which would explain the real-time data discrepancy. A possible cause was the fact that the gate-to-runway-threshold distance for the MLS system was less than that used in the VOR/DME and ILS runs.

A look at the paths flown for the DICE-turn approaches indicated the following general tendencies: (1) The runway extended path seems to have been intercepted somewhat closer to the gate for the VOR/DME and ILS than for the MLS runs; (2) the turns on the MLS in general are somewhat more shallow with less bank angle than that of the VOR/DME and ILS; and (3) VOR/DME and ILS-system turns appear to more closely match the M & S algorithm assumed radius of turn. Figures 25 and 26 are comparable approaches flown by the same pilot illustrating these tendencies. Another set of 9 DICE-turn runs was made to verify these observations. These runs used the $\pm 60^{\circ}$ MLS system but had the gate placed at the normal ILS position, 12.04 km (6.50 n.mi.) from the threshold, rather than the 8.33 km (4.50 n.mi.) used in the regular MLS runs. The results of previous ILS straight-in runs were combined with the new $\pm 60^{\circ}$ MLS (ILS gate) DICE-turn approaches to obtain an equivalent system-delivery performance. The interarrival-error standard deviation obtained was 9.7 sec and is plotted in figure 27 along with previous real-time runs for comparison.

By using the F-test at the 5-percent level of significance, the hypotheses tested for the real-time results were:

$$H_0: \ s^2 \text{ (VOR/DME and ILS)} = s^2 \ (\pm 60^{\circ} \text{ MLS with ILS gate})$$

against

$$H_1: \ s^2 \text{ (VOR/DME and ILS)} \neq s^2 \ (\pm 60^{\circ} \text{ MLS with ILS gate})$$

and

$$H_0: \ s^2 \text{ (combined } \pm 40^{\circ} \text{ and } \pm 60^{\circ} \text{ MLS)} = s^2 \ (\pm 60^{\circ} \text{ MLS with ILS gate})$$

against

$$H_1: \ s^2 \text{ (combined } \pm 40^{\circ} \text{ and } \pm 60^{\circ} \text{ MLS)} \neq s^2 \ (\pm 60^{\circ} \text{ MLS with ILS gate})$$

Unfortunately, the null hypothesis could not be rejected in either case. Since the interarrival-error standard deviation of the $\pm 60^{\circ}$ MLS with its gate distance extended was between the standard deviation of the VOR/DME and ILS and that of the combined $\pm 40^{\circ}$ and $\pm 60^{\circ}$ MLS, the F-test indicated an equality to both systems.

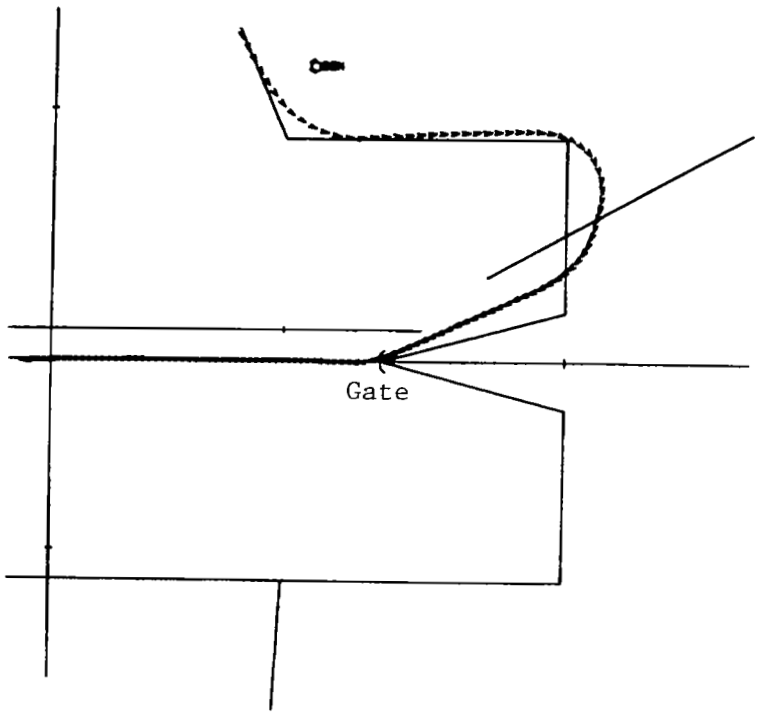

Figure 25.- Approach with VOR/DME and ILS

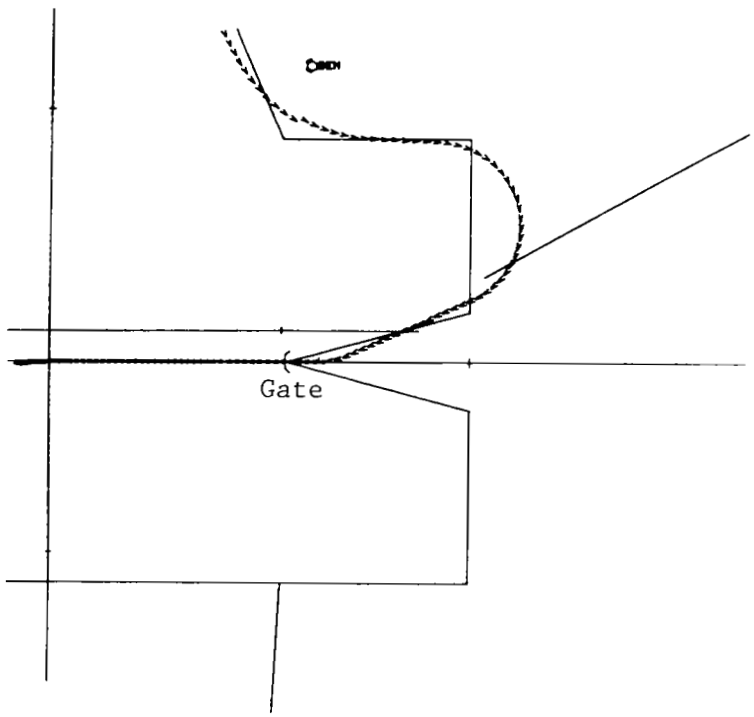

Figure 26.- Approach with VOR/DME and ±40° MLS.

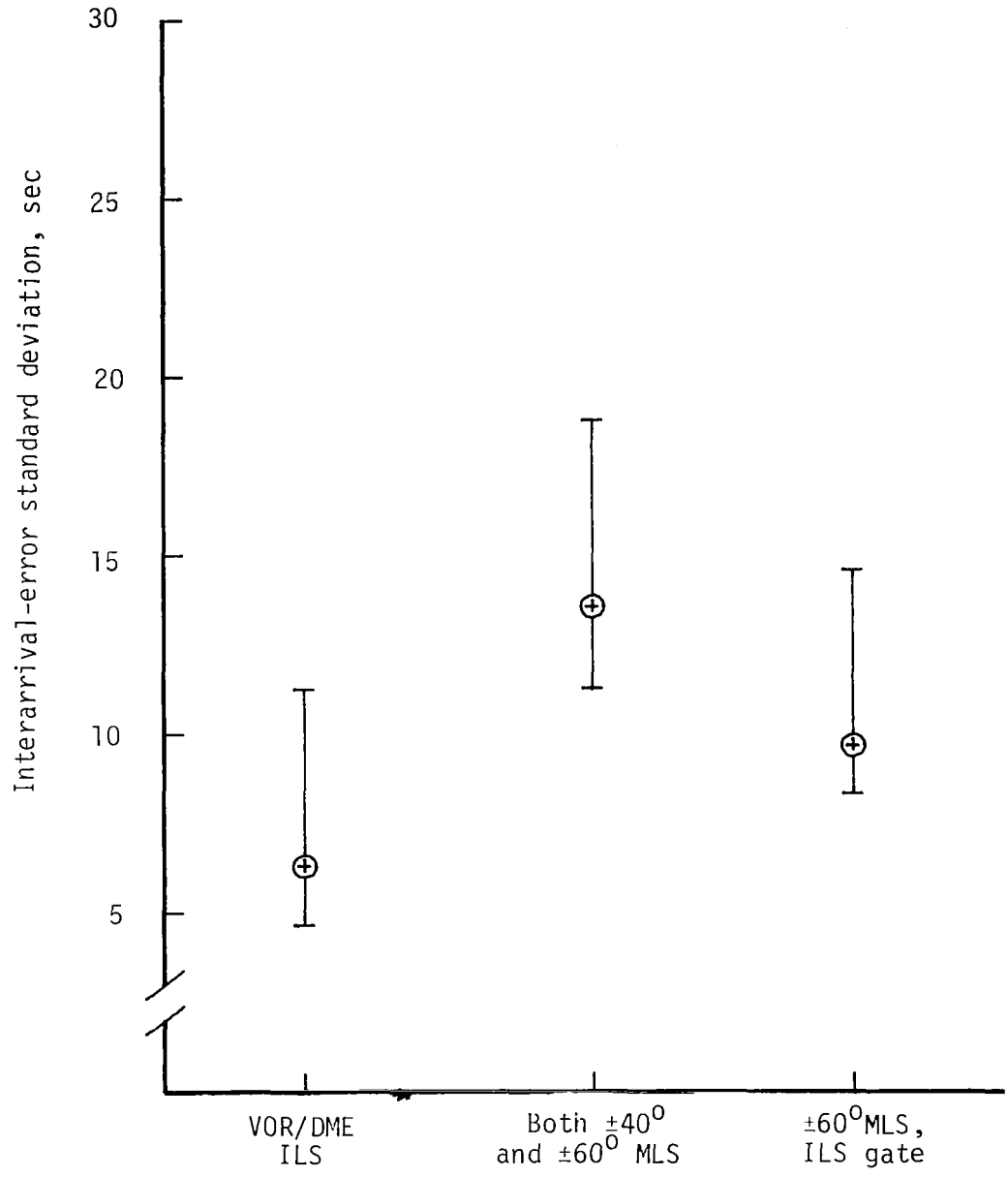

Figure 27.- Interarrival delivery precision of the real-time data runs for various final-approach navigation systems and gate locations. Confidence interval is between 90.25 percent and 99.88 percent for values shown.

In searching further for confirmation of the possible gate-location effect, distances from the gate where the runway centerline was intercepted were measured from approach plots like those of figures 25 and 26. The results of these measurements are summarized in table 10. The measured average intercept distance from the gate for the VOR/DME and ILS system was 0.39 km (0.21 n.mi.), whereas the average distance measured for the combined ±40° and ±60° MLS was 0.89 km (0.48 n.mi.). The average values obtained seem to confirm the contention that the pilots intercepted the runway centerline extension closer to the expected M & S point (the gate) when the gate was farther from the threshold. However, instead of falling relatively close to one of the aforementioned values, the average distance measured for the new ±60° MLS run with ILS gate distance was 0.67 km (0.36 n.mi.). This value is almost halfway between the values measured for the VOR/DME and ILS and for the combined ±40° and ±60° MLS runs. At least these results are consistent with the interarrival-error standard deviation measurements because for those too the ±60° MLS run with ILS gate fell between the other two measurements (fig. 27).

TABLE 10.- MEASUREMENTS OF RUNWAY-CENTERLINE-INTERCEPT DISTANCE FROM THE GATE

Navigation system	Number of runs	Average intercept distance from gate		Standard deviation	
		km	n.mi.	km	n.mi.
VOR/DME and ILS	9	0.39	0.21	1.78	0.96
Combined ±40° and ±60° MLS	18	.89	.48	1.11	.60
±60° MLS with ILS gate	9	.67	.36	.80	.43

Although the magnitude of the average runway-centerline-intercept distance from the gate seems to vary with gate distance from the runway threshold, the small amount of real-time data does not give very good statistical discrimination. For instance, the t-test for differences of mean used on the real-time results failed to indicate a definite difference in intercept distance. The hypothesis used was

$$H_0: \mu_{(\text{VOR/DME and ILS})} = \mu_{(\text{combined } \pm 40^\circ \text{ and } \pm 60^\circ \text{ MLS})}$$

against

$$H_1: \mu_{(\text{VOR/DME and ILS})} \neq \mu_{(\text{combined } \pm 40^\circ \text{ and } \pm 60^\circ \text{ MLS})}$$

where μ is the average intercept distance from the gate. Because of the relatively poor resolution of the t-test resulting from the limited number of real-time runs, the null hypothesis could not be rejected even at a 10 percent level of significance. This same result is, of course, obtained when the average intercept distance for the ±60° MLS with ILS gate is tested against the intercept distance of the other two systems. Unfortunately hypothesis testing with the real-time data available does not permit a definite conclusion as to whether

the runway-centerline-intercept distance from the gate is influenced by the gate distance from the threshold.

Although the data is not as statistically conclusive as desirable, the distance of the gate from the threshold does appear to be a factor in pilot performance. The principal causes of outer-marker-delivery time errors are (1) A pilot does not start a DICE turn at the expected time; (2) the actual turn is not made with the bank angle assumed in the ground algorithm; and (3) the intercept, or merge, point with the extended runway centerline is at a different point than the gate location which was expected with the ground ETA predictive algorithm. The latter two situations appear to be the contributing factors when the gate is moved closer to the runway. A plausible explanation for the worst delivery performance experienced when the gate was moved closer to the threshold is that the primary concern of the pilot at some point in his approach becomes that of configuring and aligning the aircraft for executing the normal, safe IFR landing required in the real-time simulation runs. Given that the pilots had experience with the EHSI map in normal TCV landings, the subconscious reaction may be to align and configure their aircraft for landing at some distance from the threshold which training and experience tells them is required for an acceptable touchdown. Another consideration is that for a given glide slope, runway-alignment maneuvers must be performed closer to the ground when the gate is moved in. All of this considered, we submit that in this investigation, the MLS gate was moved close to or inside the point where the inherent pilot concern for landing impacted the M & S system capability for precise time delivery.

Although the gate-location effect is not predictable in the fast-time study, this effect is an interesting and significant finding in view of the fact that the next generation of commercial aircraft will be equipped with EHSI displays. When the MLS system gets implemented, the possibility of moving in the gate to shorten the common IFR path will be considered (ref. 14). Combine these factors with the pressure to achieve maximum IFR capacity through precise time delivery and the same situation as that experienced in the real-time runs will exist. Although the experimental findings gave an indication of what might be expected, it is possible that further experience and training might modify the impact on delivery performance of moving the MLS gate closer to the threshold.

The effect of an onboard coupled control system in removing pilot variation is a related question. The limited results obtained raised some interesting and important issues which should be addressed in further studies.

8.0 SUMMARY OF RESULTS

The fixed-path (speed-control) metering and spacing (M & S) system described in this report assumes an aircraft two-dimensional area navigation (RNAV) capability. The chief objectives of this investigation were to evaluate the delivery performance of an earlier proposed M & S system and to determine if using the microwave landing system (MLS) for approach guidance improved the system's delivery performance over that of very high frequency omnidirectional range/distance measuring equipment and instrument landing system (VOR/DME and ILS). The primary performance measure used was the aircraft interarrival-error standard deviation at the outer marker. Facilities used in the study are the

Terminal Area Air Traffic Model (TAATM) and the Terminal Configured Vehicle (TCV) Aft Flight Deck Simulator. Both fast-time (batch-mode) and real-time pilot-in-the-loop experiments were conducted. Results of the investigation are discussed in sections 5.0, 6.0, and 7.0. The following is a list of the major findings of the investigation:

1. The fast-time simulation data show that the M & S system aircraft interarrival-error standard deviation at the outer marker is only reduced from 9.2 to 7.9 sec when the $\pm 60^{\circ}$ MLS replaces the VOR/DME as the RNAV data source during final-approach, fine-tuning, DICE-directed maneuvers. Although this is true for the particular geometry studied, further investigation indicated this result reflects the interaction of two types of approach routes. For only straight-in routes there was no verified difference between the interarrival-error standard deviation of the MLS and ILS systems; however, there was a more substantial 2.6-sec advantage for the MLS system if the geometry contained only DICE-turn final-approach routes. The DICE-turn routes have the downwind-base configuration normally used at most terminals.

2. There was no statistically significant difference between the time-delivery performance of the $\pm 40^{\circ}$ MLS system and that of the $\pm 60^{\circ}$ MLS system. For the particular M & S system studied, the wider coverage $\pm 60^{\circ}$ MLS appears to offer no time-delivery precision over the basic $\pm 40^{\circ}$ MLS system. This would appear to be true regardless of the arrival-route geometry as long as the DICE turns are made within MLS coverage.

3. Real-time VOR/DME and ILS data results were consistent with the fast-time data runs but the real-time MLS results indicated a worse delivery performance not only compared with the fast-time data but also compared with the real-time VOR/DME and ILS system as well. The gate location for the ILS runs was placed 12.04 km (6.50 n.mi.) from the threshold. Since the increased accuracy of the MLS system allows precise final intercept, the gate location for the MLS runs was moved 3.70 km (2.00 n.mi.) closer to the threshold in order to reduce the final-approach common path. Though not as statistically conclusive as desirable, the real-time data indicate that moving the gate 2.00 n.mi. closer to the runway threshold may affect the pilot's implementation of final DICE-turn maneuvering needed to achieve M & S delivery precision. It appears that if the gate is moved significantly closer to the threshold than normal, a pilot with the displays available in the TCV aft-flight-deck cockpit may tend to configure and align the aircraft for landing at the same distance he normally does rather than precisely following the M & S-derived fine-tuning DICE instructions. This raises some important issues concerning the interactions of electronic horizontal situation indicator (EHSI) displays, close-in final intercepts, and M & S systems which need further investigation.

4. The en route metering function of the M & S system studied, even though accomplished with a time-based process, only regulates the aircraft arrival rate and operates independently of the terminal schedule process. That is, the terminal scheduler has no knowledge of the metering-scheduled outer-marker time and establishes its own scheduled outer-marker time when the aircraft reaches the terminal's tentative-schedule point. This study demonstrated that most of the arrival (metering) fix holding is transferred to more fuel-efficient, higher altitude en route delay as the terminal's tentative-schedule point is moved

closer to the metering-process time point. Clearly the closer the terminal tentative-schedule time is moved to the en route metering time, the closer a coupled metering and terminal scheduling system is approached. Therefore, coupling should be incorporated in the design of a metering and spacing system utilizing relatively fixed, fuel-efficient, profile descent paths. Also, a reduction in terminal delay not only saves fuel but increases safety by reducing congestion and lowering the work load of both pilots and controllers.

5. The M & S system used in the investigation had several limitations and constraints which are discussed in section 5.0. For example, the ground rules used to assign holds tended to be conservative and inflexible, thereby creating traffic-flow gaps unnecessary for safety. Another constraint noted is the lack of information in the scheduling algorithm on the path-shortening and stretching capability available. To achieve a relatively fixed-path configuration this information, by design, is used only by the schedule-maintenance algorithm as a backup to realize a scheduled marker time. This procedure places highest priority on achieving the scheduled marker time by speed control with secondary priority on holding aircraft and resequencing depending on the aircraft location. The limitations of this process are compounded by the holding limitations mentioned previously. If the scheduler was given more knowledge of the controllability possible with path shortening and stretching, then speed control could still be given highest priority but the secondary priorities would have path change over holding. This should yield smoother traffic flow but at the expense of some variability in aircraft approach paths.

Langley Research Center
National Aeronautics and Space Administration
Hampton, VA 23665
April 6, 1981

APPENDIX A

SYSTEM INTERARRIVAL TIME-ERROR PERFORMANCE FROM SINGLE-AIRCRAFT, ROUTE-DEPENDENT ARRIVAL ERRORS

During the real-time experiments, the TCV Aft Flight Deck Simulator was treated by the Terminal Area Air Traffic Model (TAATM) as merely another aircraft in its airspace to be controlled. The time-of-arrival error at the outer marker for the TCV simulator can be independently and directly measured but any interarrival-error measurements must use a TAATM (real-time version) generated software aircraft as the "other" aircraft of a pair. Since one of the objectives of the real-time investigation was to verify fast-time TAATM performance, it would be preferable to have a "pure" real-time result not affected by the quantity to be verified. In addition, the arrival errors are different for the straight-in and DICE-turn routes used in the geometry. Therefore, there is a route interaction in the interarrival-error measurements which cannot be directly measured in the single-aircraft, real-time data case as was done in the multiple-aircraft, fast-time data runs. The development in this appendix allows the measured, piloted-cockpit error variance at the outer marker for each type of route to be converted to an equivalent-system interarrival-error variance. This interarrival-error variance is what would be expected if all aircraft in the terminal system had the same time-error characteristics as those measured for the TCV simulator.

Arrival Error of Single Aircraft

This section will show how to determine the single-aircraft arrival error when the arrival could be from either of two types of routes, each with its own delivery-error distribution. The arrival errors for each of the types of routes are independent of each other.

Let the route be defined by variable R so that R_1 has an aircraft time error of delivery distribution x such that $f(x|R_1) \sim N(u_1,\sigma_1^2)$, the notation being that the conditional distribution of x given route 1 is a normal distribution with mean u_1 and variance σ_1^2. Similarly, R_2 has an aircraft time-error distribution x such that $f(x|R_2) \sim N(u_2,\sigma_2^2)$ with probability P of each route as follows:

$$P(R_1) = P_1 \tag{A1}$$

$$P(R_2) = P_2 \tag{A2}$$

and

$$P_1 + P_2 = 1 \tag{A3}$$

APPENDIX A

The following sketch illustrates the conditional time-error distributions for each type of arrival route:

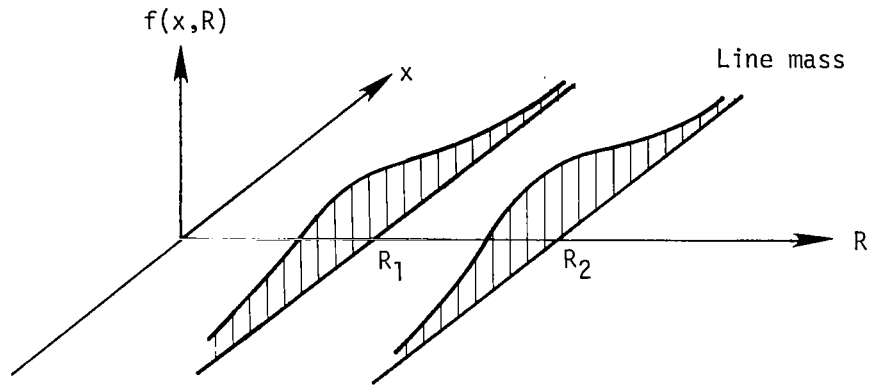

We can now state the following

$$f_x(x) = \sum^{R} f_{x,R}(x,R) = \sum_{i=1}^{2} f_x(x|R_i)P(R_i)$$

$$f_x(x) = P_1 f_x(x|R_1) + P_2 f_x(x|R_2)$$

$$f_x(x) = P_1 \frac{1}{\sigma_1\sqrt{2\pi}} e^{-\left[\frac{(x-u_1)^2}{2\sigma_1^2}\right]} + P_2 \frac{1}{\sigma_2\sqrt{2\pi}} e^{-\left[\frac{(x-u_2)^2}{2\sigma_2^2}\right]} \qquad \text{(A4)}$$

APPENDIX A

The moment-generating function for x, represented by $M_x(t)$, is determined by the following:

$$M_x(t) = E\{e^{tx}\} = \int_{-\infty}^{\infty} e^{tx} f(x)\, dx$$

$$= P_1 e^{tu_1} \int_{-\infty}^{\infty} \frac{1}{\sigma_1 \sqrt{2\pi}} e^{t(x-u_1)} e^{-\left[\frac{(x-u_1)^2}{2\sigma_1^2}\right]} dx$$

$$+ P_2 e^{tu_2} \int_{-\infty}^{\infty} \frac{1}{\sigma_1 \sqrt{2\pi}} e^{t(x-u_2)} e^{-\left[\frac{(x-u_2)^2}{2\sigma_1^2}\right]} dx \qquad \text{(A5)}$$

where $E\{e^{tx}\}$ is the expectation of e^{tx}. By using the known results for normal distributions we get

$$M_x(t) = P_1 e^{[tu_1 + (\sigma_1^2 t^2)/2]} + P_2 e^{[tu_2 + (\sigma_2^2 t^2)/2]} \qquad \text{(A6)}$$

By using the property of $M_x(t)$,

$$E\{x\} = \frac{d}{dt}\left[M_x(t)\right]\Big|_{t=0} = P_1 u_1 + P_2 u_2 \qquad \text{(A7)}$$

and

$$E\{x^2\} = \frac{d^2}{dt^2}\left[M_x(t)\right]\Big|_{t=0} = P_1(\sigma_1^2 + u_1^2) + P_2(\sigma_2^2 + u_2^2) \qquad \text{(A8)}$$

We can now obtain the variance of x (i.e., Var{x}):

$$\text{Var}\{x\} = E(x^2) - [E(x)]^2$$

$$= P_1(\sigma_1^2 + \mu_1^2) + P_2(\sigma_2^2 + \mu_2^2) - (P_1\mu_1 + P_2\mu_2)^2$$

$$\text{Var}\{x\} = P_1\sigma_1^2 + P_2\sigma_2^2 + P_1P_2(\mu_1 - \mu_2)^2 \tag{A9}$$

Interarrival Error of Two Aircraft With Known Arrival-Error Distribution

Given there are two particular aircraft arrivals such that

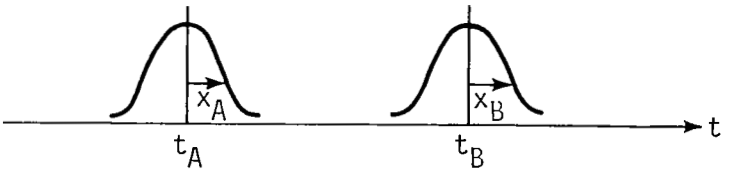

where the first aircraft A has target time t_A and error x_A and the second aircraft B has target time t_B and error x_B.

The errors x_A and x_B are independent:

$$\left.\begin{aligned} x_A &\sim N(\mu_A, \sigma_A^2) = f_x(x|A) \\ x_B &\sim N(\mu_B, \sigma_B^2) = f_x(x|B) \end{aligned}\right\} \tag{A10}$$

Therefore, the interarrival error y between A and B is

$$y = [(t_B + x_B) - (t_A + x_A)] - (t_B - t_A) = x_B - x_A \tag{A11}$$

We can thus say the following:

$$E\{y\} = \bar{x}_B - \bar{x}_A = \mu_B - \mu_A \tag{A12}$$

and

$$\begin{aligned} \mathrm{Var}\{y\} &= E\{y^2\} - [E\{y\}]^2 \\ &= E\{(x_B - x_A)^2\} - [E\{x_B - x_A\}]^2 \\ &= E\{x_B^2\} - \mu_B^2 + E\{x_A^2\} - \mu_A^2 \\ &= \mathrm{Var}\{x_B\} + \mathrm{Var}\{x_A\} \\ \mathrm{Var}\{y\} &= \sigma_A^2 + \sigma_B^2 \end{aligned} \tag{A13}$$

The interarrival error y, given the order and arrival error of each aircraft is

$$f_y(y|A,B) \sim N(\mu_B - \mu_A, \sigma_A^2 + \sigma_B^2) \tag{A14}$$

General Interarrival Error of Two Aircraft

We can now determine the interarrival time error between two aircraft when either aircraft could come from either of two types of routes with each route having its own error distribution. With the symbols already defined and from the following sketch, a new random variable C is introduced such that

$C = 1$	$(A = R_1, B = R_1)$
$C = 2$	$(A = R_1, B = R_2)$
$C = 3$	$(A = R_2, B = R_1)$
$C = 4$	$(A = R_2, B = R_2)$

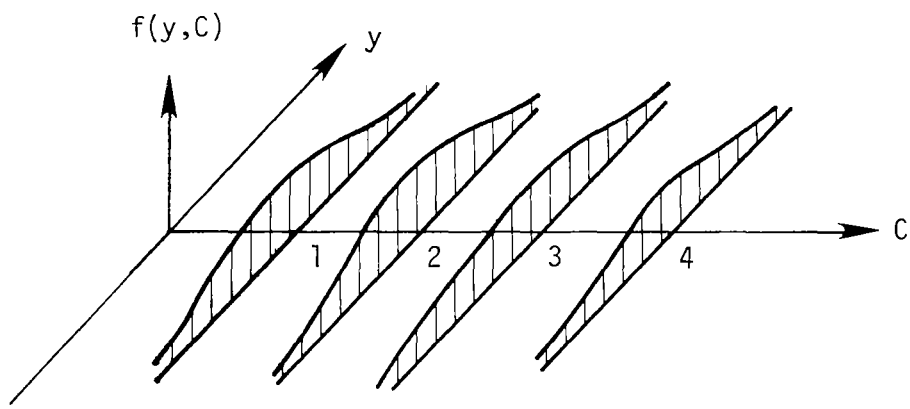

APPENDIX A

For independent arrivals the probability P is defined by:

$$\left.\begin{aligned} P(C = 1) &= P_1{}^2 \\ P(C = 2) &= P_1 P_2 \\ P(C = 3) &= P_1 P_2 \\ P(C = 4) &= P_2{}^2 \end{aligned}\right\} \qquad \text{(A1 5)}$$

If the interarrival time error between two aircraft A and B is defined by y, then

$$\left.\begin{aligned} f_y(y|C=1) &\sim N\left(0,\ \sigma_{c,1}^2\right) \sim N(0,\ 2\sigma_1{}^2) \\ f_y(y|C=2) &\sim N\left(u_{c,2},\ \sigma_{c,2}^2\right) \sim N(u_2 - u_1,\ \sigma_1{}^2 + \sigma_2{}^2) \\ f_y(y|C=3) &\sim N\left(u_{c,3},\ \sigma_{c,3}^2\right) \sim N(u_1 - u_2,\ \sigma_1{}^2 + \sigma_2{}^2) \\ f_y(y|C=4) &\sim N\left(0,\ \sigma_{c,4}^2\right) \sim N(0,\ 2\sigma_2{}^2) \end{aligned}\right\} \qquad \text{(A1 6)}$$

The moment-generating function for y, represented by $M_y(t)$, is determined by the following:

$$M_y(t) = E\{e^{ty}\} = \int_{-\infty}^{\infty} e^{ty} f(y)\, dy = P_1{}^2 \int_{-\infty}^{\infty} \frac{1}{\sigma_{c,1}\sqrt{2\pi}} e^{(ty)} e^{-\left[\frac{y^2}{2\sigma_{c,1}^2}\right]} dy$$

$$+ P_1 P_2 e^{tu_{c,2}} \int_{-\infty}^{\infty} \frac{1}{\sigma_{c,2}\sqrt{2\pi}} e^{t(y-u_{c,2})} e^{-\left[\frac{(x-u_{c,2})^2}{2\sigma_{c,2}^2}\right]} dy$$

$$+ P_2 P_1 e^{tu_{c,3}} \int_{-\infty}^{\infty} \frac{1}{\sigma_{c,3}\sqrt{2\pi}} e^{t(y-u_{c,3})} e^{-\left[\frac{(x-u_{c,3})^2}{2\sigma_{c,3}^2}\right]} dy$$

$$+ P_2{}^2 \int_{-\infty}^{\infty} \frac{1}{\sigma_{c,4}\sqrt{2\pi}} e^{(ty)} e^{-\left[\frac{y^2}{2\sigma_{c,4}^2}\right]} dy \qquad \text{(A1 7)}$$

APPENDIX A

By using the known results from normal distributions we get

$$M_y(t) = P_1^2 e^{\left(\sigma_{c,1}^2 t^2\right)/2} + P_1 P_2 e^{\left[tu_{c,2}+\left(\sigma_{c,2}^2 t^2\right)/2\right]} + P_2 P_1 e^{\left[tu_{c,3}+\left(\sigma_{c,3}^2 t^2\right)/2\right]} + P_2^2 e^{\left(\sigma_{c,4}^2 t^2\right)/2} \quad \text{(A18)}$$

$$M_y(t) = P_1^2 e^{\sigma_1^2 t^2} + P_1 P_2 e^{\left[tu_2 - tu_1 + \left(\sigma_1^2+\sigma_2^2\right)t^2/2\right]} + P_2 P_1 e^{\left[tu_1 - tu_2 + \left(\sigma_1^2+\sigma_2^2\right)t^2/2\right]} + P_2^2 e^{\sigma_2^2 t^2} \quad \text{(A19)}$$

By using these properties of $M_y(t)$,

$$E\{y\} = \frac{d}{dt}\left[M_y(t)\right]\Big|_{t=0} = 0$$

and

$$E\{y^2\} = \frac{d^2}{dt^2}\left[M_y(t)\right]\Big|_{t=0}$$

we can say the following:

$$E\{y^2\} = P_1^2(2\sigma_1^2) + 2P_1P_2\left[\left(\sigma_1^2 + \sigma_2^2\right) + \left(u_2 - u_1\right)^2\right] + P_2^2(2\sigma_2^2) \quad \text{(A20)}$$

Since $E\{y\} = 0$,

$$\text{Var}\{y\} = E\{y^2\} \quad \text{(A21)}$$

Confidence Interval of Interarrival-Error Standard Deviation

This section shows the determination of some interval around the sample estimate of interarrival-error standard deviation σ_y defined by end points

(confidence limits) for which some measure of confidence can be assigned. The terms $\sigma_{L,1}$ and $\sigma_{H,1}$ are the lower and upper bounds of the confidence interval for σ_1 determined from the chi-square such that

$$\left.\begin{aligned}\sigma_{L,1} &= b_{L,1}\sigma_1 \\ \sigma_{H,1} &= b_{H,1}\sigma_1\end{aligned}\right\} \tag{A22}$$

and $\sigma_{L,2}$ and $\sigma_{H,2}$ are the lower and upper bounds for σ_2 so that

$$\left.\begin{aligned}\sigma_{L,2} &= b_{L,2}\sigma_2 \\ \sigma_{H,2} &= b_{H,2}\sigma_2\end{aligned}\right\} \tag{A23}$$

where b_L and b_H are constants determined by the number of data samples or degrees of freedom. Therefore,

$$\left.\begin{aligned}&\sigma_{L,1} \leqq \sigma_1 \leqq \sigma_{H,1} \\ &\text{and} \quad \text{and} \quad \text{and} \\ &\sigma_{L,2} \leqq \sigma_2 \leqq \sigma_{H,2}\end{aligned}\right\} \quad \text{Arrival-error standard deviation confidence bounds}$$

$$\downarrow \quad \downarrow \quad \downarrow \qquad \text{Transform function (eq. (A20))}$$

$$\sigma_{L,y} \leqq \sigma_y \leqq \sigma_{H,y} \qquad \text{System interarrival-error confidence bound}$$

with $\sigma_{L,y}$ and $\sigma_{H,y}$ defining the confidence interval around σ_y. Since all terms are positive, the transform function for the lower bound of σ_y is obtained by substituting the lower bound for each of the routes (i.e., $\sigma_{L,1}$, $\sigma_{L,2}$) into equation (A20) to get

$$\sigma_{L,y} = \{P_1^2[2(b_{L,1}\sigma_1)^2] + 2P_1P_2\left[(b_{L,1}\sigma_1)^2 + (b_{L,2}\sigma_2)^2 + (u_2 - u_1)^2\right] + P_2^2[2(b_{L,2}\sigma_2)^2]\}^{1/2} \tag{A24}$$

A similar substitution yields the upper bound. If the degrees of freedom are the same for the data from both routes, then

$$b_{L,1} = b_{L,2} = b_L \tag{A25}$$

APPENDIX A

By substituting into equation (A24),

$$\sigma_{L,y} = b_L\left\{2P_1{}^2\sigma_1{}^2 + 2P_1P_2\left[\left(\sigma_1{}^2 + \sigma_2{}^2\right) + \left(\frac{\mu_2 - \mu_1}{b_L}\right)^2\right] + 2P_2{}^2\sigma_2{}^2\right\}^{1/2} \tag{A26}$$

Rewriting $\sigma_{L,y}$ in terms of σ_y from equation (A20) yields

$$\sigma_{L,y} = b_L\left[\sigma_y{}^2 - 2P_1P_2(\mu_2 - \mu_1)^2\left(1 - \frac{1}{b_L{}^2}\right)\right]^{1/2} \tag{A27}$$

A similar process for the upper bound gives

$$\sigma_{H,y} = b_H\left[\sigma_y{}^2 - 2P_1P_2(\mu_2 - \mu_1)^2\left(1 - \frac{1}{b_H{}^2}\right)\right]^{1/2} \tag{A28}$$

A procedure to define the end points of a confidence interval has been determined. Now some measure of confidence is needed for the interval. The following sketch illustrates the confidence limits:

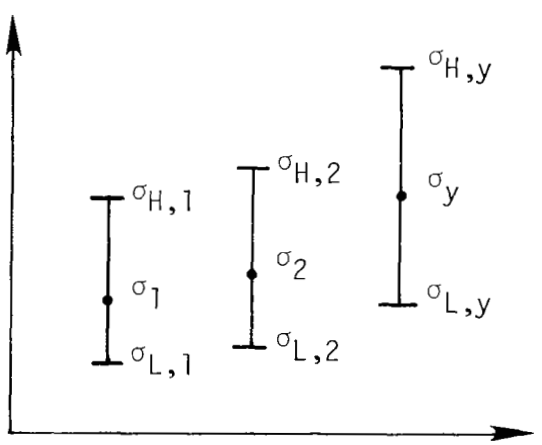

If $P = 0.9500$ that σ_1 is within the interval $\sigma_{L,1} \leq \sigma_1 \leq \sigma_{H,1}$ and also the same probability that σ_2 is within the interval $\sigma_{L,2} \leq \sigma_2 \leq \sigma_{H,2}$, then $P = 0.9025$ that σ_1 and σ_2 are both within their respective confidence bounds. If both $\sigma_{L,1} \leq \sigma_1 \leq \sigma_{H,1}$ and $\sigma_{L,2} \leq \sigma_2 \leq \sigma_{H,2}$ are true, then $\sigma_{L,y} \leq \sigma_y \leq \sigma_{H,y}$ is also ture. See eq. (A24).) If

$P = 0.025$ that $\sigma_1 > \sigma_{H,1}$ and the same probability that $\sigma_1 < \sigma_{L,1}$

and

$P = 0.025$ that $\sigma_2 > \sigma_{H,2}$ and the same probability that $\sigma_2 < \sigma_{L,2}$

then

$P = 6.25 \times 10^{-4}$ that both $\sigma_1 > \sigma_{H,1}$ and $\sigma_2 > \sigma_{H,2}$ and the same probability that both $\sigma_1 < \sigma_{L,1}$ and $\sigma_2 < \sigma_{L,2}$

Therefore, $P = 1.25 \times 10^{-3}$ that σ_1 and σ_2 are both above or both below their respective confidence bounds. From equation (A24), when these conditions exist σ_y is outside its confidence bounds defined by $\sigma_{H,y}$ and $\sigma_{L,y}$. The result of this exercise is a bounded probability interval for the confidence interval of σ_y. If $(\sigma_{L,1},\sigma_{H,1})$ and $(\sigma_{L,2},\sigma_{H,2})$ define 95.000-percent confidence intervals for σ_1 and σ_2, respectively, then σ_y will fall between $\sigma_{L,y}$ and $\sigma_{H,y}$ somewhere between 90.250 to 99.875 percent of the time. This gives a feeling for the confidence which can be placed on the interval defined by $\sigma_{L,y}$ and $\sigma_{H,y}$.

Fast-Time Experimental Verification

The two types of routes used in the system studied were the straight-in BYERS route and the two-DICE-turn approach of all the other arrival routes. As a verification for equation (A20), the aircraft arrival-error standard deviation was obtained from a fast-time, no-BYERS-traffic data run and also for an all-BYERS sample. These arrival-error standard deviations were combined in equation (A20) to obtain the calculated system interarrival-error standard deviation. Figure A1 shows this calculated value was indeed quite close to the measured system interarrival-error standard deviation of the normal-system, all-route data run.

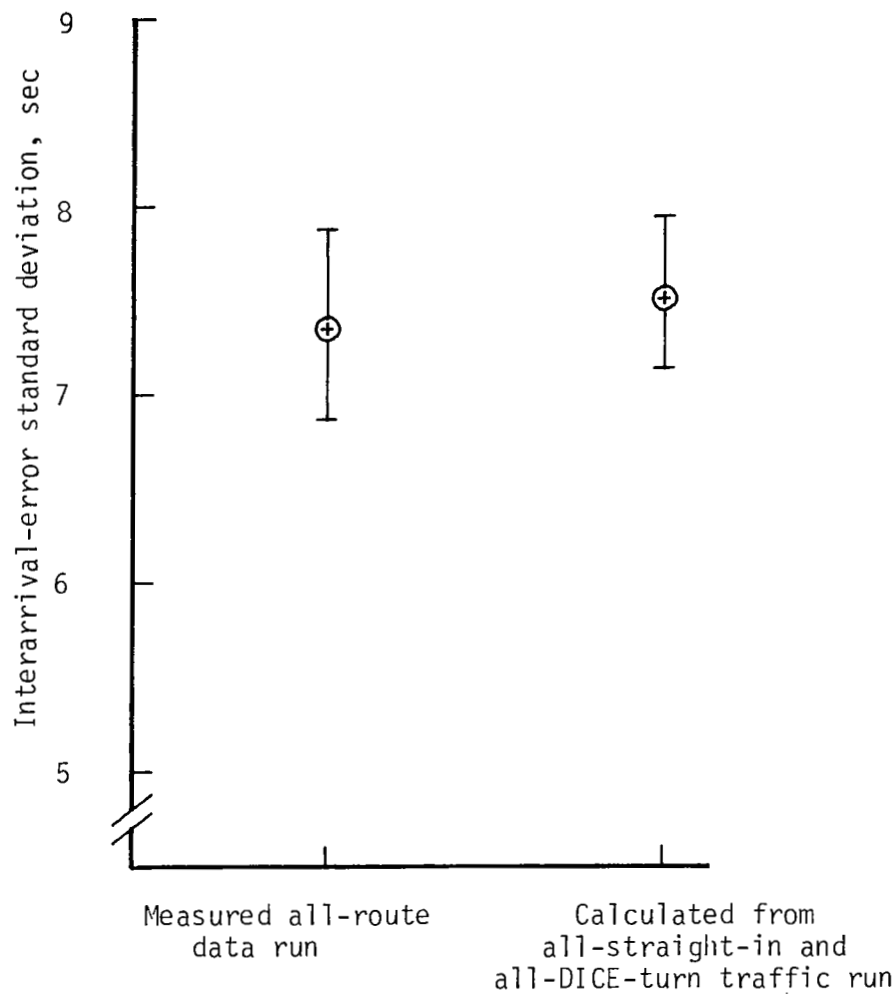

Figure A1.- Interarrival delivery precision from a measured, normal all-route data run and calculated value from arrival precision of an all straight-in and all-DICE-turn traffic sample. Final approach with ±60° MLS navigation; no wind error; confidence interval of 95.00 percent for measured values shown and between 90.25 and 99.88 percent for calculated value.

APPENDIX B

SPEED-CONTROL ALGORITHM (SPDOPT)

The nominal speed on a given flight-path segment for an aircraft is the highest acceptable speed for that aircraft dependent on its position within the terminal area and its performance class. The schedule-maintenance logic of the M & S system, however, is capable of selecting an alternate speed if a speed option has been specified for the segment and if the control logic has determined that an alternate speed should be chosen to achieve a desired SMT. Assuming that V_{I_H} and V_{I_L} are the permissible high and low indicated airspeeds for a given segment, the speed-control algorithm is responsible for choosing an indicated airspeed V_{I_S} such that $V_{I_L} \leqq V_{I_S} \leqq V_{I_H}$.

This appendix details the equations used to calculate a ground speed V_{S_1} equivalent to V_{I_S} when speed control is applied on a segment for a given aircraft. The velocity limitations on the segment and all succeeding segments on the route are presented to the algorithm as indicated airspeeds. In order to perform estimated-time-of-arrival calculations, however, the algorithm first converts these velocities to equivalent ground speeds for the altitudes and wind speeds which are predicted to be encountered by the aircraft. The desired ground speed V_{S_1} calculated with the algorithm is also converted to its equivalent indicated airspeed before delivery as a speed command to the aircraft. The following discussion includes the equations used to convert indicated airspeeds and accelerations to their equivalent ground speeds and accelerations as well as a derivation of the equations used to calculate the desired ground speed V_{S_1}.

Relationship of Indicated and Ground Speeds/Accelerations

By using a second-order approximation, ground speed V_g is defined by the following:

$$V_g = \bar{k}(1 + \alpha h + \beta h^2)V_I - \bar{w} \qquad (B1)$$

where

h	altitude
V_I	indicated airspeed
$\bar{w}$	wind vector
$\bar{k}$	crab-angle an descent-angle correction factor
α,β	constants

APPENDIX B

The approximate ground acceleration a_1 for segment 1 S_1 is

$$a_1 = a_I(1 + \alpha h_0 + \beta h_0^2) + bV_{I_i}(\alpha + 2\beta h_0) \tag{B2}$$

where, for $\bar{k} \cong 1$ and

$$\frac{dV_g}{dt} = \frac{\partial V_g}{\partial h}\frac{dh}{dt} + \frac{\partial V_g}{\partial V_I}\frac{dV_I}{dt}$$

the following definitions apply:

a_I constant indicated-airspeed acceleration (negative acceleration for arrival case), $\frac{dV_I}{dt}$

b constant descent rate, $\frac{dh}{dt}$

α $= 1.48060 \times 10^{-5}$

β $= 9.07143 \times 10^{-11}$

h_0 initial altitude at the start of S_1

V_{I_i} initial indicated airspeed

Likewise, where h_1 is the initial altitude at the start of segment 2 S_2, the approximate ground acceleration a_2 for S_2 is

$$a_2 = a_I(1 + \alpha h_1 + \beta h_1^2) + bV_{I_1}(\alpha + 2\beta h_1) \tag{B3}$$

where V_{I_1} is the maximum possible indicated airspeed on S_1. Similarly, where h_2 is the initial altitude at the start of segment 3 S_3, the approximate ground acceleration a_3 for S_3 is

$$a_3 = a_I(1 + \alpha h_2 + \beta h_2^2) + bV_{I_2}(\alpha + 2\beta h_2) \tag{B4}$$

where V_{I_2} is the maximum possible indicated airspeed on S_2.

APPENDIX B

Definition of Terms Used in No-Speed-Overlap Case on Succeeding Segments

Figure B1 illustrates the no-speed-overlap case for segments S_n for n = 1, 2, and 3 where

V_{i_1} initial ground speed on S_1

V_{H_1} highest possible ground speed on S_1

V_{L_1} lowest possible ground speed on S_1

V_{H_2} highest possible ground speed on S_2

V_{L_2} lowest possible ground speed on S_2

V_{H_3} highest possible ground speed on S_3

V_{S_1} desired ground speed on S_1

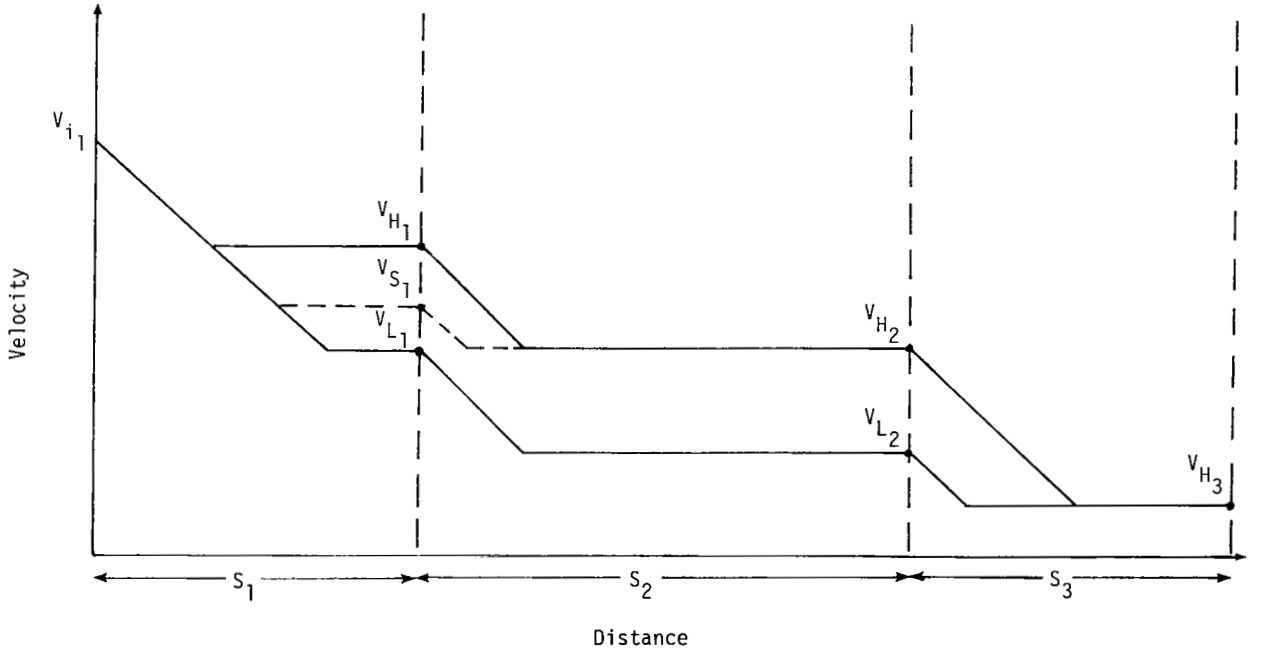

Figure B1.- No-speed-overlap case on succeeding segments.

For this case $V_{i_1} \geq V_{H_1} \geq V_{S_1} \geq V_{L_1} \geq V_{H_2} \geq V_{L_2}$. In all cases $V_{i_1} \geq V_{H_1}$ or V_{H_1} is set equal to V_{i_1}. The determination of V_{S_1} requires the expression of $XLLT(V_{S_1})$ and $ETAR(V_{S_1})$ as explicit functions of V_{S_1}. The following two sections of this appendix define $XLLT(V_{S_1})$ and $ETAR(V_{S_1})$ for this case.

APPENDIX B

Computation of $XLLT(V_{S_1})$ for No Speed Overlap on Succeeding Segments

The term $XLLT(V_{S_1})$ is defined as the time of arrival at the OM if S_1 is flown at V_{S_1} and the other segments are flown at their lowest respective velocities. Figure B2 illustrates the time, distance, and velocity relationships used to determine $XLLT(V_{S_1})$. We can say

$$XLLT(V_{S_1}) = XLLT(V_{H_1}) + \Delta XLLT_{S_1} + \Delta XLLT_{S_2} \tag{B5}$$

where

$$\Delta XLLT_{S_1} = (t_1 + t_2) - (t_1' + t_2') \tag{B6}$$

and

$$\Delta XLLT_{S_2} = (t_3 + t_4) - (t_3' + t_4') \tag{B7}$$

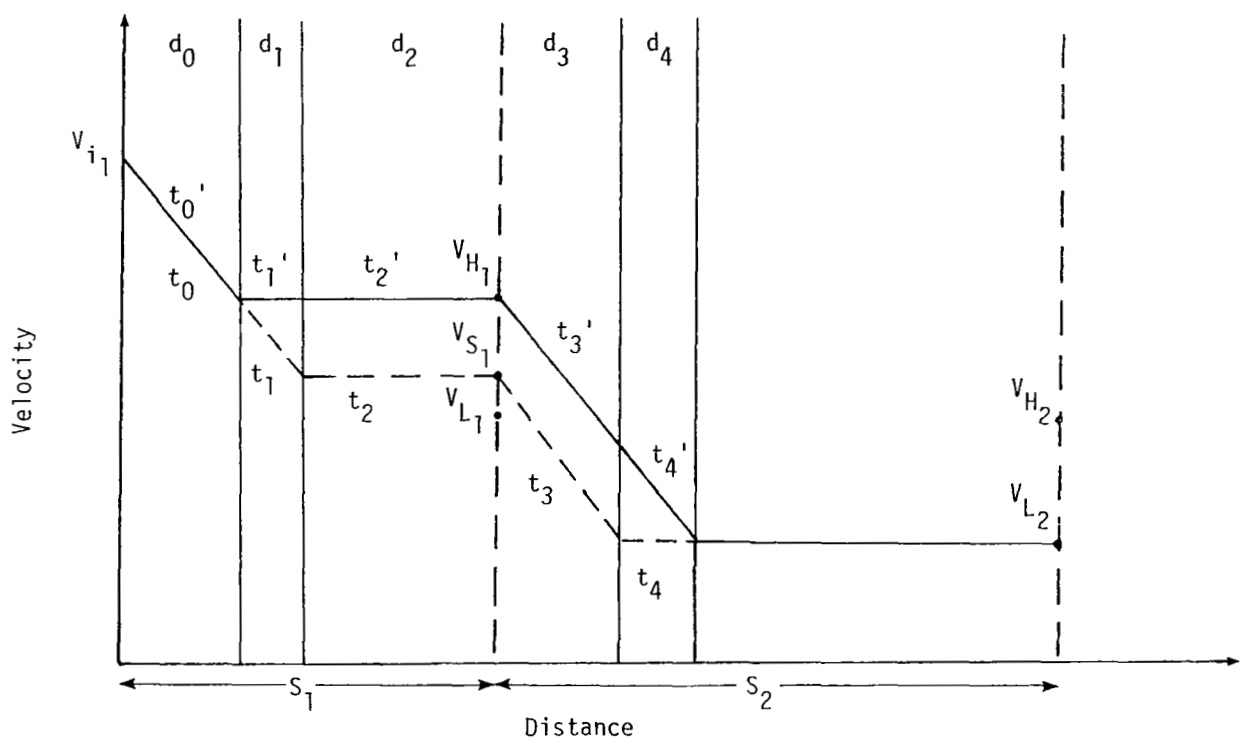

Figure B2.- Time, distance, and velocity diagram to illustrate $XLLT(V_{S_1})$.

APPENDIX B

The value $XLLT(V_{H_1})$ is defined in a manner similar to $XLLT(V_{S_1})$ with the exception that S_1 is flown at V_{H_1}. This value is calculated external to the speed-control algorithm and is presented as an input constant to the routine. By referring to figure B2 and assuming constant acceleration, we can write the following equations:

$$t_0 = \frac{V_{H_1} - V_{i_1}}{a_1} \tag{B8}$$

$$t_1 = \frac{V_{S_1} - V_{H_1}}{a_1} \tag{B9}$$

$$t_2 = \frac{d_2}{V_{S_1}} = \frac{(S_1 - d_0) - d_1}{V_{S_1}} \tag{B10}$$

$$d_0 = \left(\frac{V_{H_1} + V_{i_1}}{2}\right) t_0 = \frac{V_{H_1}^2 - V_{i_1}^2}{2a_1} \tag{B11}$$

$$d_1 = \left(\frac{V_{S_1} + V_{H_1}}{2}\right) t_1 = \frac{V_{S_1}^2 - V_{H_1}^2}{2a_1} \tag{B12}$$

$$t_1' + t_2' = \frac{d_1 + d_2}{V_{H_1}} = \frac{S_1 - d_0}{V_{H_1}} \tag{B13}$$

Therefore,

$$\Delta XLLT_{S_1} = \left(\frac{V_{S_1} - V_{H_1}}{a_1}\right) + \left(S_1 - \frac{V_{H_1}^2 - V_{i_1}^2}{2a_1}\right)\left(\frac{1}{V_{S_1}} - \frac{1}{V_{H_1}}\right) - \left(\frac{V_{S_1}^2 - V_{H_1}^2}{2a_1 V_{S_1}}\right) \tag{B14}$$

Again referring to figure B2 we can write

$$t_3 = \frac{V_{L_2} - V_{S_1}}{a_2} \tag{B15}$$

$$t_4 = \frac{d_4}{V_{L_2}} \tag{B16}$$

$$t_3' + t_4' = \frac{V_{L_2} - V_{H_1}}{a_2} \tag{B17}$$

$$d_3 = \left(\frac{V_{L_2} + V_{S_1}}{2}\right) t_3 = \frac{V_{L_2}^2 - V_{S_1}^2}{2a_2} \tag{B18}$$

$$d_3 + d_4 = \left(\frac{V_{L_2} + V_{H_1}}{2}\right) (t_3' + t_4') = \frac{V_{L_2}^2 - V_{H_1}^2}{2a_2} \tag{B19}$$

$$d_4 = \frac{V_{S_1}^2 - V_{H_1}^2}{2a_2} \tag{B20}$$

Therefore,

$$\Delta XLLT_{S_2} = \frac{V_{H_1} - V_{S_1}}{a_2} + \frac{V_{S_1}^2 - V_{H_1}^2}{2a_2 V_{L_2}} \tag{B21}$$

Computation of $ETAR(V_{S_1})$ for No Speed Overlap on Succeeding Segments

The term $ETAR(V_{S_1})$ is the estimated time of arrival at the outer marker using V_{S_1} on S_1 and the highest velocities permitted on the remaining segments. Figure B3 illustrates the segment-speed relationship used to determine $ETAR(V_{S_1})$. We can write $ETAR(V_{S_1})$ as

$$ETAR(V_{S_1}) = ETAR(V_{H_1}) + \Delta ETAR_{S_1} + \Delta ETAR_{S_2} \tag{B22}$$

The expressions for $\Delta ETAR_{S_1}$ and $\Delta ETAR_{S_2}$ are similar to those used for $\Delta XLLT_{S_1}$ and $\Delta XLLT_{S_2}$ with V_{L_2} replaced by V_{H_2}. By using equation (B14) and by replacing V_{L_2} by V_{H_2} in equation (B21), then

APPENDIX B

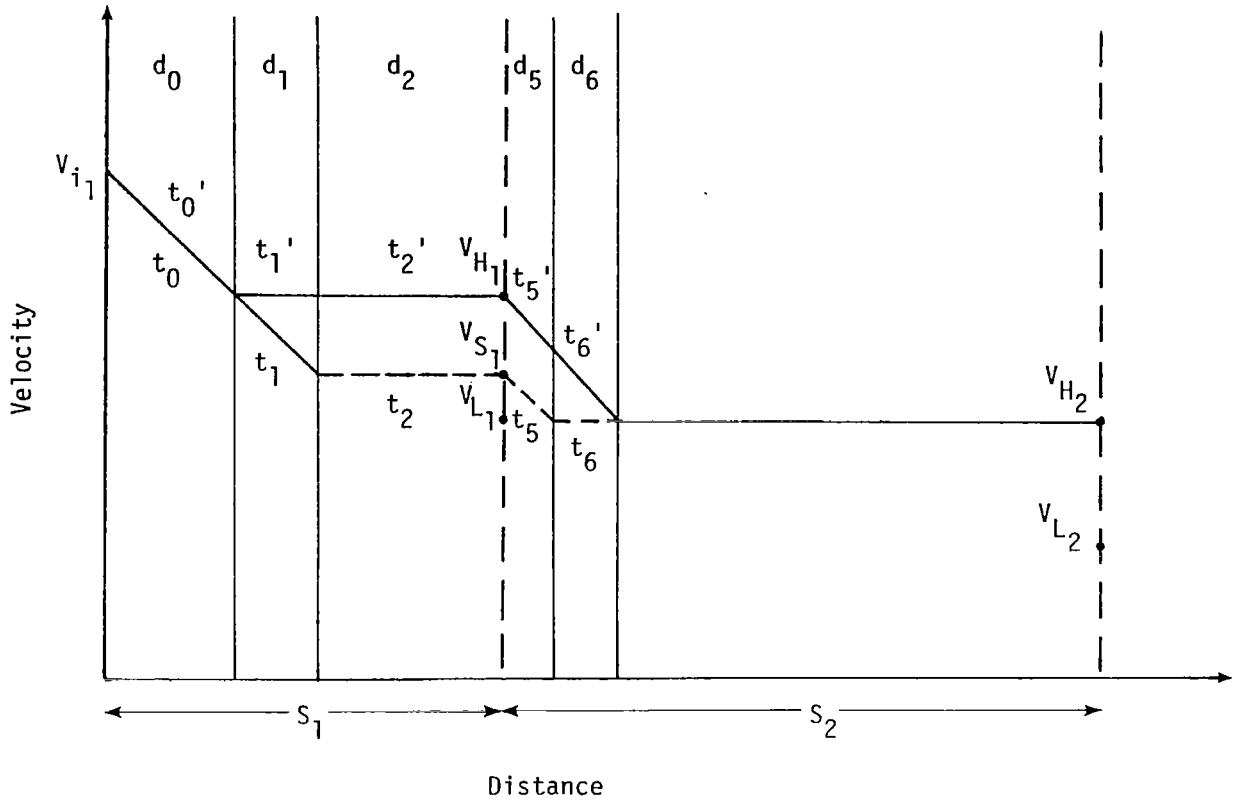

Figure B3.- Time, distance, and velocity diagram to illustrate $\mathrm{ETAR}(V_{S_1})$.

$$\Delta \mathrm{ETAR}_{S_1} = \left(\frac{V_{S_1} - V_{H_1}}{a_1}\right) + \left(S_1 - \frac{V_{H_1}^2 - V_{i_1}^2}{2a_1}\right)\left(\frac{1}{V_{S_1}} - \frac{1}{V_{H_1}}\right) - \left(\frac{V_{S_1}^2 - V_{H_1}^2}{2a_1 V_{S_1}}\right) \tag{B23}$$

and

$$\Delta \mathrm{ETAR}_{S_2} = \frac{V_{H_1} - V_{S_1}}{a_2} + \frac{V_{S_1}^2 - V_{H_1}^2}{2a_2 V_{H_2}} \tag{B24}$$

The value $\mathrm{ETAR}(V_{H_1})$ is defined in a manner similar to $\mathrm{ETAR}(V_{S_1})$ with the exception that S_1 is flown at V_{H_1}. This value is calculated external to the speed-control algorithm and is presented as an input constant to the routine.

APPENDIX B

Solution of Speed Control for No-Speed-Overlap Case on Succeeding Segments

The criteria used to determine the segment velocity V_{S_1} are the following:

$$SMT = XLLT'(V_{S_1}) \tag{B25}$$

and

$$SMT = ETAR(V_{S_1}) + k'[FDELAY(V_{S_1})] \tag{B26}$$

where k' is empirically defined as

$$k' = k + (1 - k)\left(\frac{V_{H_1} - V_{S_1}}{V_{H_1} - V_{L_1}}\right) = \left[k + \frac{(1 - k)V_{H_1}}{V_{H_1} - V_{L_1}}\right] + \left[\frac{-(1 - k)}{V_{H_1} - V_{L_1}}\right]V_{S_1}$$

$$= k_1 + k_2 V_{S_1} \tag{B27}$$

where k_1 and k_2 are the bracketed terms in the preceding equation. The value $XLLT'(V_{S_1})$ is defined as the outer-marker arrival time if S_1 is flown at V_{S_1} and the remaining segments are flown assuming a percentage of the future delay capability $FDELAY(V_{S_1})$ will be used in order to achieve the desired SMT. This percentage approaches 100 percent as V_{S_1} approaches V_{L_1}. The value $FDELAY(V_{S_1})$ is determined with the following equation:

$$FDELAY(V_{S_1}) = XLLT(V_{S_1}) - ETAR(V_{S_1}) \tag{B28}$$

The following drawing illustrates these functions:

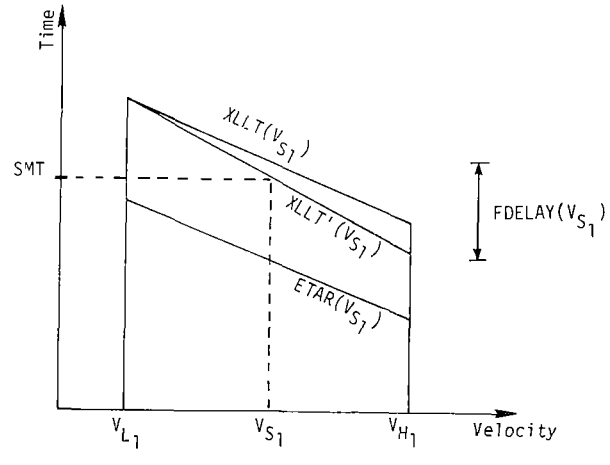

APPENDIX B

If equations (B5), (B14), and (B21) are applied to equation (B28) for $XLLT(V_{S_1})$ and equations (B22), (B23), and (B24) are used for $ETAR(V_{S_1})$, then

$$FDELAY(V_{S_1}) = \left[FDELAY(V_{H_1}) - \frac{V_{H_1}^2}{2a_2}\left(\frac{1}{V_{L_2}} - \frac{1}{V_{H_2}}\right)\right] + \left[\frac{1}{2a_2}\left(\frac{1}{V_{L_2}} - \frac{1}{V_{H_2}}\right)\right]V_{S_1}^2$$

$$= FD_1 + FD_2\left(V_{S_1}^2\right) \tag{B29}$$

where FD_1 and FD_2 are the bracketed terms in the preceding equation. If we substitute equations (B23) and (B24) into equation (B22), the result is

$$ETAR(V_{S_1}) = \frac{1}{V_{S_1}}\left[S_1 + \frac{V_{i_1}^2}{2a_1}\right] + \left[ETAR(V_{H_1}) - \frac{S_1}{V_{H_1}} + \left(\frac{V_{H_1}^2 - V_{i_1}^2}{2a_1V_{H_1}}\right) - \frac{V_{H_1}^2}{2a_2V_{H_2}} - V_{H_1}\left(\frac{1}{a_1} - \frac{1}{a_2}\right)\right] + V_{S_1}\left[\frac{1}{2a_1} - \frac{1}{a_2}\right] + V_{S_1}^2\left[\frac{1}{2a_2V_{H_2}}\right]$$

$$= \frac{ET_1}{V_{S_1}} + ET_2 + ET_3(V_{S_1}) + ET_4(V_{S_1}^2) \tag{B30}$$

where ET_1, ET_2, ET_3, and ET_4 are the bracketed terms in the preceding equation.

Substituting the final forms of equations (B27), (B29), and (B30) into equations (B25) and (B26) yields the following:

$$(V_{S_1})SMT = ET_1 + ET_2(V_{S_1}) + ET_3(V_{S_1}{}^2) + ET_4(V_{S_1}{}^3) + k_1FD_1(V_{S_1}) + k_2FD_1(V_{S_1}{}^2) + k_1FD_2(V_{S_1}{}^3) + k_2FD_2(V_{S_1}{}^4) \quad \text{(B31)}$$

which can be written in the form of a polynomial in V_{S_1}:

$$AV_{S_1}{}^4 + BV_{S_1}{}^3 + CV_{S_1}{}^2 + DV_{S_1} + E = 0 \quad \text{(B32)}$$

where

$$A = k_2(FD_2)$$

$$B = ET_4 + k_1(FD_2)$$

$$C = ET_3 + k_2(FD_1)$$

$$D = ET_2 + k_1(FD_1) - SMT$$

$$E = ET_1$$

Solution of Speed Control for Speed-Overlap Case on Succeeding Segments

Thus far in the discussion we have only considered the situaton for no speed overlap on adjacent segments, that is, $V_{L_1} \geqq V_{H_2}$. For the overlap case in which the speed ranges are equal on segments 1 and 2, that is, $V_{H_1} = V_{H_2}$ and $V_{L_1} = V_{L_2}$, a restriction must be placed on V_{H_2} as a function of V_{S_1} in order to determine a desirable V_{S_1}. The ground rules for the M & S system do not allow for increases in speed on succeeding segments. Therefore, whenever $V_{S_1} \leqq V_{H_2}$, the highest velocity permitted on segment 2 must be equal to V_{S_1}, that is V_{H_2} set equal to V_{S_1}. Figure B4 illustrates this speed overlap case for segments S_n for $n = 1, 2$, and 3. By going through a similar development as was done for the no-overlap case, a polynomial in V_{S_1} can be determined:

$$AV_{S_1}{}^4 + BV_{S_1}{}^3 + CV_{S_1}{}^2 + DV_{S_1} + E = 0 \quad \text{(B33)}$$

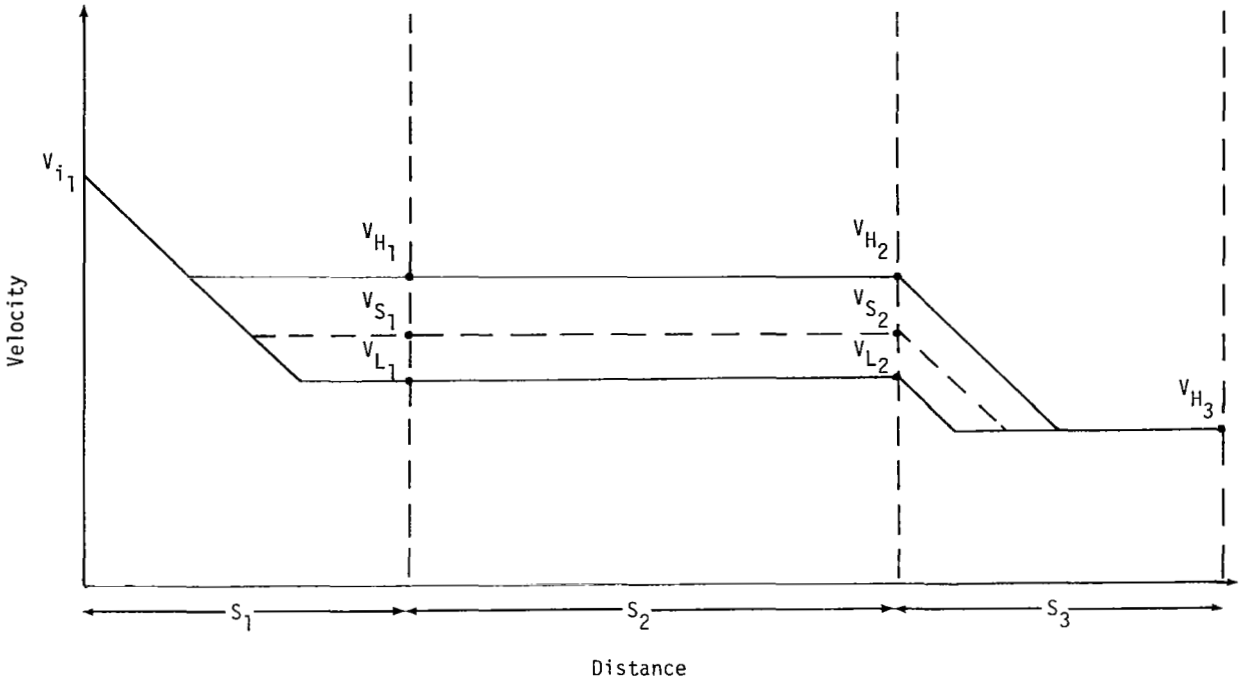

Figure B4.- Speed-overlap case on succeeding segments.

where

$$A = k_2(FD_5)$$

$$B = k_1(FD_6) + k_2(FD_5)$$

$$C = ET_7 + k_1(FD_5) + k_2(FD_4)$$

$$D = ET_6 + k_1(FD_4) + k_2(FD_3) - SMT$$

$$E = ET_5 + k_1(FD_3)$$

for which the following apply:

$$k_1 = k + \frac{(1 - k)V_{H_1}}{V_{H_1} - V_{L_1}}$$

$$k_2 = -\frac{1 - k}{V_{H_1} - V_{L_1}}$$

APPENDIX B

$$c_1 = \frac{1 + \alpha h_2 + \beta h_2^2}{1 + \alpha h_1 + \beta h_1^2}$$

$$FD_3 = \frac{c_1 V_{H_1}^2}{2a_3} - \frac{S_2}{c_1}$$

$$FD_4 = FDELAY(V_{H_1}) + V_{H_1}\left(\frac{1}{a_2} - \frac{c_1}{a_3}\right) - \frac{V_{H_1}^2}{2a_2 V_{L_2}} + \frac{S_2}{c_1 V_{H_1}}$$

$$FD_5 = \frac{c_1}{2a_3} - \frac{1}{a_2}$$

$$FD_6 = \frac{1}{2a_2 V_{L_2}}$$

$$ET_5 = S_1 + \frac{S_2}{c_1} + \frac{V_{i_1}^2}{2a_1} - \frac{c_1 V_{H_1}^2}{2a_3}$$

$$ET_6 = ETAR(V_{H_1}) - V_{H_1}\left(\frac{1}{a_1} - \frac{c_1}{a_3}\right) - \left(S_1 + \frac{S_2}{c_1} - \frac{V_{H_1}^2 - V_{i_1}^2}{2a_1}\right)\frac{1}{V_{H_1}}$$

$$ET_7 = \frac{1}{2a_3} - \frac{c_1}{2a_3}$$

APPENDIX C

GENERAL DESCRIPTION OF RNAV

Position and Track Information

In order to obtain the distances and angles needed in the RNAV equations, the aircraft estimated position must first be determined. With (X_A,Y_A) defined as the actual aircraft position and (X_V,Y_V) as the VOR/DME location, a line can be drawn from the VOR/DME station to the aircraft, as shown in figure C1(a). The angle θ of this line from north N and its length ρ are determined from

$$\left.\begin{aligned} \rho &= \sqrt{(X_A - X_V)^2 + (Y_A - Y_V)^2} \\ \theta &= \frac{\pi}{2} - \tan^{-1}\left(\frac{X_A - X_V}{Y_A - Y_V}\right) \end{aligned}\right\} \tag{C1}$$

If $\Delta\rho$ and $\Delta\theta$ are the combined airborne and ground errors, then the aircraft location errors $(\Delta X,\Delta Y)$ are determined from

$$\begin{bmatrix} \Delta X \\ \Delta Y \end{bmatrix} = \begin{bmatrix} -\rho \sin\theta & \cos\theta \\ \rho \cos\theta & \sin\theta \end{bmatrix} \begin{bmatrix} \Delta\theta \\ \Delta\rho \end{bmatrix} \tag{C2}$$

The location errors are added to the aircraft's position to simulate the raw-navigation measured location (X_M,Y_M):

$$\left.\begin{aligned} X_M &= X_A + \Delta X \\ Y_M &= Y_A + \Delta Y \end{aligned}\right\} \tag{C3}$$

The measured or input cross-track error D_{in} can now be determined. A straight line is drawn between the two waypoints defining the current aircraft path as shown in figure C1(a). The distance S from the measured aircraft position to waypoint 2 is

$$S = \sqrt{(X_M - X_{P,2})^2 + (Y_M - Y_{P,2})^2} \tag{C4}$$

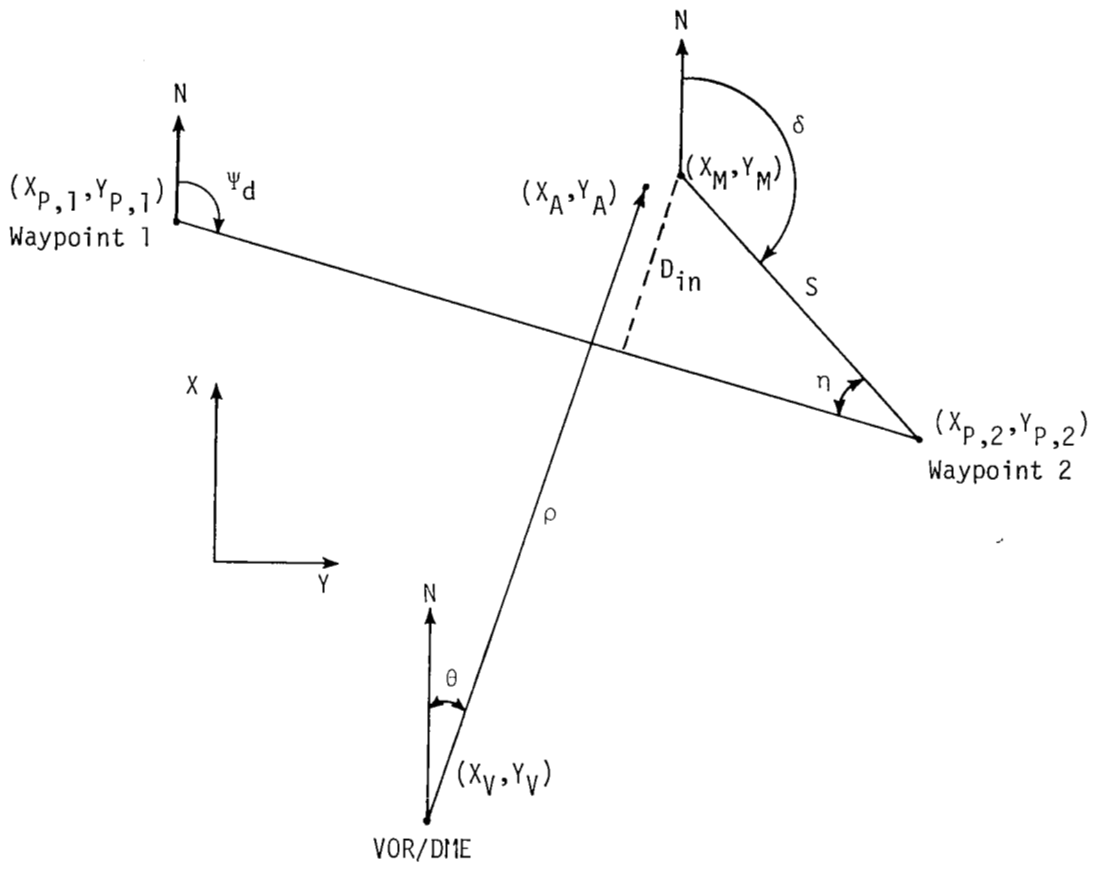

(a) Position location.

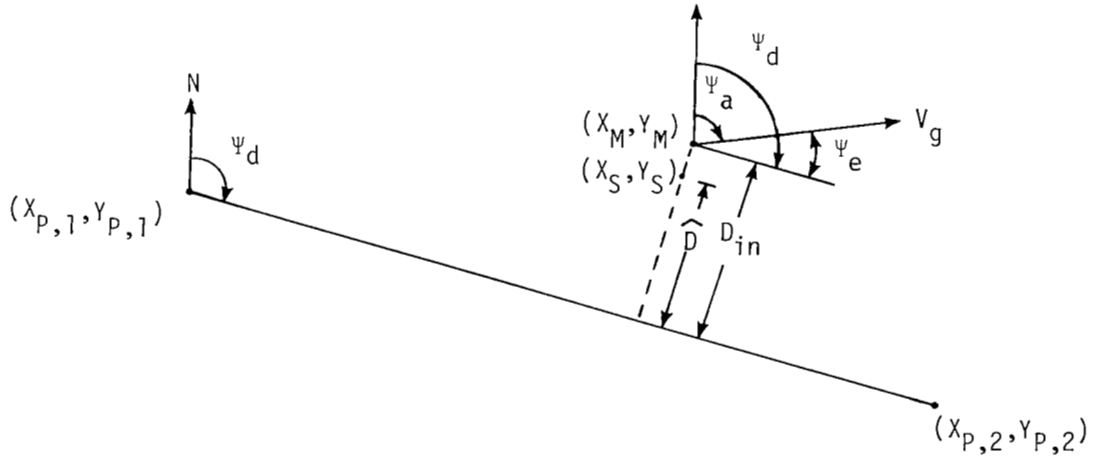

(b) Track-angle error and cross-track rate.

Figure C1.- Area navigation model.

and, the bearing angle δ is

$$\delta = \frac{\pi}{2} - \tan^{-1}\left(\frac{X_{P,2} - X_M}{Y_{P,2} - Y_M}\right) \tag{C5}$$

The bearing angle Ψ_d from waypoint 1 to waypoint 2 is determined from

$$\Psi_d = \frac{\pi}{2} - \tan^{-1}\left(\frac{X_{P,2} - X_{P,1}}{Y_{P,2} - Y_{P,1}}\right) \tag{C6}$$

Angle η is determined from

$$\eta = \delta - \Psi_d \tag{C7}$$

The perpendicular offset of the aircraft's measured position from the course defined by waypoints 1 and 2 is the cross-track error D_{in} and is given by

$$D_{in} = -S \sin \eta \tag{C8}$$

If part of figure C1(a) is slightly redrawn in figure C1(b) with an aircraft ground velocity V_g and a ground-track angle Ψ_a, then a track-error angle Ψ_e is defined as follows:

$$\Psi_e = -(\Psi_d - \Psi_a) \tag{C9}$$

The cross-track deviation rate $\dot{D}$ is

$$\dot{D} = V_g \sin \Psi_e \tag{C10}$$

In order to smooth the raw navigation input data, a simple complementary-type filtering is done on the track position. If the following are defined as

D	aircraft position distance off track
D_{in}	navigation-measured distance off track given by equation (C8)
$\hat{D}_n$	estimated position of D at time n after smoothing

APPENDIX C

$\dot{D}_n$ track-rate information at time n

$D_{p,n}$ predicted position at n using $\hat{D}_{n-1}$ and $\dot{D}_n$

then the smoothing function used is

$$\hat{D}_n = D_{p,n} + K_f(D_{in} - D_{p,n}) = \hat{D}_{n-1} + \Delta t\dot{D}_n + K_f[D_{in} - (\hat{D}_{n-1} + \Delta t\dot{D}_n)] \quad (C11)$$

where Δt is the position update time and K_f is a constant selected at 0.25. The filter action is shown in the following sketch:

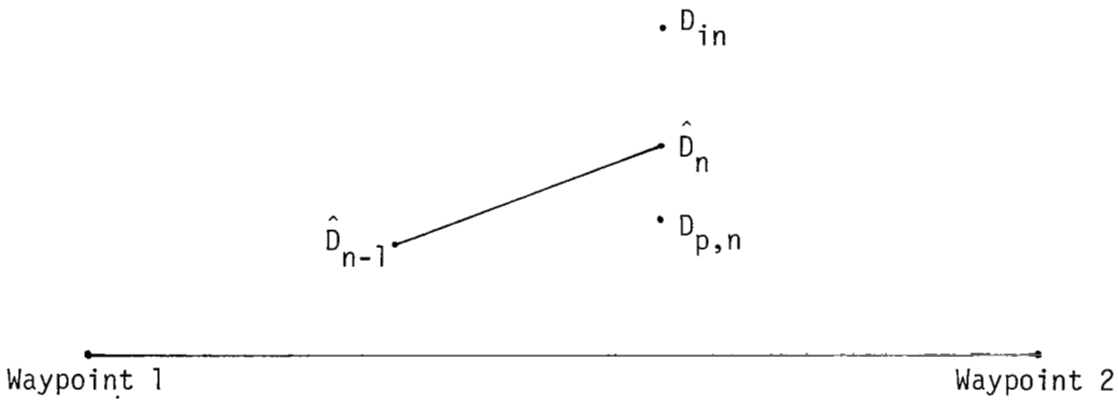

The term $\hat{D}_n$ defines the smoothed estimated position of D at time n, which is shown as (X_S, Y_S) in figure C1(b).

Figure C2 contains the horizontal path control algorithm for RNAV guidance (see ref. 15), for which the following apply:

Φ_d desired bank angle

V_a true airspeed

R radius of curvature when flying a curved path

APPENDIX C

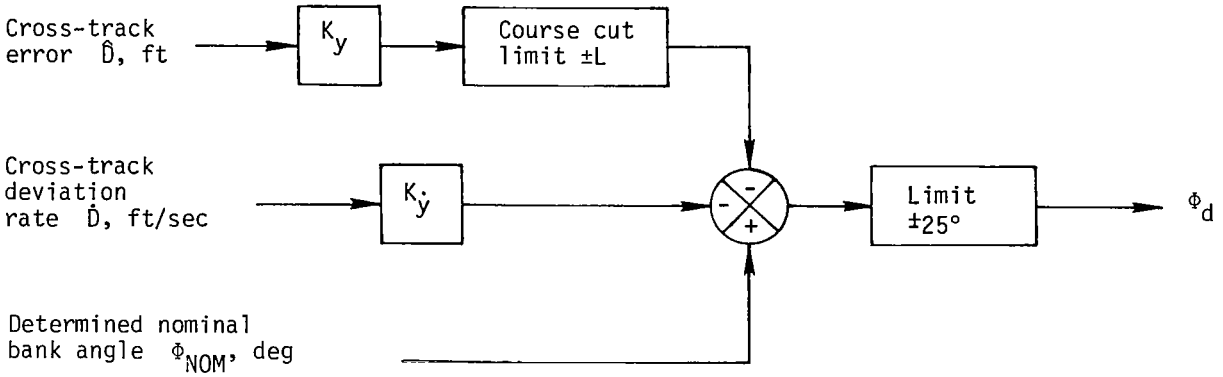

$$\Phi_{NOM} = \begin{cases} \pm 20^\circ \text{ when in RNAV turn} \\ 0^\circ \text{ otherwise} \end{cases}$$

$$K_y = \frac{K_{\dot{y}}^2}{7.12}$$

$$K_{\dot{y}} = \begin{cases} 0.5 \text{ for IAS} < 100 \text{ knots} \\ 0.68 - 0.0018 \text{ IAS for } 100 \leq \text{IAS} \leq 300 \text{ knots} \\ 0.14 \text{ for IAS} > 300 \text{ knots} \end{cases}$$

$$L = V_a K_{\dot{y}} \sin \Psi_I$$

$$\Psi_I = \begin{cases} 30^\circ \text{ for } x < 30^\circ \\ 90^\circ \text{ for } x > 90^\circ \\ x \text{ otherwise} \end{cases}$$

$$x = \frac{470|\hat{D}|}{V_a^2} - 30^\circ$$

Figure C2.- Horizontal path-control algorithm for RNAV guidance. (1 ft = 0.3048 m; constants will change if metric values are substituted.)

APPENDIX C

Turn Anticipation

For an RNAV aircraft flying from waypoint A to B to C as in figure C3, the objective of turn anticipation is to start the aircraft turning toward waypoint C at a point F such that the aircraft flies a smooth path toward segment BC with no overshoot of the course. As the aircraft flies from A to B (fig. C3) the following calculation is made to determine the distance d from B to initiate roll-in to the nominal bank angle Φ_{NOM} of the turn:

$$d = R \tan\left(\frac{\Delta\Psi}{2}\right) + r_i \tag{C12}$$

where $\Delta\Psi$ is the change in heading between segments AB and BC, R is the radius of curvature defined by

$$R = \frac{V_a^2}{g \tan \Phi_{NOM}} \tag{C13}$$

for $\Phi_{NOM} = 20^o$, and r_i is the roll-in distance to establish the nominal bank angle:

$$r_i = \Delta t V_a \tag{C14}$$

with Δt as the time required to roll into nominal bank:

$$\Delta t = \frac{\Phi_{NOM}}{\dot{\Phi}_{Limit}} \tag{C15}$$

where $\dot{\Phi}_{Limit} = 4$ degrees per second. A roll-out distance is also established to make a smooth merge with course BC. A normal bank angle of 0^o is desired at the start of the straight segment if the aircraft is on course and track. The distance r_o shown in figure C3 is the distance along the curved path from the end of the turn when roll-out is started:

$$r_o = \frac{\Phi_{NOM}}{\dot{\Phi}_{Limit}} V_a \tag{C16}$$

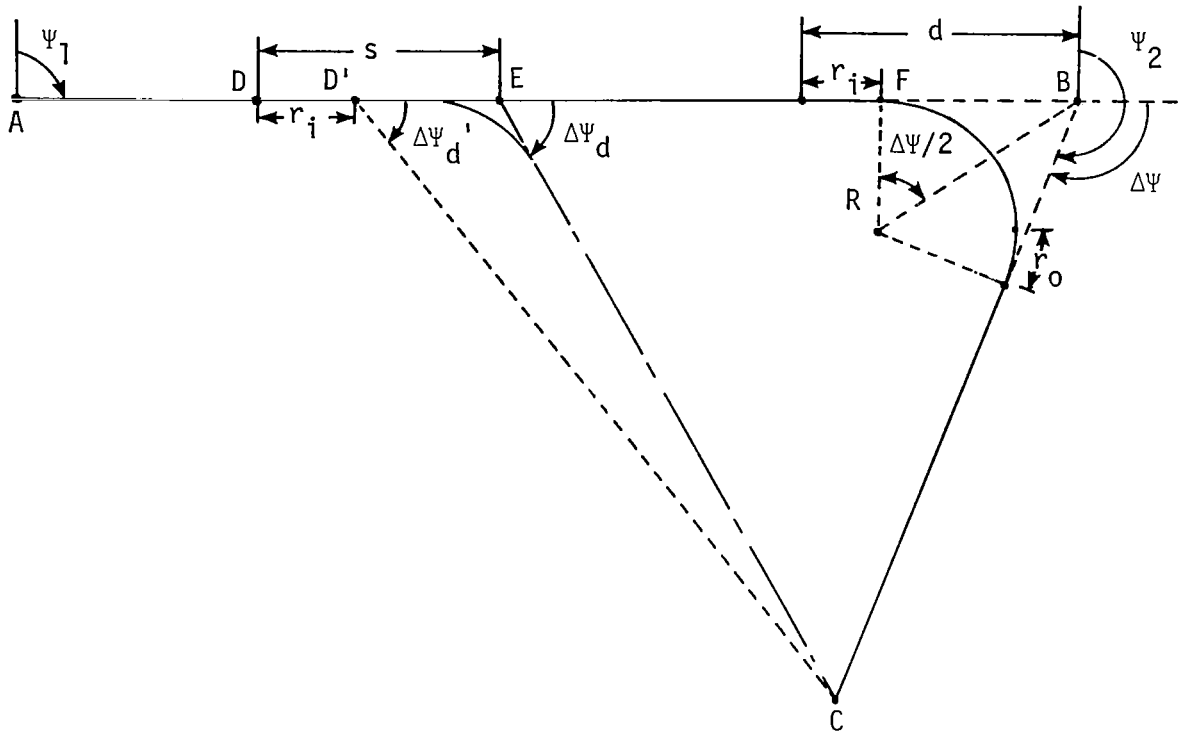

Figure C3.- Geometry of RNAV turn-anticipation and direct-to procedure.

Direct-To Function

When a direct-to message is issued to the aircraft directing it to turn immediately to C from its path AB, a calculation similar to that done for turn anticipation is performed. Equation (C12) is executed in an iterative process to determine distance s in figure C3. In the iterative process a line is constructed from the point D' to the point C. The point D' is achieved by adding the roll-in distance r_i to the point D where the direct-to message occurs. Then equation (C12) is executed using $\Delta\Psi_d'$ instead of $\Delta\Psi$. This yields the first approximation for s. This value for s is then added to point D yielding a first approximation for E. The process is then repeated by constructing the line from E to C and continuing as before until the process has been performed five times. The purpose of this iteration is to obtain a good approximation for s. The function converges fairly rapidly, so five iterations were deemed adequate.

A good estimate of s is needed because a direct-to RNAV constructs an imaginary waypoint a distance s from point D as shown in figure C3. This point is constructed so that the aircraft beginning its turn at D will fly to the path EC similar to the way it does toward BC in turn anticipation, that is, a smooth path having no overshoot.

APPENDIX D

METERING AND SPACING LOGICAL FLOW CHARTS

Logical flow charts for the major M & S sequencing, scheduling, and schedule-maintenance control routines are presented in this appendix. Explanations of the speed-option and DICE procedures are contained in the main body of the report. The logical flow charts which are included consist of the following:

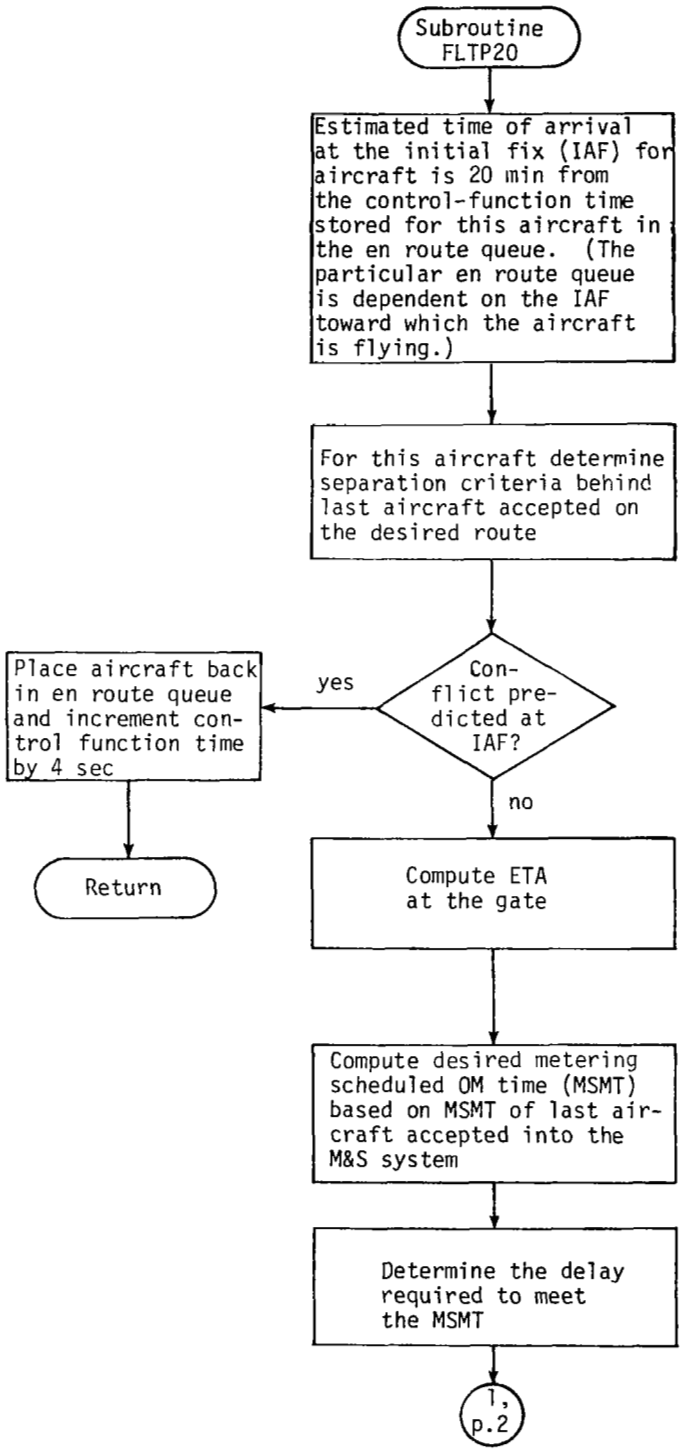

(a) Page 1 of FLTP20 subroutine.

Figure D1.- Twenty-minute flight-plan message (FLTP20).

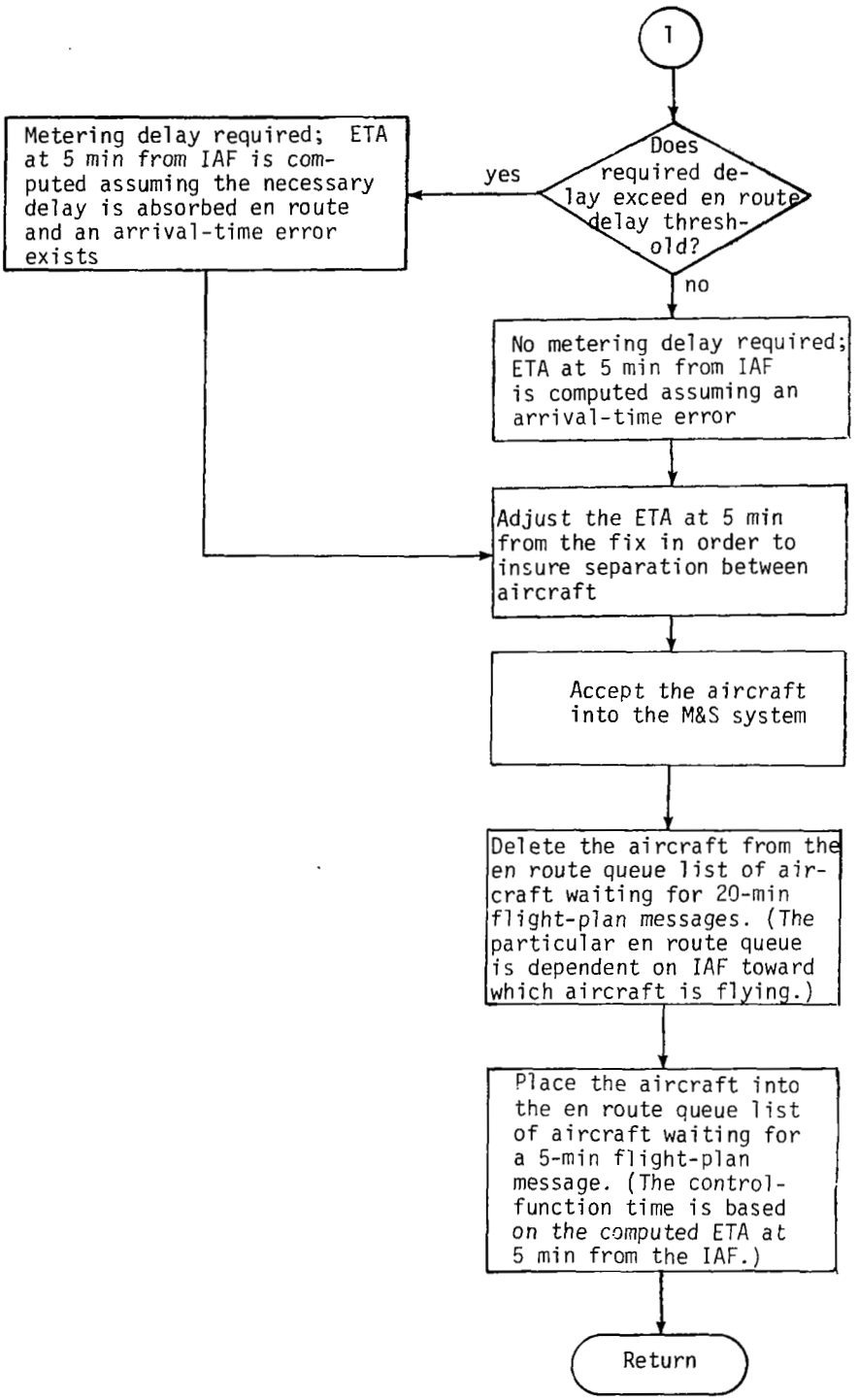

(b) Page 2 of FLTP20 subroutine.

Figure D1.- Concluded.

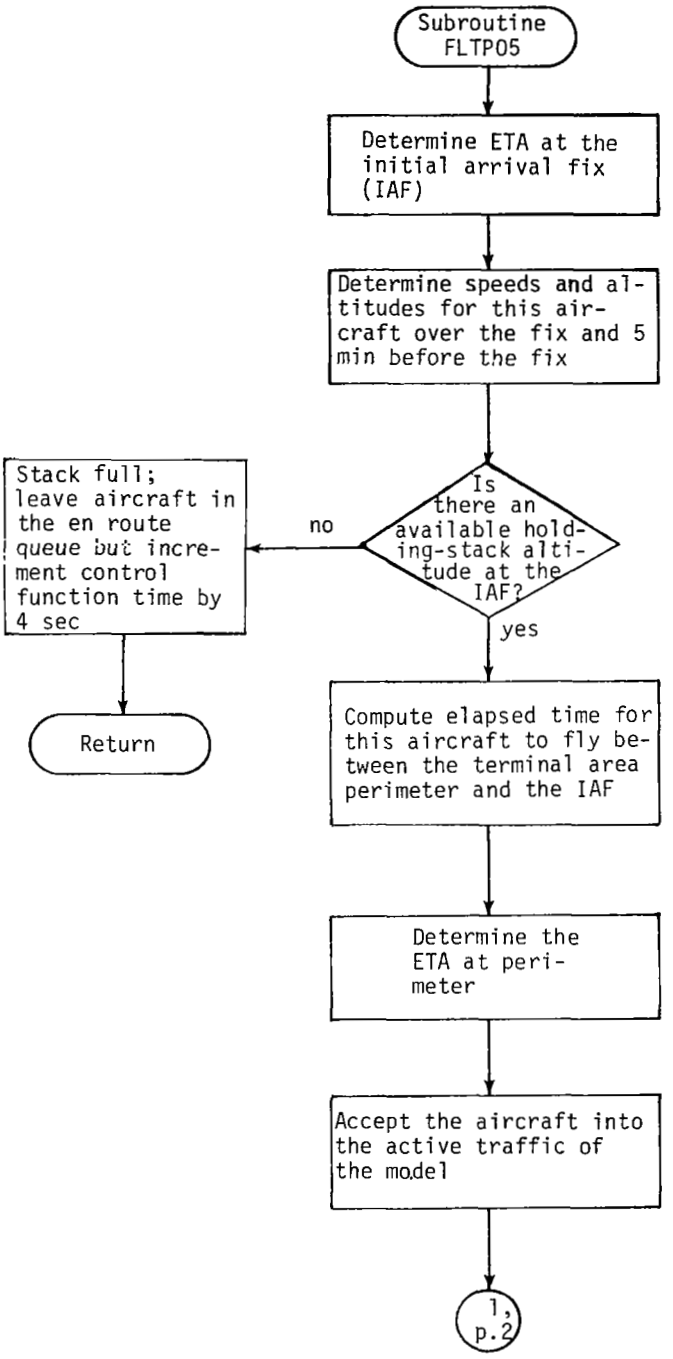

(a) Page 1 of FLTP05 subroutine.

Figure D2.- Five-minute flight-plan message (FLTP05).

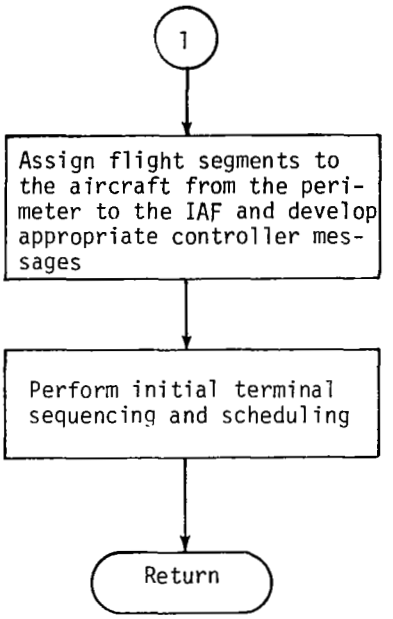

(b) Page 2 of FLTP05 subroutine.

Figure D2.- Concluded.

APPENDIX D

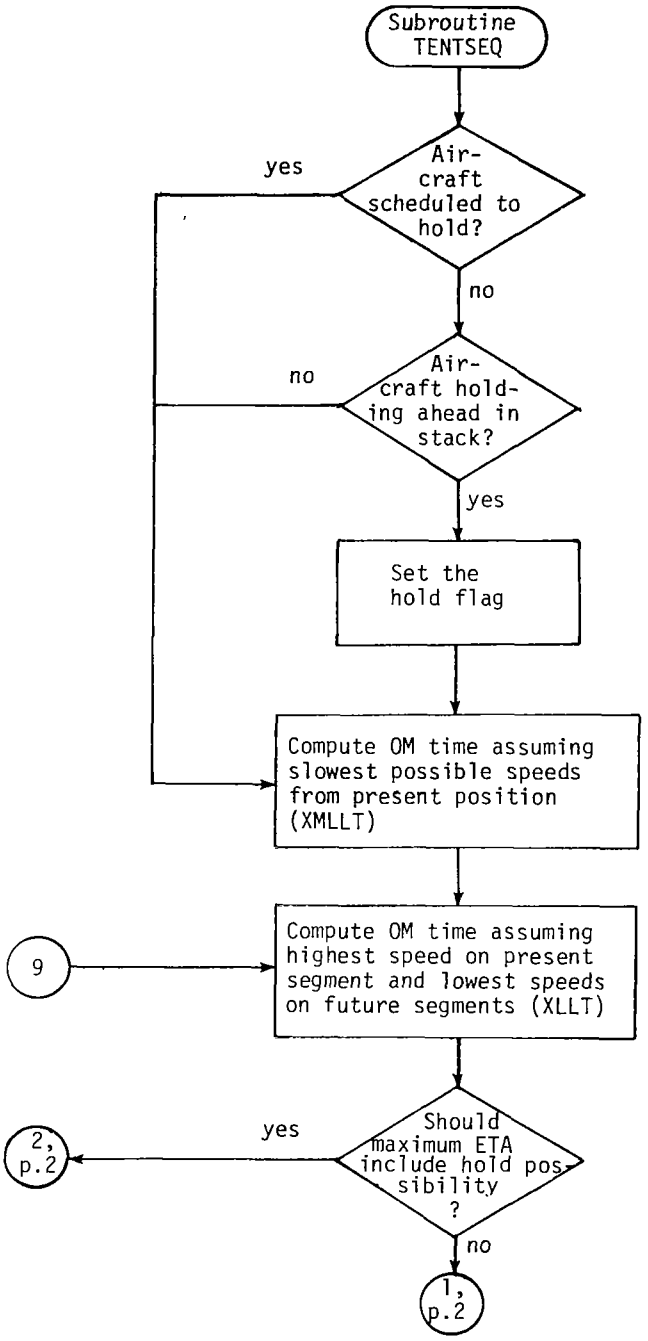

(a) Page 1 of TENTSEQ subroutine.

Figure D3.- Master control routine for schedule determination and maintenance (TENTSEQ).

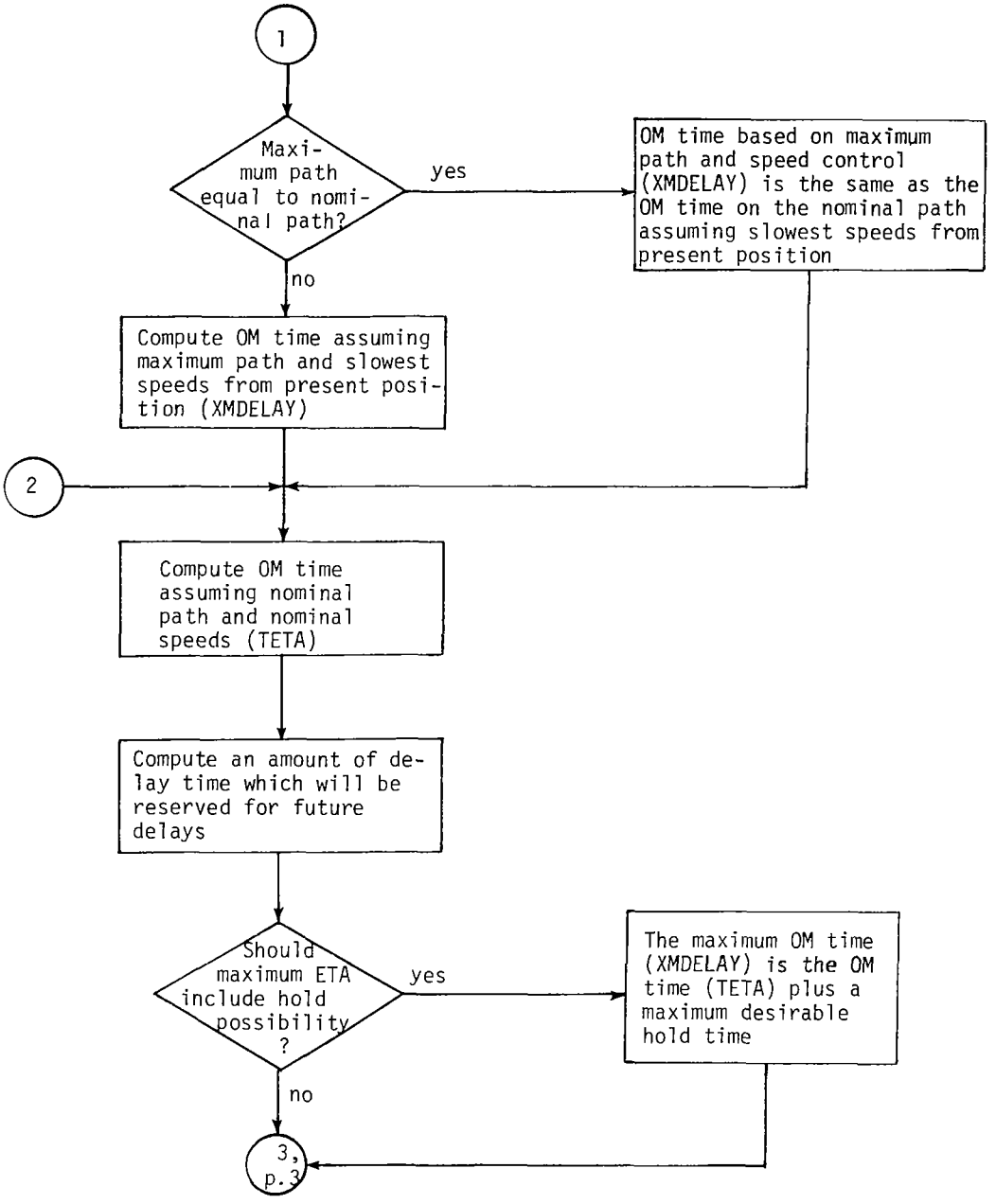

(b) Page 2 of TENTSEQ subroutine.

Figure D3.- Continued.

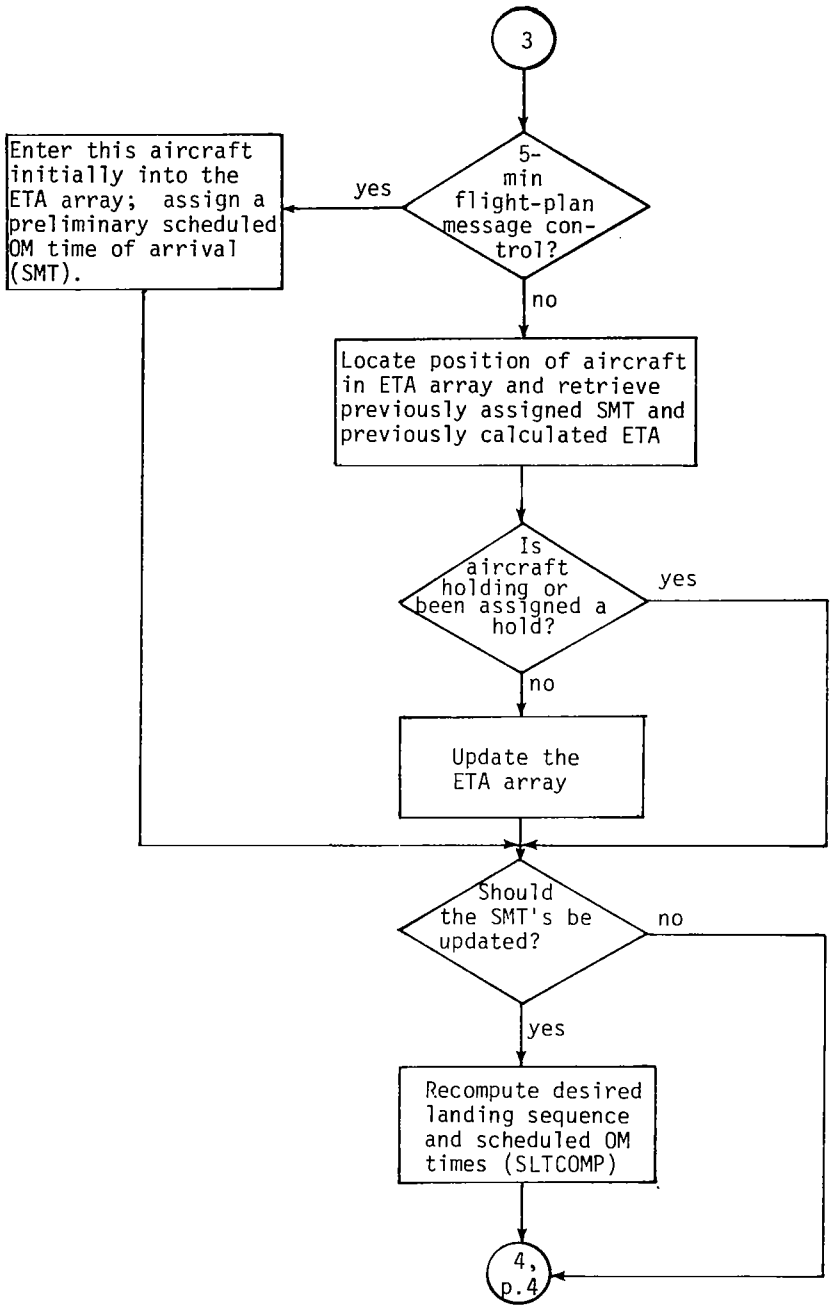

(c) Page 3 of TENTSEQ subroutine.

Figure D3.- Continued.

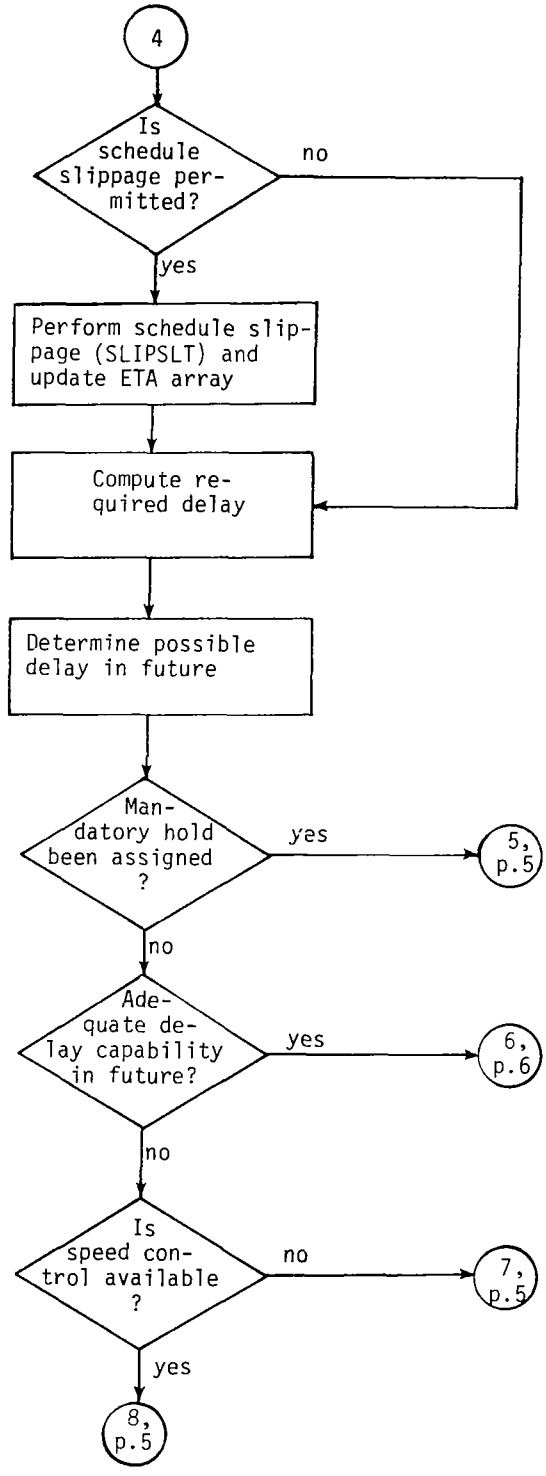

(d) Page 4 of TENTSEQ subroutine.

Figure D3.- Continued.

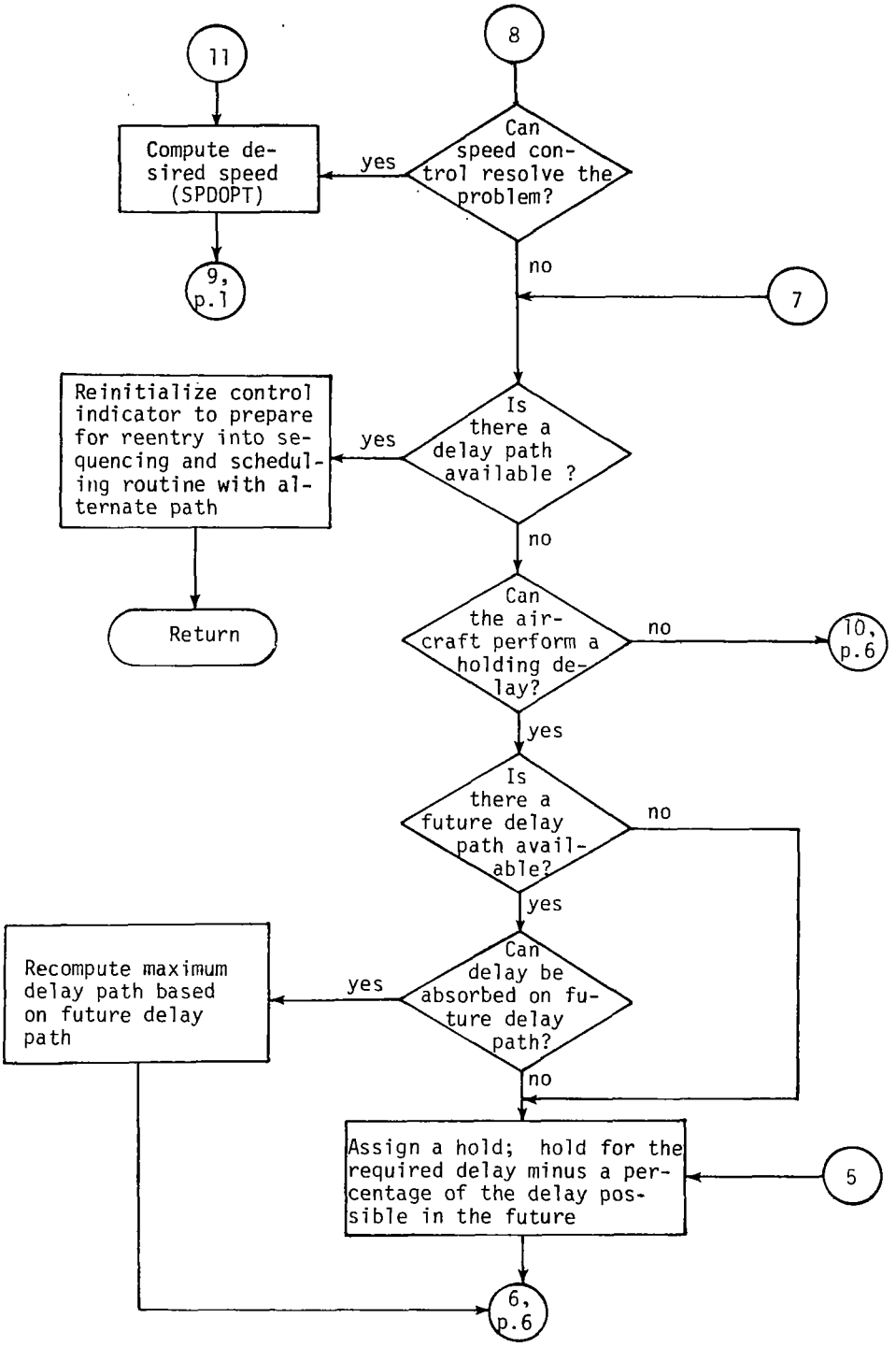

(e) Page 5 of TENTSEQ subroutine.

Figure D3.- Continued.

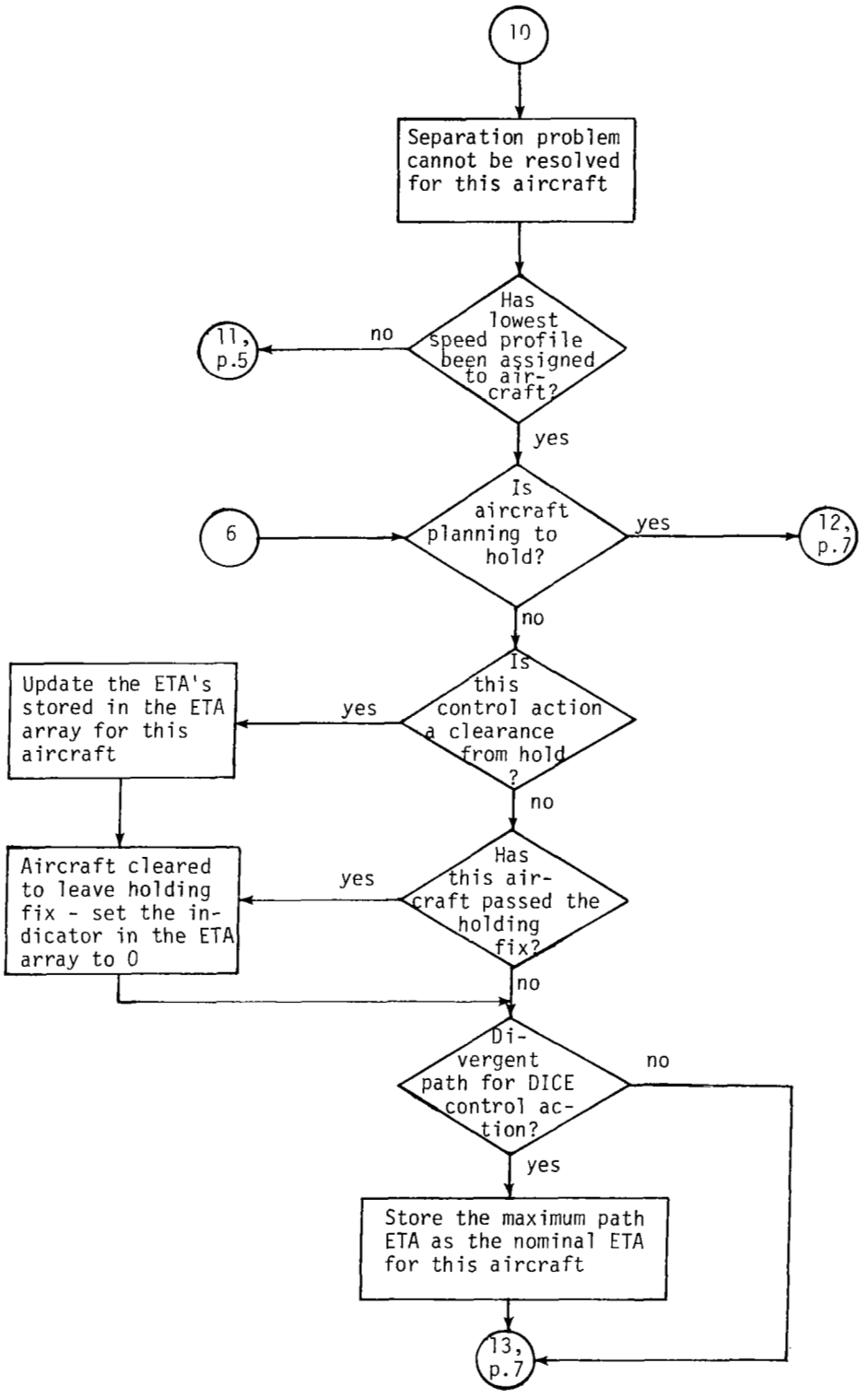

(f) Page 6 of TENTSEQ subroutine.

Figure D3.- Continued.

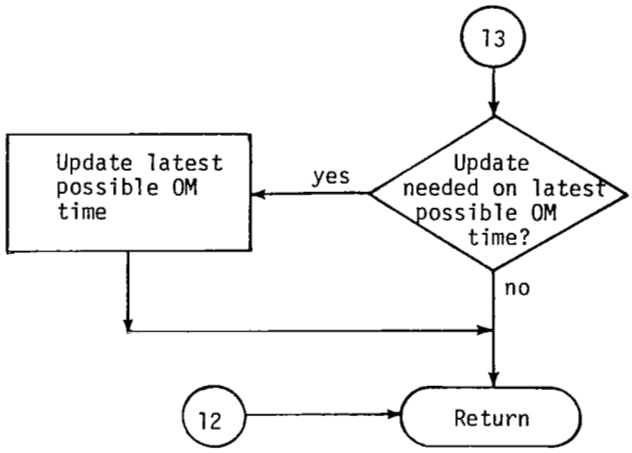

(g) Page 7 of TENTSEQ subroutine.

Figure D3.- Concluded.

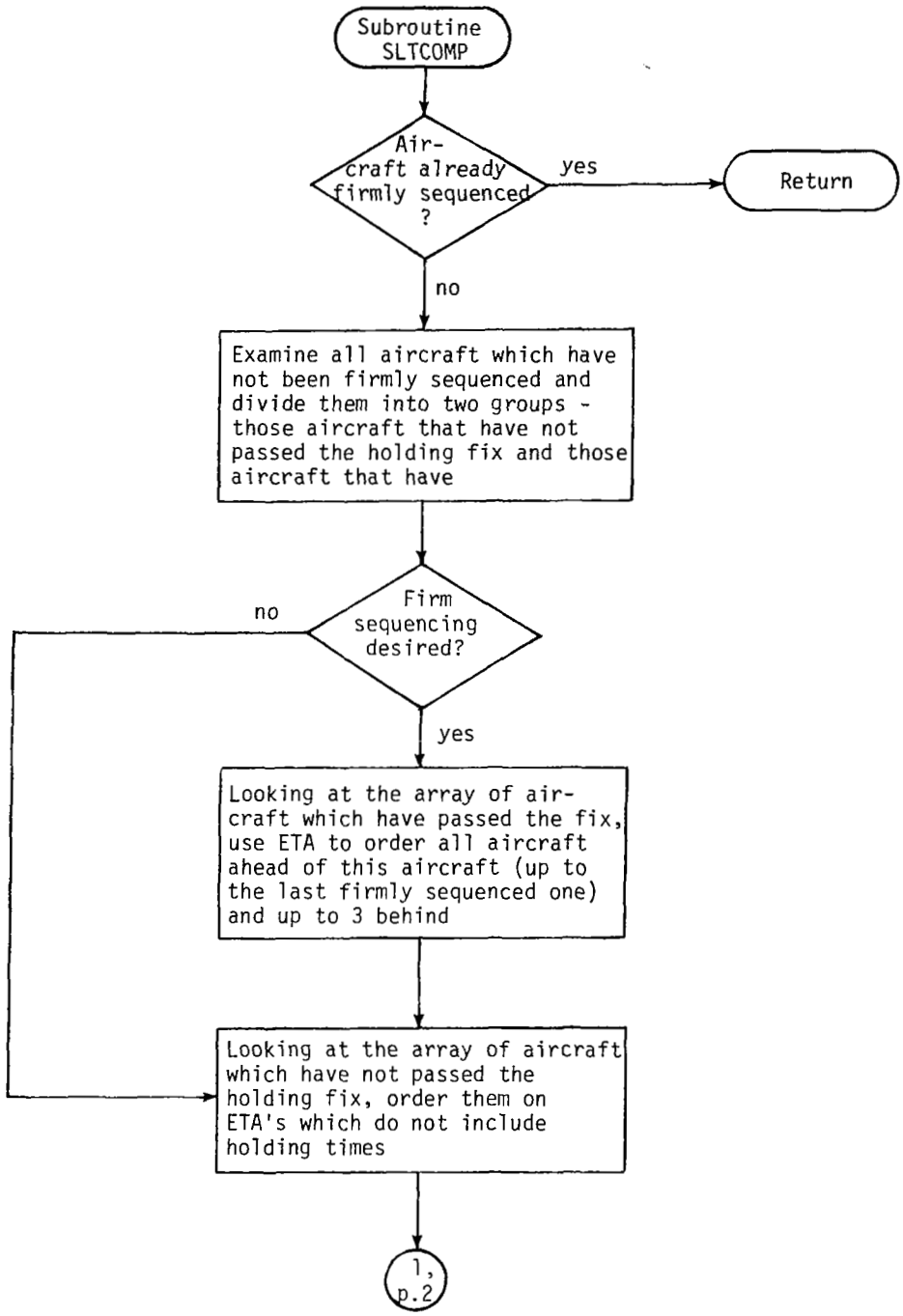

(a) Page 1 of SLTCOMP subroutine.

Figure D4.- Schedule time-of-arrival computation (SLTCOMP).

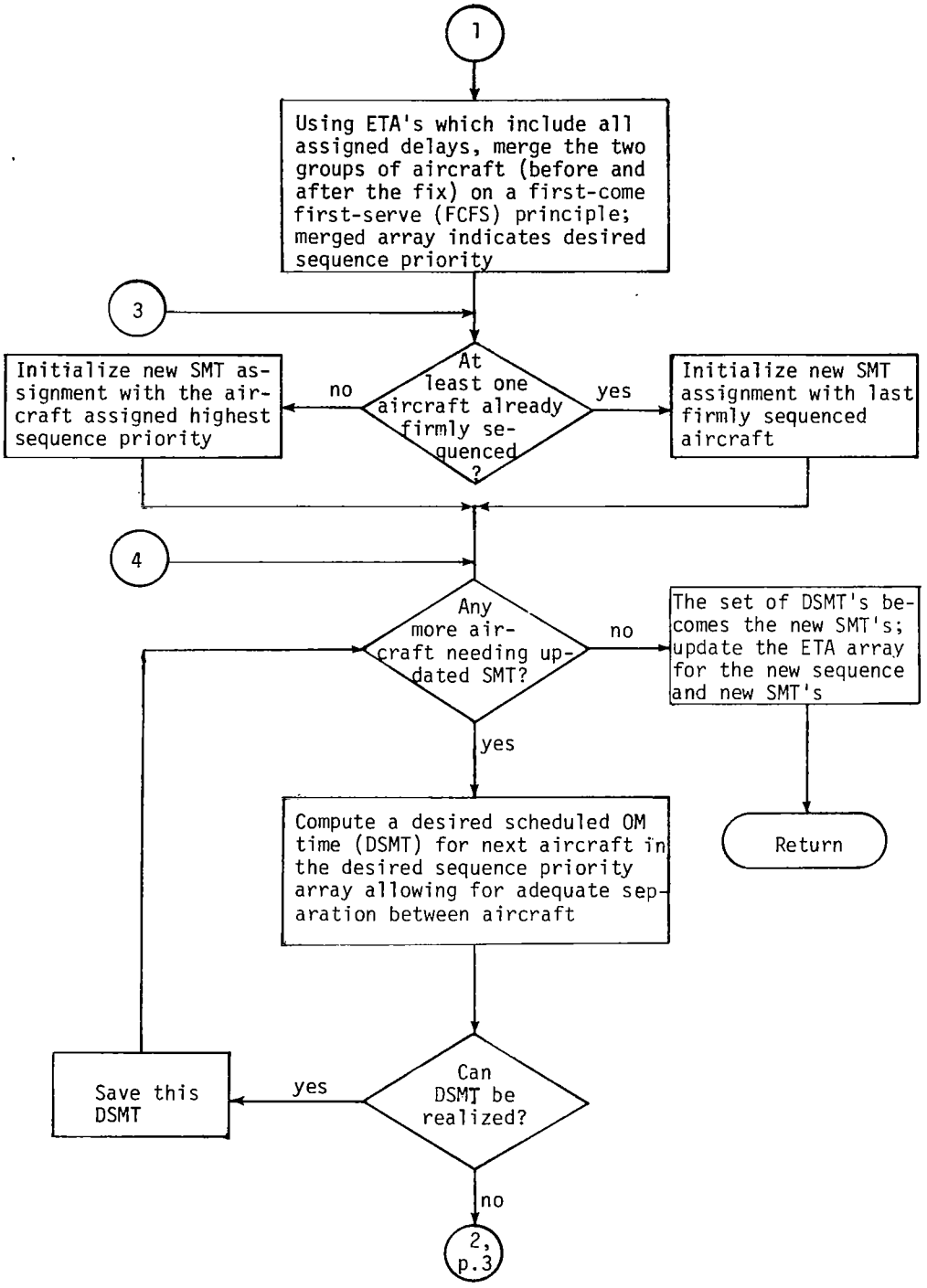

(b) Page 2 of SLTCOMP subroutine.

Figure D4.- Continued.

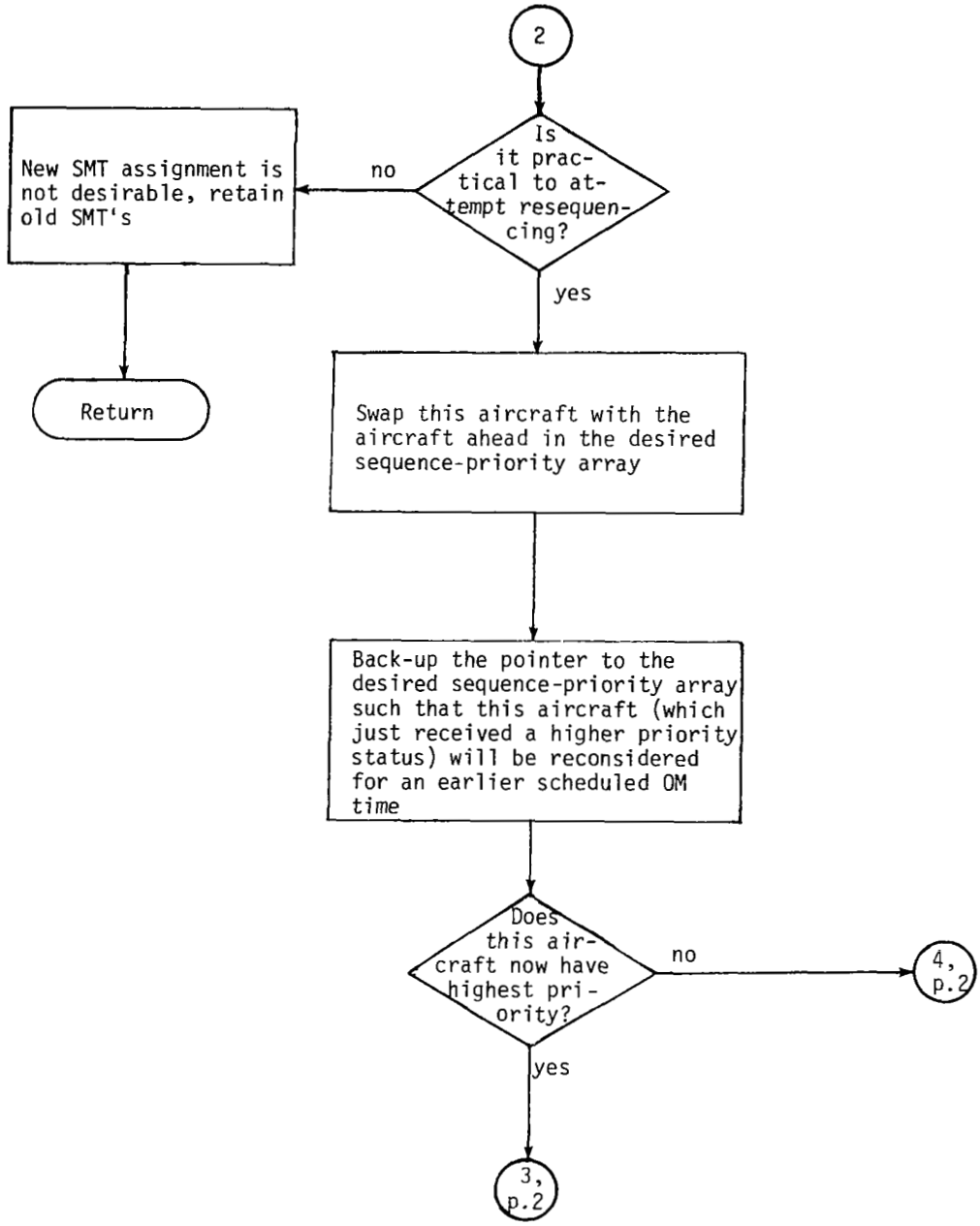

(c) Page 3 of SLTCOMP subroutine.

Figure D4.- Concluded.

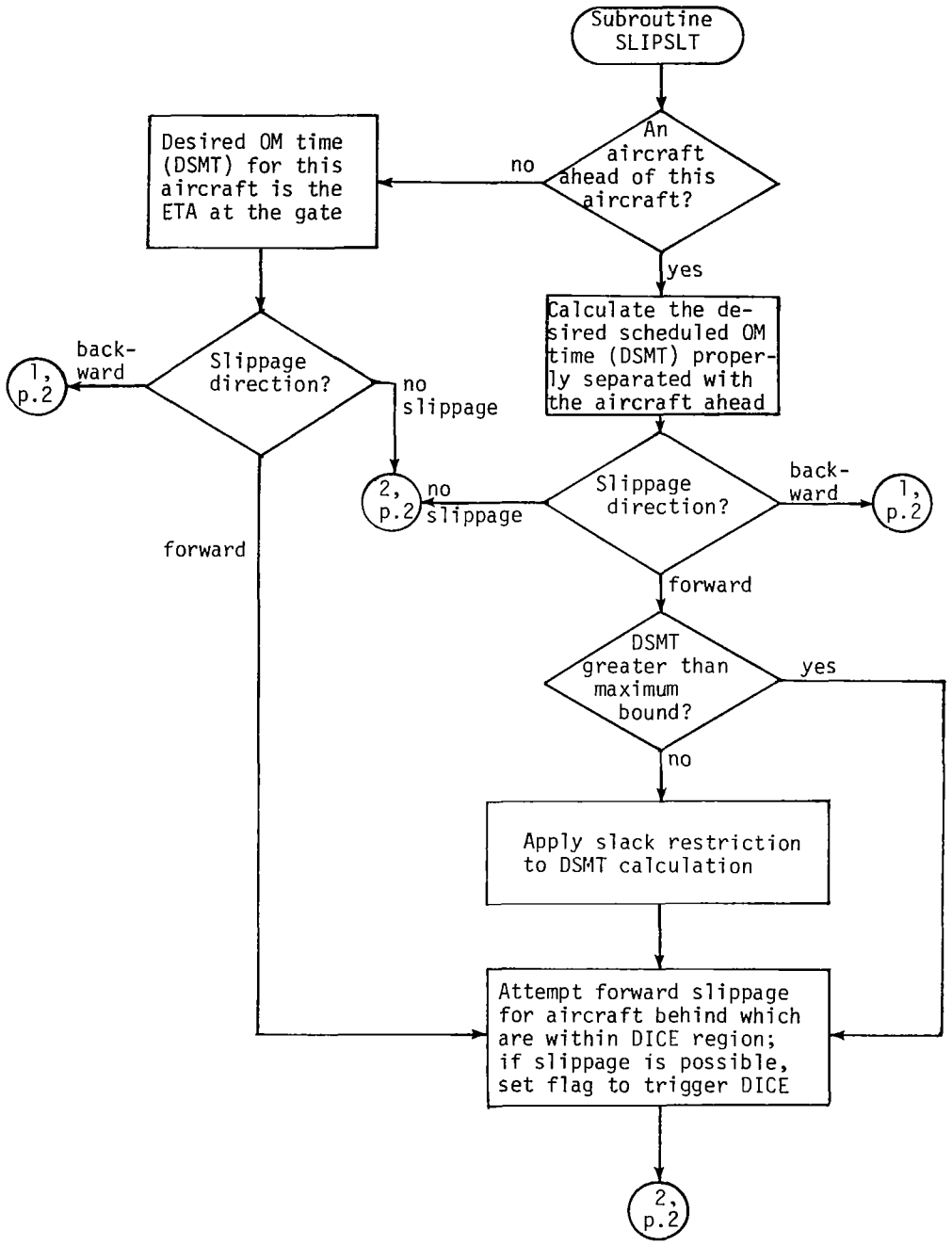

(a) Page 1 of SLIPSLT subroutine.

Figure D5.- Schedule slippage (SLIPSLT).

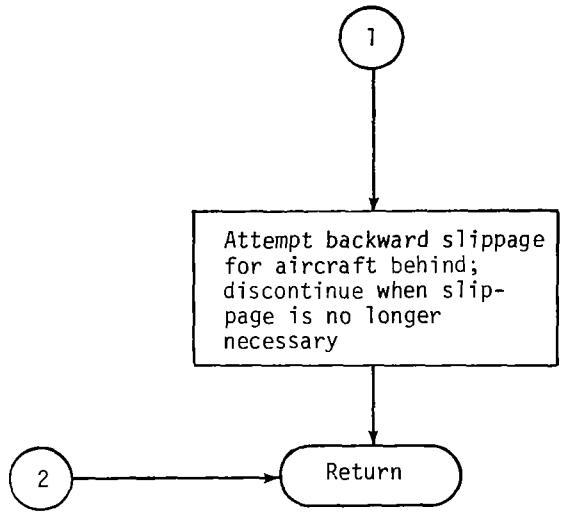

(b) Page 2 of SLIPSLT subroutine.

Figure D5.- Concluded.

REFERENCES

1. Horowitz, B. M.; and Sternfels, P. R.: Automated Metering and Spacing at Denver. MTR-6281 (Contract No. DOT-FA70WA-2448), MITRE Corp., Oct. 1972.

2. Mohleji, S. C.; and Horowitz, B. M.: Metering and Spacing System Simulation of Terminal Arrivals at Denver's Stapleton Airport. MTR-6327, MITRE Corp., Feb. 1973.

3. Mohleji, S. C.: Automated Metering and Spacing With Area Navigation. MTR-6431, MITRE Corp., June 1973.

4. Gados, R. G.; Mohleji, S. C.; and Gabrieli, H.: A Proposed Metering and Spacing System for Denver. MTR-6865 (Contract No. DOT-FA69NS-162), MITRE Corp., Mar. 1975.

5. Mohleji, Satish C.: Error Analysis of a Ground-Based Metering and Spacing System Using MLS. MTR-6796 (Contract No. DOT-FA69NS-162), MITRE Corp., Nov. 1974.

6. Britt, C. L., Jr.; Credeur, L.; Davis, C. M.; and Capron, W.: Research in Ground-Based Near-Terminal Area 4D Guidance and Control. ICAS Paper 76-57, Oct. 1976.

7. Research Triangle Inst.: Vehicle Dependent Aspects of Terminal Area Guidance and Control. NASA CR-144987, 1976.

8. Research Triangle Inst.: Study of the Impact of Air Traffic Management Systems on Advanced Aircraft and Avionic Systems. NASA CR-132278, 1973.

9. Staff of NASA Langley Research Center and Boeing Commercial Airplane Company: Terminal Configured Vehicle Program - Test Facilities Guide. NASA SP-435, 1980.

10. Capron, W. R.; and Rodgers, W. G.: An Operator/User Guide for the Terminal Area Air Traffic Model (TAATM) Fast-Time and Real-Time Simulation Programs. NASA CR-165662, 1981.

11. Davis, C. M.; and Montoya, R. J.: Research on Airborne Traffic Situation Displays. Volume I: Development of a Traffic Situation Display (TSD) Research Capability Utilizing the Terminal Area Air Traffic Model (TAATM). NASA CR-159269, 1980.

12. Harris, Richard M.: Future ATC Technology Improvement and the Impact on Airport Capacity. Plans and Developments for Air Traffic Systems, AGARD-CP-188, Feb. 1976, pp. 20-1 - 20-14.

13. Houck, Jacob A.: Operation and Evaluation of the Terminal Configured Vehicle Mission Simulator in an Automatic Terminal Area Metering and Spacing ATC Environment. NASA paper presented at the Summer Computer Simulation Conference (Toronto, Canada), July 16-18, 1979.

14. White, William F., compiler: Flight Demonstrations of Curved, Descending Approaches and Automatic Landings Using Time Reference Scanning Beam Guidance. NASA TM-78745, 1978.

15. McKinstry, R. Gill: Guidance Algorithms and Non-Critical Control Laws for ADEDS and AGCS. Doc. D6-41565, Boeing Co., 1974.

1. Report No.	2. Government Accession No.	3. Recipient's Catalog No.
NASA TP-1844		

4. Title and Subtitle	5. Report Date
EVALUATION OF MICROWAVE LANDING SYSTEM (MLS) EFFECT ON THE DELIVERY PERFORMANCE OF A FIXED-PATH METERING AND SPACING SYSTEM	August 1981
	6. Performing Organization Code: 534-04-13-51

7. Author(s)	8. Performing Organization Report No.
Leonard Credeur, Christina M. Davis, and William R. Capron	L-14069
	10. Work Unit No.

9. Performing Organization Name and Address	11. Contract or Grant No.
NASA Langley Research Center Hampton, VA 23665	
	13. Type of Report and Period Covered: Technical Paper

12. Sponsoring Agency Name and Address	14. Sponsoring Agency Code
National Aeronautics and Space Administration Washington, DC 20546	

15. Supplementary Notes

Leonard Credeur: Langley Research Center.
Christina M. Davis: Research Triangle Institute, Research Triangle Park, North Carolina.
William R. Capron: Kentron International, Inc., Hampton, Virginia.

16. Abstract

A simulation study was conducted to evaluate the delivery performance of an earlier proposed fixed-path metering and spacing (M & S) system and to determine if using the microwave landing system (MLS) improved the system's performance over that achieved with the instrument landing system (ILS). The M & S algorithms described assume an aircraft two-dimensional area navigation capability. The three navigation systems compared were: (1) very high frequency omnidirectional range/distance measuring equipment (VOR/DME) and ILS, (2) VOR/DME and ±40° MLS, and (3) VOR/DME and ±60° MLS. Other factors studied were M & S tentative schedule point location, route-geometry effects, and approach-gate-location effects. The study was made with a computerized terminal-area air trafic model and the results compared with those obtained by interaction with a full-crew, pilot-in-the-loop cockpit simulation. Summarized results are: (1) the MLS offers some improvement over VOR/DME and ILS if all approach routes contain computer-assisted turns (i.e., no straight-in routes); (2) pilot reaction to moving the gate closer to the runway threshold may adversely affect M & S performance; and (3) coupling en route metering to terminal scheduling transfers most of the terminal holding to more full-efficient, higher altitude en route delay.

17. Key Words (Suggested by Author(s))	18. Distribution Statement
Microwave landing system Metering and spacing Flow control Area navigation Interarrival-time error	Unclassified - Unlimited Subject Category 04

19. Security Classif. (of this report)	20. Security Classif. (of this page)	21. No. of Pages	22. Price
Unclassified	Unclassified	131	A07

For sale by the National Technical Information Service, Springfield, Virginia 22161

NASA-Langley, 1981